Universidade do Minho
Escola de Engenharia

Helena Sofia Cardoso Oliveira

Gating Design of a bathtub body in Brass alloy cast by Low-Pressure Die Casting

October 2023

Gating Design of a bathtub body in Brass alloy cast by Low-Pressure Die Casting
Helena Oliveira
UMinho | 2023

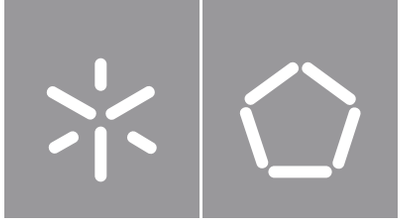

Universidade do Minho
Escola de Engenharia

Helena Sofia Cardoso Oliveira

Gating Design of a bathtub body in Brass alloy cast by Low-Pressure Die Casting

Master's Dissertation
Integrated Master's Degree in Mechanical Engineering
Specialization in Advanced Manufacturing

Work supervised by:
Professor Hélder Jesus Fernandes Puga

October 2023

ACKNOWLEDGEMENTS

This milestone marks the culmination of a significant chapter in my life, encompassing five years of learning, personal growth, and discovering my passion. In light of this achievement, I am filled with boundless gratitude for the numerous people who have played a key role in my journey. Their contributions deserve acknowledgement and my heartfelt thanks:

First and foremost, I express my immense gratitude to my mentor, Professor Hélder Puga, your unwavering belief in my abilities and willingness to offer guidance during the most challenging moments have been instrumental. Your support and encouragement have shown me that perseverance and skill lead to fulfilling outcomes.

To my beloved parents, Rosa and Carlos, your unbending belief in me has been a constant source of strength. Your unconditional love laid the foundation for my accomplishments, and I owe much of my success to you.

To my wonderful big sister, Margarida, my "partner in crime", your presence and support have been invaluable. Thank you for your kind words during times of need and for demonstrating me the way through obstacles. You are, undoubtedly, my best friend forever!

To Eng. Iker and Eng. Igor from ESI Group Support, your tireless assistance with the software has been paramount. Your dedication and expertise have been vital in making this work a reality. Thank you very much for your help!

To Metalúrgica Central da Trofa, Lda., for welcoming me, sharing your knowledge and offering support whenever needed.

I want to express my profound fondness to my godparents, Margarida and Luís. Thank you for your tremendous support throughout these years and for always being a part of my life. Your values and inspiration made this work possible, and I owe you that!

To my cherished grandmother, Felicidade, your love and support throughout these five years have been a constant source of inspiration and strength. I would also like to thank my other “grandmother”, Tia Nanda, for everything you did for me throughout my life. Your values made me who I am today!

To my extended family - my aunt and uncle, Ana and Rui, and my cousins, André and Rodrigo - thank you for your encouragement and unconditional support and love during this journey.

To my closest friends, Filipe, Damião, Sara, and Sílvia, with whom I had the pleasure to have by my side through thick and thin. Whether joyful or challenging, our shared moments have made this ride easier and more fun. May our friendship remain forever unbreakable!

At last but not least, I would like to express my heartfelt appreciation to Beatriz, whom I had the pleasure to meet at Metalúrgica Central da Trofa, Lda.. Thank you for your kind words, relentless support, and valued friendship during difficult times. I will never forget our time together, and I hope we keep in touch!

I extend my heartfelt gratitude to all who have contributed to this work, directly or indirectly. Your role has enriched the depth of this endeavour.

A todos, o meu obrigada!

"We've always defined ourselves by the ability to overcome the impossible. These moments when we dare to aim higher, to break barriers, to reach for the stars, to make the unknown known. We count these moments as our proudest achievements."

- Cooper, movie *Interstellar*.

STATEMENT OF INTEGRITY

I hereby declare having conducted this academic work with integrity. I confirm that I have not used plagiarism or any form of undue use of information or falsification of results along the process leading to its elaboration.

I further declare that I have fully acknowledged the Code of Ethical Conduct of the University of Minho.

ABSTRACT

In manufacturing, Low-Pressure Die Casting (LPDC) has stood out as a versatile and innovative solution, notably recognized in various sectors, particularly in the production of taps. Due to its ability to produce high-quality castings with minimal waste, this technology has gained significant prominence today. However, foundries face several challenges, mainly related to inadequate casting designs, resulting in defects that lead to the rejection of components. Addressing this issue, the present dissertation provides a transparent and objective description of the development of a filling system applied to the LPDC, using simulation software (QuikCAST) to reduce the occurrence of defects.

Chapter 1 introduces the current problem observed in casting simulations, along with the objective of the work - the development of a filling system through numerical simulation. Additionally, a brief overview of the document's structure is provided.

Chapter 2 describes the casting technology employed, Low-Pressure Die Casting, covering its sequence and highlighting prevalent defects.

The copper alloy and the mould material used in this work are described in Chapter 3. This chapter covers the most significant characteristics of each material for the numerical simulation.

Chapter 4 describes the numerical simulation process used in the QuikCAST software, with two types of simulation being used: Thermal Die Cycling to determine the temperature of dies and Filling Process simulation. This chapter also presents the study case used in the dissertation (bathtub water mixer) and all considerations regarding core design and the filling system.

The main focus of this work is Chapter 5, with three candidate solutions being proposed to reduce the high rejection rate of parts. Each solution was carefully designed, considering the key aspects of casting filling systems development. Simulation played a crucial role, allowing the prediction and evaluation of the proposed systems. The selected solution demonstrated overall positive results, including a high casting yield (60%), a low defect percentage, and no air inside the cavity. These outcomes indicate a reduced rejection rate of cast parts and improvement in the company's production process.

Chapter 6 summarizes the entire project, providing an overview of the work and offering insights for future research. In a broader context, this project demonstrated the feasibility of implementing simulation software in foundries to reduce costs and time-to-market.

KEYWORDS

CASTING SIMULATION, LOW-PRESSURE DIE CASTING, DEFECTS PREDICTION, QUIKCAST, BRASS.

RESUMO

Na manufatura, a Fundição por Baixa Pressão tem-se destacado como uma solução versátil e inovadora visivelmente reconhecida em diversas áreas, nomeadamente na produção de torneiras. Por produzir fundidos de alta qualidade com um reduzido desperdício, esta tecnologia tem-se destacado atualmente. No entanto, as fundições enfrentam diversos desafios, maioritariamente relacionados com projetos de fundição inadequados, levando ao surgimento de defeitos que resultam na rejeição de peças. Tendo em vista o problema, a presente dissertação descreve, de forma clara e objetiva, o desenvolvimento de um sistema de enchimento, aplicado à Fundição por Baixa Pressão, com recurso a *software* de simulação (QuikCAST), de forma a mitigar o surgimento de defeitos.

O Capítulo 1 apresenta o problema atualmente verificado nas fundições a nível de simulação de fundição, bem como o objetivo do trabalho – desenvolvimento de um sistema de enchimento através de simulação numérica. Para além disso, apresenta uma descrição sumária da estrutura do documento.

O Capítulo 2 refere-se à tecnologia de fundição empregue, a Fundição por Baixa Pressão, com a sequência de fundição e especial destaque aos defeitos recorrentes.

A liga de cobre e da moldação utilizadas são descritas no Capítulo 3. Aqui, destacam-se as características mais preponderantes para a simulação numérica de cada material.

O Capítulo 4 descreve pormenorizadamente o processo de simulação numérica, com dois tipos de simulação empregues: *Thermal Die Cycling*, para determinar as temperaturas das coquilhas e *Filling Simulation* relativa ao enchimento da cavidade. É ainda apresentado o caso de estudo (misturadora de água de banheira), bem como todas as considerações do projeto de machos e do sistema de enchimento.

O foco principal deste trabalho é o Capítulo 5, apresentando três soluções para reduzir a elevada rejeição. Cada solução foi cuidadosamente projetada, de acordo com o desenvolvimento de sistemas de enchimento. A simulação foi crucial, permitindo a previsão e a avaliação dos mesmos. A solução selecionada apresentou um elevado rendimento de cacho (60%), reduzidos defeitos e a ausência de ar. Estes resultados reduzem a rejeição de fundidos e melhorias no processo de produção da empresa.

O Capítulo 6 resume o trabalho realizado e propondo trabalhos futuros. Assim, este projeto demonstrou a viabilidade da implementação de *software* de simulação em fundições para redução de custos e diminuição do *time-to-market*.

PALAVRAS-CHAVE

SIMULAÇÃO DE FUNDIÇÃO, FUNDIÇÃO POR BAIXA PRESSÃO, PREVISÃO DE DEFEITOS, QUIKCAST, LATÃO.

INDEX

FIGURE INDEX

TABLE INDEX

LIST OF ACRONYMS

AISI	American Iron and Steel Institute;
CAD	Computer Aided Design;
CPDC	Counter Pressure Die Casting;
DAS	Dendritic Arm Spacing;
FDM	Finite Differences Method;
FDU	Foundry Degassing Unit;
FEM	Finite Elements Method;
GF	George Fisher;
HPDC	High Pressure Die Casting;
HTC	Heat Transfer Coefficient;
ISO	International Organisation for Standardisation;
LPDC	Low Pressure Die Casting;
MCT	*Metalúrgica Central da Trofa, Lda*;
N-S	Navier-Stokes Equations;
PDE	Partial Differential Equations;
SI	*Système International d'Unités*;
VOF	Volume-of-Fluid Equation.

LIST OF SYMBOLS

Latin Symbols

Symbol	Description	Unit
A	Surface Area	m^2
C_p	Specific Heat	$\mathrm{J} \cdot \mathrm{K}^{-1}$
d	Diameter	m
F	Volume-of-Fluid Function	[-]
g	Gravitational Acceleration	$\mathrm{m/s}^2$
h	Heat Transfer Coefficient	$\mathrm{W}/(\mathrm{m}^2 \cdot \mathrm{K})$
k	Thermal Conductivity	$\mathrm{W}/(\mathrm{m} \cdot \mathrm{K})$
N_R	Reynold's Number	[-]
P	Permeability	[-]
p	Pressure	bar
Q	Heat	W
T	Temperature	°C
t	Time	s
u, v, w	Liquid Metal Velocity	m/s
Y	Height	m
V	Volume	m^3

Greek Symbols

Symbol	Description	Unit
ε	Emissivity	[-]
μ	Kinematic Viscosity	m^2/s
ρ	Density	$\mathrm{kg/m}^3$

Chapter 1 - INTRODUCTION

In the modern industrial fields, simulation software finds wide-ranging applications across various domains, encompassing structural, thermal, and other domains. These tools are employed to forecast and ascertain potential negative outcomes that may arise during the subsequent stages of component manufacturing.

Like other manufacturing sectors, the primary aspiration of foundries is to produce impeccable components within the shortest achievable timeframe. This overarching goal drives industries to adopt simulation technology to address their challenges progressively and effectively.

Simulation technology offers a valuable solution for comprehensively analysing and optimising various manufacturing processes. By simulating the casting process, industries can predict potential defects, optimise designs, and assess the effects of different parameters without needing physical prototypes. It not only accelerates the development cycle but also contributes to more sustainable practices by reducing the consumption of resources. As a result, integrating simulation software into foundry operations becomes a logical step forward, aligning with the broader trend of leveraging digital tools to achieve greater efficiency, accuracy, and competitiveness in the manufacturing landscape.

In manufacturing, Low-Pressure Die Casting (LPDC) has emerged as a versatile solution applicable to various everyday applications, notably within the sanitary industry. Acknowledge for producing high-quality cast products with minimal waste, LPDC technology has gained traction. Nevertheless, contemporary casting industries grapple with many challenges, prominently centred around insufficient or inadequate casting designs. This deficiency often leads to the emergence of defects that subsequently prompt the rejection of castings. Shrinkage Porosity stands out among the prevalent defects, underscoring the significance of optimizing gating systems to mitigate the risk of premature solidification during the casting process.

1.1. MOTIVATION

Casting simulation offers the capability to visualize and analyze critical stages of the casting process, encompassing mould cavity filling, solidification, and cooling. This predictive capability proves invaluable in identifying and anticipating defects, including shrinkage and gas porosity, runouts, and cold shuts. As a result, it serves as a reliable resource for optimizing casting systems, avoiding the need for extensive shop-floor trials. Within the realm of casting geometry development, certain factors exert significant influence [1]:

i. Material properties influence casting behaviour, including alloy characteristics such as chemical composition, density, specific heat, thermal conductivity, and viscosity.

ii. Geometry considerations encompass internal and external corners, cored holes, ribs, pockets, and the arrangement and number of cavities. These elements impact heat transfer to the mould.

iii. The manufacturing process and alloy chosen can lead to process-specific issues. Turbulence during cavity filling, for instance, may cause oxidation at the metal front, while the chosen technology may result in erosion or degradation of the casting mould, if selected incorrectly.

Given the considerations, accurate and comprehensive casting software becomes paramount in achieving high-quality, defect-free parts. Achieving perfect casting software is a challenging endeavour, as it is recognized that minor shortcomings in the design process can have a significant impact. While design typically accounts for around 5% of the total production cost, inadequate design can contribute to over 80% of the overall manufacturing expenses. Casting defects resulting from suboptimal design can lead to a high rejection rate. Thus, developing well-designed casting systems supported by suitable software is crucial to optimizing products and reducing time-to-market [2].

According to Figure 1, the application of casting software offers a multitude of benefits, as outlined below [1–3]:

i. **Prediction of Metal Behavior**: Casting software enables the prediction of metal flow dynamics within a cavity.

ii. **Solidification Insight**: The software predicts solidification behaviour and associated problems, such as shrinkage porosity, a prevalent defect that can be mitigated through simulation.

iii. **Thermal Stress Estimation**: The software estimates thermal stresses post-solidification and thermal treatment, aiding in identifying potential issues.

iv. **Gating System Design and Optimization**: Casting software facilitates the design and optimization of gating systems while predicting defect positions. This reduces the need for extensive shop floor trials that can escalate manufacturing costs, encompassing processes like tool fabrication/modification, metal melting, pouring, and other steps.

v. **Market Share Expansion**: Using simulation software instils confidence in companies, even when handling intricate casting geometries, which can expand a company's market share.

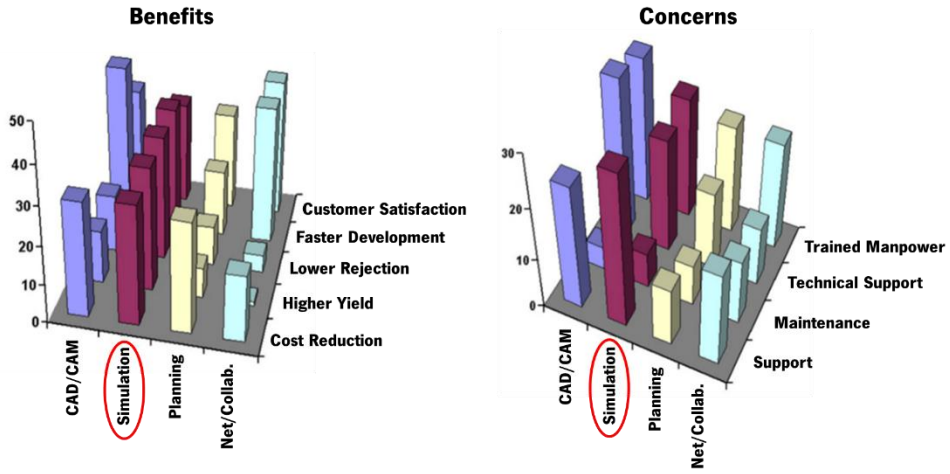

Figure 1: Benefits and inconveniences of using casting simulation software in industries.

By improving casting software's capabilities, industries can enhance their casting processes, reduce defects, and achieve more efficient and cost-effective manufacturing outcomes.

Casting simulation, while beneficial, is not without its drawbacks, which encompass the following [1, 3]:

i. **High Implementation Cost**: The use of casting simulation involves substantial upfront costs, encompassing software licensing, hardware requirements, and potential training expenses.

ii. **Dependence on Expertise**: The accurate interpretation and utilization of simulation results require skilled technical personnel proficient in the software, which is essential to ensure outcomes align with expectations.

iii. **External Program Dependence**: Casting simulation relies on external programs, such as Computer-Aided Design (CAD) software, to model casting and gating system geometries. This interdependence can lead to complexities in data exchange and compatibility.

Despite these challenges, the potential to optimize casting processes and enhance product quality makes casting simulation valuable in various industries.

1.2. AIM

This study aims to assess the feasibility of utilizing the QuikCAST casting simulation software within brass foundry processes, specifically for producing a Bathtub Body at *Metalúrgica Central da Trofa, Lda.*, using the Low-Pressure Die Casting technology. The research will examine essential properties of the Brass alloy employed by the company (ISO CuZn39Pb1Al-B), encompassing its chemical composition, thermal conductivity, solidus and liquidus temperatures, phase diagrams, microstructure, and other pertinent attributes. This exploration will provide insights into the alloy's fundamental characteristics.

Subsequently, crucial aspects of the LPDC process will be investigated, including mathematical principles, casting sequencing, and other relevant concepts. Significant parameters that substantially influence this technology will also be comprehensively explored.

At last, the study will involve developing a casting system using the QuikCAST software, alongside identifying and predicting potential casting defects. Subsequent assessments and discussions will be conducted between numerical and experimental results. The envisaged outcome is to facilitate the application of the numerical model in predicting casting defects for future gating system developments, thereby providing Metalúrgica Central da Trofa, Lda. with a valuable tool to enhance casting quality in various other models.

1.3. METALÚRGICA CENTRAL DA TROFA, LDA

Metalúrgica Central da Trofa, Lda., Figure 2, is a company located in Vila Nova de Famalicão, Braga, Portugal, established in the early 1960s. Initially, the company focused on casting brass, with a particular emphasis on taps and valves. Over the years, the company diversified its product offerings and expanded into various applications, including bathtub mixer and water-meter shell. Today, Metalúrgica

Central da Trofa, Lda. specializes in producing non-ferrous materials, primarily copper-zinc alloys known as brasses. Additionally, they offer services such as machining, polishing, and product packaging [4].

Figure 2: The company *Metalúrgica Central da Trofa, Lda.*.

The company's product range includes various fittings, bathroom accessories, and other household components related to water systems. Furthermore, the company produces brass items, including water meters and valves, used for control and direction water and other fluids [4].

(a) (b)

Figure 3: Examples of components produced by *Metalúrgica Central da Trofa, Lda.* (a) water valves and (b) fittings.

1.4. Document Structure

The document is structured so that each chapter provides a comprehensive overview of the steps undertaken in the project's development to enhance reader comprehension. Within each chapter, practical applications and underlying assumptions are thoroughly discussed, supported by fundamental theoretical concepts from metallurgy and foundry practices. The strategy entails the following steps:

1. Gain a comprehensive understanding of Low-Pressure Die Casting and its key parameters.

2. Utilise the QuikCAST casting software to design a comprehensive gating system to minimise rejection rates.

3. Perform a comparative analysis between numerical simulations and experimental outcomes.

The current chapter introduces key aspects concerning the utilization of casting simulations in industries and the challenges currently faced. Additionally, a concise history of the company is provided, shedding light on the origin of the issues at hand. The chapter also outlines the study's objectives and the document's overall structure.

Chapter 2 delves into the specific casting technology employed: Low-Pressure Die Casting. A central focus of this chapter is a thorough exploration of common defects inherent to it (Chapter 2.3), elaborating on typical defects encountered in this method.

Chapter 3 presents a comprehensive overview of the copper alloy under investigation (ISO CuZn39Pb1Al-B). The critical parameters for simulation, such as chemical composition, phase diagram, microstructure, thermal properties, and melt treatment, are detailed. The material utilized for the tools, AISI H13 steel, is also mentioned.

Chapter 4 provides an in-depth examination of the entire process of simulating LPDC. Beginning with a discussion on the numerical model used by the QuikCAST software, the study delves into the specific case this project addresses. Modifications made to create the casting model, core design, and gating design are also elaborated. The complexities and solutions associated with designing gating channels are discussed. Furthermore, the numerical model employed in QuikCAST for Low-Pressure Die Casting technology is presented. This chapter also describes the two types of simulations conducted: Thermal Die Casting and Filling (and solidification). Critical parameters for each simulation are elucidated.

In Chapter 5, the outcomes obtained for the study case are showcased, featuring a comprehensive comparison between experimental and numerical results. The microstructures of areas with defects and those without apparent flaws are visualized using optical microscopy, facilitating meaningful comparisons.

Chapter 6 summarizes the project's findings and presents comprehensive conclusions on the topics explored. Furthermore, the key challenges of the project and future work are also explored.

1.5. Chapter References

[1] B. Ravi, "Casting Simulation and Optimisation: Benefits, Bottlenecks and Best Practices Casting Simulation and Optimisation: Benefits, Bottlenecks, and Best Practices," *Indian Foundry Journa*, pp. 1–11, Jan. 2008, [Online]. Available: https://www.researchgate.net/publication/228975218

[2] THERCAST®, "WHY SHOULD YOU USE SIMULATION SOFTWARE FOR YOUR MOLTEN METAL CASTING?," *Transvalor Americas*, Aug. 16, 2022. https://blog.transvalorusa.com/articles/use-simulation-software-for-your-molten-metal-casting (accessed Aug. 19, 2023).

[3] B. Ravi and G. L. Datta, "Co-operative Virtual Foundry for Cost-Effective Casting Simulation," in *54th Indian Foundry Congress, Pune, 2006*, 2006, pp. 1–12. [Online]. Available: https://www.researchgate.net/publication/228886765

[4] Metalúrgica Central da Trofa, Lda., "Metalúrgica Central da Trofa, Lda.," 2023. https://mct.com.pt/ (accessed Aug. 18, 2023).

Chapter 2 - Low-Pressure Die Casting

Low-Pressure Die Casting (LPDC), also known as permanent low-pressure mould, is a widely known casting process used to produce metal parts, like automotive parts (wheels and cylinder heads) or taps, that uses pressure to fill a cavity, despite what happens in gravity casting [1–2].

Unlike High-Pressure Die Casting (HPDC), the LPDC pressure range varies between 0.1 bar to 1 bar, required to lift the molten metal from the furnace, placed below the dies, up into the mould. LPDC is typically used in small to medium parts, until 150 kg[1], mostly made from alloys with low melting points, such as aluminium, magnesium, or copper alloys [3–5].

2.1. Casting sequence

In practice, the LPDC process has been demonstrated to be impressively automated and very productive. Generally, the procedure used for pouring metal with this type of technology can be described as follows [7–9]:

[1] Parts with more than 150 kg can also be obtained with Low-Pressure Die Casting, but only in exceptional cases due to the high cost of the dies [6].

1. The molten metal is transferred to another furnace (also called a holding furnace), beneath the moulds, at the same temperature as the previous furnace.

2. Then, air or other inert gas (for instance, nitrogen) is pressurised through small holes, in the furnace, pushing the metal to the riser towards the dies. Later, a gating system fills the mould cavity with metal (Figure 4).

3. During solidification, the pressure applied to the air or gas remains constant until most of the casting has solidified inside the cavity.

4. The pressure is then released, and the molten metal in the riser tube falls, by gravity, to the furnace, which can be reused.

5. Lastly, casting is removed from the dies for additional finishing operations.

Figure 4 shows a schematic representation of a typical LPDC machine. Note that in some LPDCs' equipments, the riser tube is heated using a gas burner to avoid premature solidification of the molten metal during cavity filling [6].

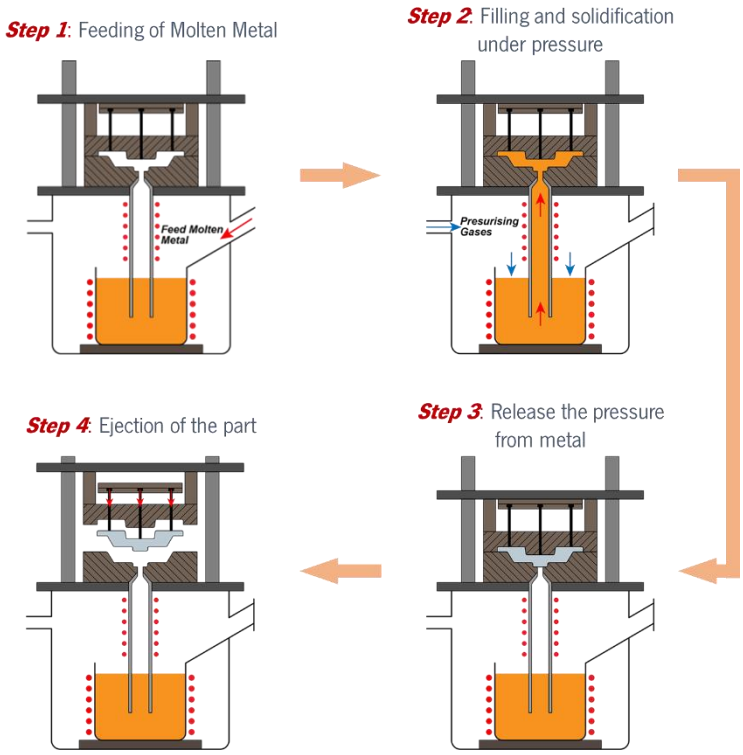

(a)

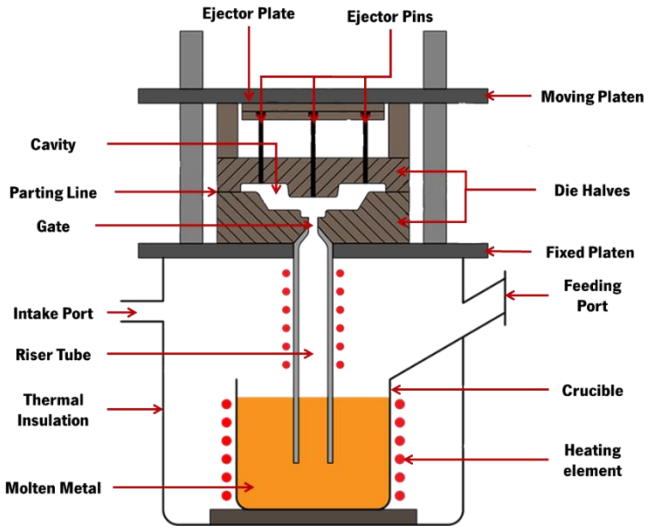

(b)

Figure 4: Low-Pressure Die Casting (a) casting sequence and (b) machine.

2.2. Advantages and Disadvantages of Low-Pressure Die Casting

Low-Pressure Die Casting has been used nowadays in many foundries/applications, due to its various advantages [3, 9, 11]:

i. **High metallurgical quality** – as metal enters the cavity quiescently, with a non-turbulent filling pattern, some unwanted aspects, like metal overturning, impact, and splash, can be avoided. During solidification, gas pressure stays constant for a short time, enabling natural compensation of the metal. Therefore, some casting defects, such as shrinkage porosities, can be reduced since molten metal is fed continuously to the cavity (for that reason, this process is often used for producing axisymmetric parts like automobile wheels).

ii. **High flexibility** – this process can be used in complex geometries with different wall thicknesses, sizes, heights, and configurations. It can be used for non-ferrous alloys like aluminium and copper and ferrous alloys like steel and cast irons.

iii. **Simplicity of gating system** – the gating system is generally straightforward, and the use of feeders can be omitted most of the time. Thus, machining costs are lower.

iv. **Good castability** – when metal enters mould under pressure, its fluidity increases, as well as the specimens' yield (over 90%), which is suitable for castings requiring high mechanical strength.

v. **Low percentage of slag/dross** – typically, slag develops at the surface of molten metal. However, due to the design of the machine (Figure 4), slag that might be in molten metal is removed because of the riser tube that connects the furnace to the moulds. Moreover, as stated before, molten metal moves

slowly towards the cavity (there is some stability during filling), and the probability of including oxides due to turbulent flow also decreases, raising casting purity.

vi. **Possibility of process automatization** – LPDC machines are simple and, most of the time, very compact, which enhances process automatization.

vii. **Lower capital investment** – Low-Pressure Die Casting machines are much more economical than High-Pressure Die Casting machines due to their dimensions and the complexity of the process itself.

Notice that components obtained with this technology usually reveal finer grain size and smaller dendrite arm spacing, thanks to the high solidification rates of Low-Pressure Die Casting and the inverted solidification pattern presented (casting feeding comes from underneath). However, this process also has some negative aspects like [3, 4, 12]:

i. **Slow time casting cycles** – LPDC has slow time casting cycles due to the quiescent filling, unlike in high-pressure die casting.

ii. **Minimum casting thickness** – although this technique is excellent for complex thin wall pieces, there is a minimum thickness value of approximately 3 mm, contrary to what happens in HPDC.

2.3. Common Defects associated with Low-Pressure Die Casting

Although casting simulation software helps us predict and avoid the most common casting defects encountered, it is still crucial to understand them, especially those typically found in LPDC castings. In many cases, these castings have flaws that can jeopardise their final performance, resulting in the rejection of components [13].

Also, when a defect is smaller than the microstructural features of the molten metal, for example, if it is smaller than dendritic arm spacing (DAS), it ceases to be a significant aspect. Hence, as stated in (Nunes) [4], “the more compact the defect, the less damage will be suffered.”.

As shown in Figure 5, casting defects may occur as a direct result, or not, of multiple aspects, underlining those related to negligence during metal pouring (represented in red - Figure 5), the variables associated with using poor gating systems (shown in orange - Figure 5) and also those connected to impurities/uncleanliness of the alloy (pictured in yellow - Figure 5).

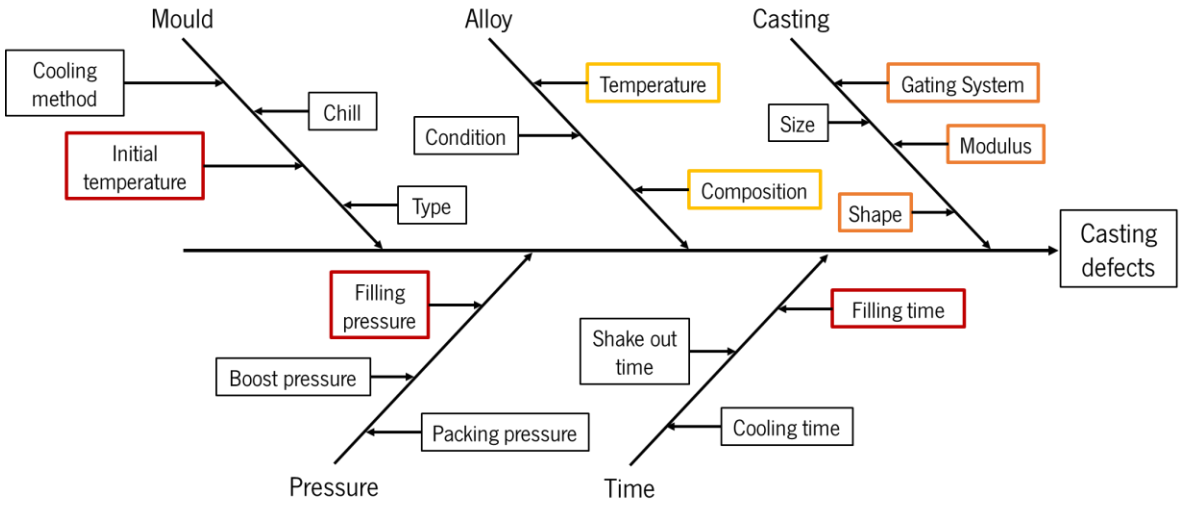

Figure 5: Effect of different variables on casting defects' appearance.

As stated by [14–15], casting defects can be divided into six main categories:

i. **Gas porosities**, including blisters, blowholes, open holes, and pinholes.

ii. **Metallurgical defects**, comprising hot tears.

iii. **Mould material defects**, with cuts/washes, drops, metal penetration, rat tails and swells.

iv. **Pouring metal defects**, including cold shuts, inclusions, misruns, and slag inclusions.

v. **Casting shape defects**, concerning mismatches/shifts and warping.

vi. **Shrinkage defects**, in which are associated with closed shrinkage defects (micro and macroporosity) and open shrinkage defects (caved surfaces and pipes).

Although there is a wide range of flaws, this chapter intends to present the most prevalent defects encountered in parts manufactured by Low-Pressure Casting and highlight some considerations for each one.

2.3.1. Gas Porosities

Gas porosities are discrete and separate holes, typically round or oval, that may appear in casting parts after cooling, with a smooth surface and bright colour. This type of defect can be identified by visual inspection during machining or by using X-ray technology if the area of the defect is not machined. According to (Nunes), this kind of flaw has two primary sources: entrained air, which has a wide range of process causes and dissolved gas, which is a fully metallurgical control problem.

Moreover, it is crucial to identify the subsurface pores created due to turbulent gating systems. Thus, these flaws are distinct from those generated *in situ* during solidification, also known as shrinkage

porosities (further discussed in Chapter 2.3.4). Subsurface pores are characterized as being smaller than 5 mm, so it does not have sufficient buoyancy to come up into a metal surface defect [16].

The leading cause of gas defects in brass alloys is air entrainment inside the cavity, in which its position and dimensions depend on the component's alloy and geometry. According to Figure 6, the hydrogen solubility in copper suffers a sudden drop between liquid and solid phases that augments the inclusion of hydrogen in the alloy, enhancing gas porosity formation [2].

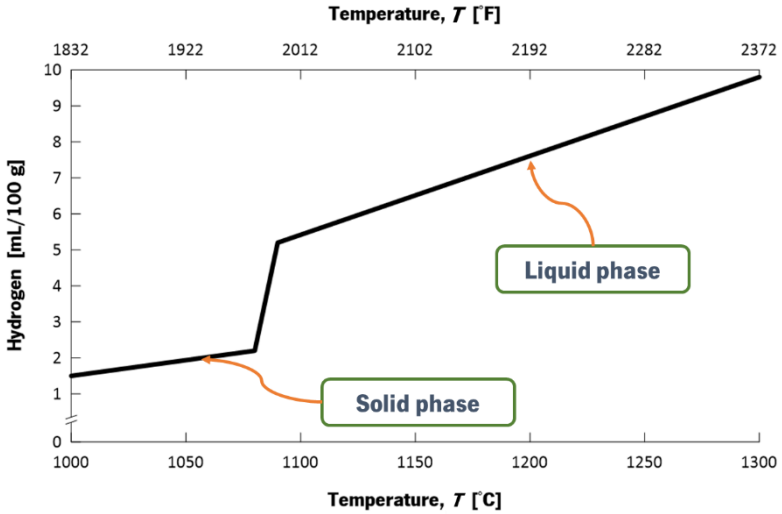

Figure 6: Hydrogen solubility in copper alloys with temperature.

As stated in [4, 10], some built-in causes of gas porosities may be described as:

i. Hydrogen released from the molten metal alloys – as stated before (Figure 6), the higher the pouring temperature, the higher the probability of hydrogen solubilizing into the alloy.

ii. Other complex gases that arise during liquid metal filling – metal gets into mould cavity quite often with high speed or pressure. If the alloy cannot flow steadily, it generates turbulence, and gases arise, leading to other casting imperfections.

iii. Gases from mould and core coatings – when metal is poured, the contact between liquid metal and mould/core-used agents causes gas volatilization and, consequently, defects.

To minimize these flaws (Figure 7), a few tips/considerations can be easily followed, such as:

i. Assure that the molten is clean and dry.

ii. Regularly apply degassing treatment to liquid metal.

iii. Design an adequate venting system.

iv. Avoid using excessive lubricants and other chemical agents.

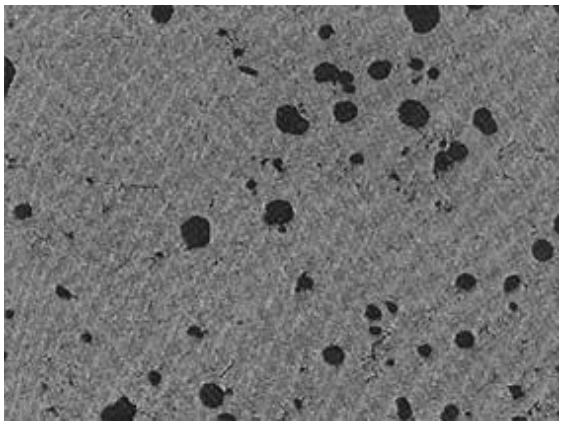

Figure 7: Gas porosity defect.

2.3.2. Pouring Metal Defects

Pouring Metal Defects are flaws related to how metal pouring is conducted and the geometry of gating systems is projected. Misruns and cold shuts are the most prevalent defects encountered.

Misrun is a casting defect that frequently comes up during the filling of cavity mould and occurs when liquid metal is too cold to flow to the borders of the component before solidification starts. Consequently, the cavity becomes deficient and incomplete, and misrun is the unfilled space in the mould (Figure 8).

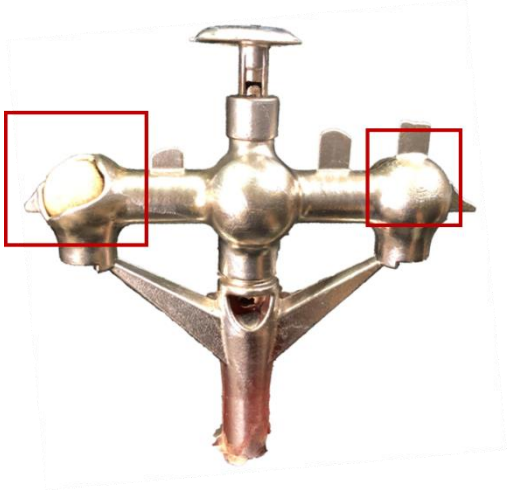

Figure 8: Misrun defect in a brass component from the company MCT.

Misruns may emerge due to several causes, but in 90% of the cases, liquid metal fluidity (i.e., the metal becomes too viscous near the end of the mould), mould design and the use of poor gating systems are the main reasons. Hence, to avoid these issues, the best approach is to adopt some good practices, such as [18]:

i. Avoid cold dies - it will not be able to maintain metal temperatures.

ii. Design an adequate gating system – the filling time is probably excessively low.

Cold shuts, also known as cold lap points, are seams that can occur in casting when the molten metal comes together from two different gates to the cavity but has not merged, usually in pieces with small to medium wall thickness. So, this type of defect appears when solidification progresses [4].

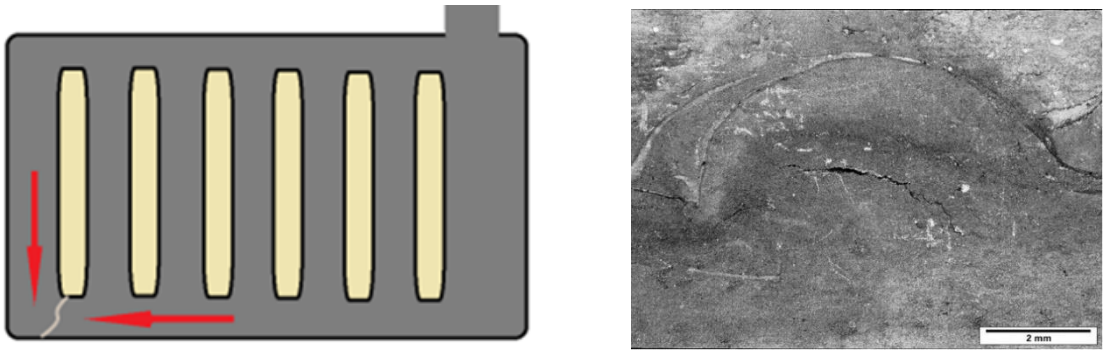

(a) (b)

Figure 9: Cold shut (a) schematic representation and (b) in a real casting piece.

As mentioned above, the root cause for cold shuts is premature solidification of the molten metal during filling, and it is mainly due to low temperature of mould and metal, insufficient casting height or poor metal treatment before pouring (ingots may contain contaminations/inclusions that needed to be removed). However, to prevent these weaknesses, some precautions might be adopted [4, 19]:

i. Increase the pouring or die temperatures to avert the alloy's premature solidification.

ii. Design an adequate gating system – the filling time is probably excessively low.

iii. Ensure that casting pressure is sufficient, considering its geometry/dimensions – use high pressure/speed ranges for larger pieces to minimize solidification of metal front; nonetheless, keep in mind that excessive values of pressure/speed cause turbulence, which, in turn, generates gas porosity.

iv. Optimize the gating system to reduce excessive filling times.

2.3.3. Casting Shape Defects

Casting shape defects affect the final shape of castings after alloy solidification, in which parts do not meet 2D design requirements, causing a high rejection rate.

Mismatches or **shifts** consist of misalignment of the upper and lower dies (Figure 10), corresponding to a horizontal displacement, according to (Wong) [15], and can also correspond to mispositioning of cores, in which the displacement occurs vertically.

Figure 10: Mismatch/shift defect.

Thus, mismatches may be associated with carelessness in core placing or, occasionally, core shift due to high molten metal velocity during filling. To minimize this defect, it is best to check if the match plate is positioned correctly [15].

Warping is another typical flaw that occurs over time, in which dimensions change in the final product due to thermal stresses and shrinkage differences induced by temperature differences between mould and molten metal (Figure 11).

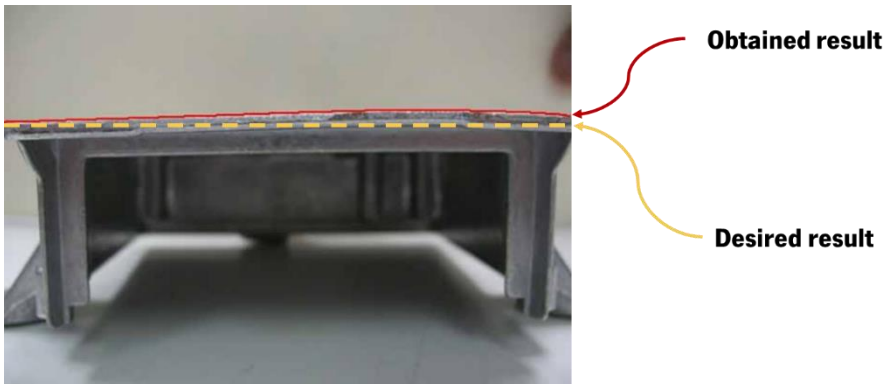

Figure 11: Warping casting defect.

Warping may appear as a result of the following [20]:

i. Inappropriate design of a gating system that does not allow fast filling.
ii. Low mould resistance (more critical in sand than die casting).
iii. Incorrect shrinkage pattern allowance regarding total part geometry.

Hence, according to (Paul, Takele), to minimize warping presence, some procedures can be taken, like [20]:

i. Monitor pouring temperature.
ii. Assure that mould and cores are stiff.
iii. Project an excellent venting system, and, if necessary, divide the gate into multiple ingates - multipoint gating system (Figure 12).

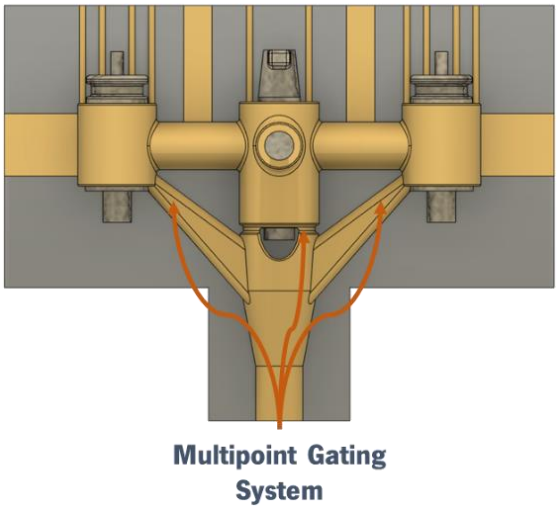

Figure 12: Multipoint gating system.

2.3.4. Shrinkage Porosity

Shrinkage porosities are metallurgical defects that form, as it states, during the solidification. It is a series of holes originating from the lack of feeding metal at the end of solidification. At all times, shrinkage is restricted to the centre of a section, which can extend to the casting surface if local die temperatures are excessive.

As metal solidifies, it contracts, which will be discussed later in this chapter, forming small cavities inside parts, practically identical to gas porosities [4].

After pouring, components cool down and solidify, which causes contraction of parts. Therefore, there are three types of solidification contraction (Figure 13): Liquid-liquid contraction, Liquid-solid contraction, and Solid-solid contraction.

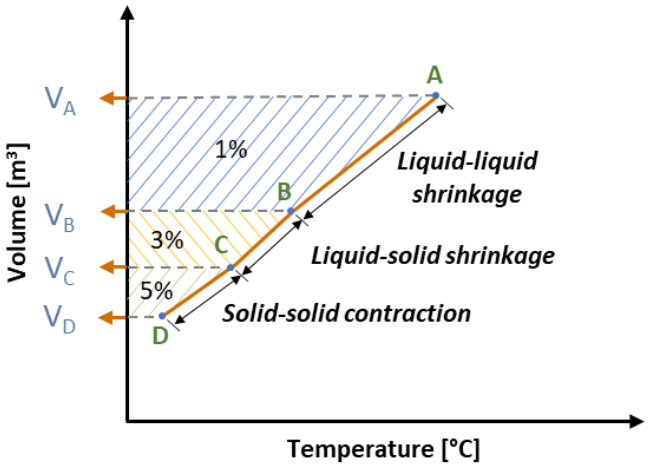

Figure 13: Shrinkage allowances for the copper alloy ISO CuZn39Pb1Al-B.

(a) Liquid-liquid contraction:

This type of contraction occurs while alloy temperature drops from pouring temperature to the melting point due to the liquid cooling.

(b) Solid-solid contraction:

Solid-solid contraction appears after casting has solidified and as it cools down from solidus to room temperature. To ensure that the final measurement of the part corresponds to the desired sizes, it is necessary to assign a slightly larger pattern that should also be considered in part design because it is one of the primary causes of warping and cracking.

(c) Liquid - solid contraction:

Liquid-solid contraction is the one that brings more concern to the foundries because of the solidification rate of the alloy. The most crucial aspect of this contraction is that all shrinkage is concentrated at the last areas of the casting to solidify. Hence, it is necessary to add an "extra volume" - known as a riser, in case of Gravity Casting - to the last points of solidification so that good castings are obtained.

During the design of feeding systems, the engineer should pay attention to the last areas to solidify, where risers should be put additionally. When done correctly, shrinkage porosity moves from the casting to the risers, which makes castings free of shrinkage porosity, since risers are removed later.

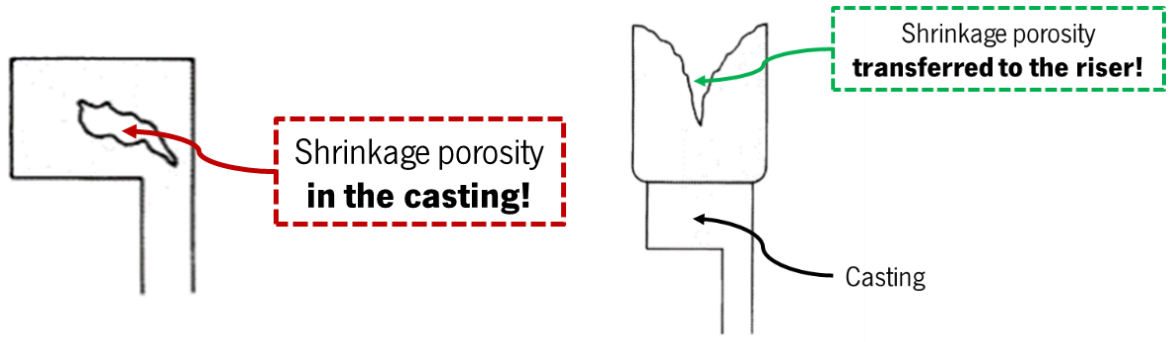

Figure 14: (a) Casting without riser - shrinkage porosity at the last point to solidify (Hot spot) - and (b) casting with a riser - no shrinkage defect encountered.

Macro or shrinkage porosity (open defects - Figure 15) is one of the possible shrinkage defects appearing in locations where insufficient feeding of liquid metal prevails to minimize volumetric shrinkage associated with liquid-solid contraction. Moreover, this flaw emerges due to the loss of directional solidification, resulting in the liquid is surrounded by solid fraction [23].

Microporosity is smaller in scale than macroporosity, with no more than 300 μm in diameter. This shrinkage defect can be classified as a closed shrinkage defect, according to Figure 15 [23].

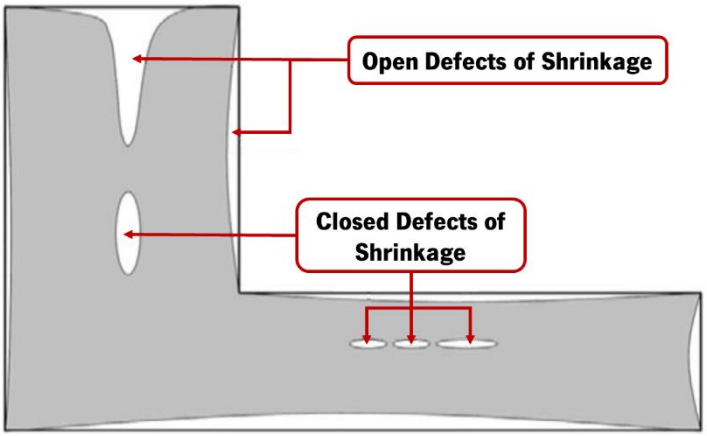

Figure 15: Closed and opened shrinkage defects.

Shrinkage porosities may appear due to:

i. Inappropriate design of a gating system that does not allow fast filling.
ii. Low mould resistance (more critical in sand than die moulds).
iii. Incorrect shrinkage pattern allowance regarding total part geometry.

Shrinkage allowance is a correction factor applied to the pattern to compensate for the contraction of the metal casting as it solidifies to room temperature. In this case, the pattern is intentionally made larger than the final desired dimensions, allowing solidification and cooling contraction of the part - sometimes, it may appear as Patternmaker's Shrinkage. Hence, full contraction is volumetric; however, it is typically represented linearly [4].

In Table 1, it is represented some typical shrinkage allowances for various alloys, like steel, aluminium, cast iron and brass. Note that these allowances should be used carefully (to predict natural casting shrinkage) because other factors impact on final dimensions of parts, like casting shape, section thickness, and mould stiffness [4].

Table 1: Typical shrinkage allowances for various alloys.

Alloy	Allowance	Approximate shrinkage [%]	Shrinkage allowance [mm/m]
Steel	1/64	1.6	15/7
Gray Cast Iron	1/100	1.0	8/4
Ductile Cast Iron	1/120	0.8	7/8
Aluminium	1/77	1.3	13/1
Brass	1/70	1.4	14/4

According to Figure 16, along yy-axis, casting has no restriction in terms of contraction, and, in this case, the design dimensions assigned should be larger, as shown in Table 1. Nonetheless, along xx-axis, casting shrinkage is constrained by the core used to make the central hole, implying that no (or negligible) shrinkage allowance is applied to this feature [4].

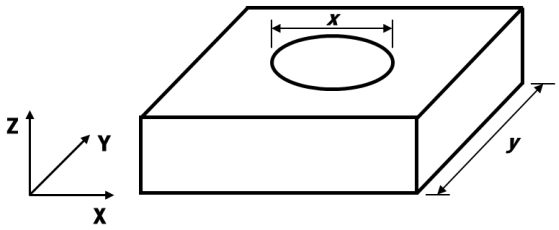

Figure 16: Casting shrinkage directions – along yy, the part can contract freely; however, along direction xx, part shrinkage is limited by the core.

Machine finish allowance refers to the compensation given to parts that require finish machining after casting, in which it is necessary to provide a small amount of metal. This type of allowance depends on many factors, such as [4]:

i. size and shape of the casting.
ii. casting surface roughness and surface defects.
iii. distortion and dimensional tolerances of casting.

2.4. CHAPTER REFERENCES

[1] CMQ, *Low Pressure Permanent Mold Process*, (Jul. 31, 2012). Accessed: Mar. 04, 2023. [Online Video]. Available: https://www.youtube.com/watch?v=s9T1RWhRrh0

[2] J. R. Davis, Davis & Associates, and W. W. Scott, *ASM Specialty Handbook - Copper and Copper Alloys*, 1st ed. 2001. [Online]. Available: www.asminternational.org

[3] "Low Pressure Die Casting: A Simple Guide to Understand the Process," *Rapid Direct*, Jun. 09, 2022. https://www.rapiddirect.com/blog/low-pressure-die-casting/ (accessed Mar. 08, 2023).

[4] R. M. Nunes, *ASM Handbook - Casting*, 4th ed., vol. 15. ASM International, 1998.

[5] R. Ye, "Die casting materials & when to use them," *3ERP*, Dec. 08, 2021. https://www.3erp.com/blog/die-casting-materials-when-to-use-them/ (accessed Mar. 04, 2023).

[6] J. R. Brown, *Foseco Non-Ferrous Foundryman's Handbook*, 11th ed.

[7] M. Fisher, "Low-Pressure vs. High-Pressure Die Casting," *McDonald Diecasting*, Nov. 04, 2019. https://www.mcdonald-diecasting.co.uk/die-cast-guides/low-pressure-vs-high-pressure-die-casting/2019/11/04/ (accessed Mar. 04, 2023).

[8] Kurtz Ersa Magazine, "Low-pressure vs. high-pressure die casting," *Kurtz Ersa Magazine*, 2016. https://www.ke-mag.com/issue-42/article/low-pressure-vs-high-pressure-die-casting.html (accessed Mar. 09, 2023).

[9] L. Zhejiang Wanfeng Technology Development Co., "Advantages of low pressure die casting (LPDC)," *Zhejiang Wanfeng Technology Development Co., Ltd*, Oct. 06, 2021. https://www.wanfengdiecasting.com/info/advantages-of-low-pressure-die-casting-lpdc-62264154.html (accessed Mar. 04, 2023).

[10] Dolin Casting, "13 Die Casting Defects and How to Avoid Them - Dolin Aluminum Casting," *Dolin Casting*, Aug. 28, 2020. https://www.dolincasting.com/13-die-casting-defects-and-how-to-avoid-them.html#Deformation (accessed Mar. 14, 2023).

[11] A. A. Luo, "Magnesium casting technology for structural applications," *Journal of Magnesium and Alloys*, vol. 1, no. 1, pp. 2–22, Mar. 2013, doi: 10.1016/j.jma.2013.02.002.

[12] Pyrotek, "Low-Pressure Die Casting Process," *Pyrotek*. https://www.pyrotek.com/primary-solutions/aluminium/foundry/metal-casting-foundry/low-pressure-die-casting/ (accessed Mar. 09, 2023).

[13] Y. Wang, S. Wu, L. Niu, X. Xue, J. Zhang, and X. Wenfeng, "Optimization of low-pressure die casting process parameters for reduction of shrinkage porosity in ZL205A alloy casting using Taguchi method," *Proc Inst Mech Eng B J Eng Manuf*, vol. 228, no. 11, pp. 1508–1514, Jan. 2014, doi: 10.1177/0954405414521065.

[14] Jonah, "Casting Misruns: What They Are And How To Fix Them," *Workshop Welding*, Nov. 03, 2019. https://workshopwelding.com/casting-misruns-what-they-are-and-how-to-fix-them/ (accessed Mar. 16, 2023).

[15] S. Wong, "21 Casting Defects and How to Prevent Them in Your Products," *In Touch Quality*, Sep. 18, 2018. https://www.intouch-quality.com/blog/21-casting-defects-and-how-to-prevent-them-in-your-products#Misruns (accessed Mar. 04, 2023).

[16] Campbell and John, *Complete Casting Handbook: Metal Casting Processes, Metallurgy, Techniques and Design*, 1st ed., vol. 1. 2011.

[17] "Different types of Castings defects," *Mechanical Engineering*. http://mechanicalinventions.blogspot.com/2012/11/different-types-of-castings-defects.html (accessed Mar. 07, 2023).

[18] Jonah, "What Is Cold Shut In Casting," *Workshop Welding*, Nov. 03, 2019. https://workshopwelding.com/what-is-cold-shut-in-casting/ (accessed Mar. 16, 2023).

[19] "Cold shuts," *Foundry Lexicon*. https://www.giessereilexikon.com/en/foundry-lexicon/Encyclopedia/show/cold-shuts-3854/?cHash=3106c915839dbe114f489d925281b7f0 (accessed Mar. 16, 2023).

[20] L. P. Raut and P. K. Tawele, "Warpage in casting: A Review," *International Journal of Advance Research in Engineering*, vol. 2, no. 4, pp. 2394–2444, Apr. 2015, [Online]. Available: https://www.researchgate.net/publication/275350480

[21] H. Nguyen, "Knowledge of Gating system: types of gating system, gating ratio, diagram," *Vietnam Cast Iron*, 2020. https://vietnamcastiron.com/gating-system/ (accessed Mar. 22, 2023).

[22] EUROPEAN STANDARD NORME EUROPÉENNE EUROPÄISCHE NORM, "Copper and copper alloys - Ingots and castings," *EUROPEAN STANDARD NORME EUROPÉENNE EUROPÄISCHE NORM*, pp. 1–76, Sep. 2017.

[23] B. Zhang, S. Cockcroft, D. Maijer, J. Zhu, and A. Phillion, "Casting Defects in Low-Pressure Die-Cast Aluminum Alloy Wheels," pp. 1–8, 2005.

[24] R. Radiša, N. Dučić, S. Manasijević, N. Marković, and Ž. Ćojbašić, "Casting improvement based on metaheuristic optimization and numerical simulation," *Facta Universitatis, Series: Mechanical Engineering*, vol. 15, no. 3, pp. 397–411, 2017, doi: 10.22190/FUME170505022R.

Chapter 3 - CASTING AND MOULD MATERIALS

3.1. CASTING ALLOY: ISO CUZN39PB1AL-B (ISO CB757S)

As it is well known, casting pure copper is particularly difficult because it is highly vulnerable to some casting defects such as surface cracking, (shrinkage) porosity and internal cavities. Therefore, Alloying improves the casting characteristics of copper, like zinc, beryllium, nickel, silicon, and many others. These elements are known as alloy elements [1].

Regarding the type of metal used to manufacture parts in LPDC, the company *Metalúrgica Central da Trofa, Lda.* use mostly copper alloys in this casting process. One of these is the copper alloy ISO CB757S, a copper-zinc alloy (or brass), which can contain about 40% Zn. According to (Davis) [2], there are six subcategories of cast brasses: red and leaded red; semi red and leaded semi-red; yellow and leaded yellow, in which the metal alloy ISO CuZn39Pb1Al-B is associated with; high-strength and leaded high-strength yellow (manganese bronzes); silicon brasses and bronzes; copper-bismuth (Cu-Bi); copper selenium bismuth (Cu-Se-Bi) brasses.

Also, copper-based casting alloys can be split into three main groups as per solidification ranges are concerned [2]:

(a) Group I alloys:

These alloys have a relatively small freezing range, meaning the liquidus and solidus temperatures are far apart at approximately 50°C. Note that yellow and yellow brasses belong to this group, and so is ISO CB757S, as is the case of brasses, manganese and aluminium bronzes, nickel bronzes, etc.

(b) Group II alloys:

These alloys have a freezing range of 50°C to 110°C.

(c) Group III alloys:

At last, alloys belonging to Group III have a freezing range of more than 110°C, which, in some cases, can be higher than 170°C.

Note: As is expected in any cast component, the microstructure consists of dendritic structures, preferably aligned. In alloys with a lower cooling rate (i.e., longer solidification time), such as brasses from Group II and III, dendritic structures are denser, and the microstructure is coarser. On the other hand, increasing the cooling rate (i.e., decreasing solidification time), like the brasses from Group I, makes the microstructure finer because dendritic arm spacing, DAS, is smaller.

Hence, ISO CuZn39Pb1Al-B presents the following appealing aspects [2]:

i. high corrosion resistance.
ii. excellent castability.
iii. reasonably low cost.
iv. good machinability, especially in finishing operations.

3.1.1. CHEMICAL COMPOSITION

Like many other metal alloys, ISO CB757S is well known for solidifying under dendrites structures; despite that, microsegregation and microporosity in these ingots are low because they solidify within small temperature ranges.

The ISO standards set some limits on the percentage of chemical elements present in each alloy for better classification of metals. Therefore, for ISO CB757S its chemical composition limits are presented in Table 2.

Table 2: Chemical composition limits, in wt%, for the alloy ISO CuZn39Pb1Al-B.

Chemical element	Cu	Pb	Sn	Zn	Fe	Ni	Al	Mn	Si
Min. [wt%]	58.0	0.2	-	32.0	-	-	0.3	-	-
Max. [wt%]	63.0	1.5	0.5	40.0	0.3	0.2	0.9	0.05	0.05

To approximate the casting software results to what is expected, it is necessary first to study and obtain the chemical composition of the brass used in the company, then enter it into the program. Therefore, the company tested a bar for its chemical composition, as shown in Table 3.

Table 3: Real chemical composition, in wt%, for the brass.

Chemical element	Cu	Pb	Sn	Zn	Fe	Ni	Al	Mn	Si
Percentage cont. [wt%]	60	0.9	0.15	38	0.1	0.1	0.78	0	0.01

According to Table 3, the percentage of zinc, Zn, is below 40 wt.%, which confirms that ISO CB757S is a yellow brass, as predicted before.

When the temperature of the metal is close to its melting point, zinc, Zn, tends to vaporise, so founders add aluminium, Al, to increase fluidity and prevent zinc vaporisation. However, aluminium should not be added indiscriminately: preferably, its percentage should be between 0.15% and 0.35%. Above these limits, the likelihood of shrinkage porosity during solidification increases and risers are required [1].

3.1.2. PHASE DIAGRAM AND MICROSTRUCTURE

With the chemical composition of the alloy (Table 3), it is possible to obtain the phase diagram of the copper alloy, which is essential to determine some characteristics that are important for casting simulation, in general.

Phase diagrams are crucial to describe the expected behaviour of the alloy microstructure as a function of temperature – the chemical composition acts as an input value. Note that brasses are Cu-Zn alloys; therefore, the phase diagrams depend only on the percentage of zinc.

Hence, analysing this type of graph makes it possible to assess which phases are thermodynamically stable in an alloy and can be expected during solidification. In Figure 17, it is presented the copper-zinc binary phase diagram.

In terms of microstructure, copper-zinc alloys can be divided into four main categories, according to the phases displayed, described as follows:

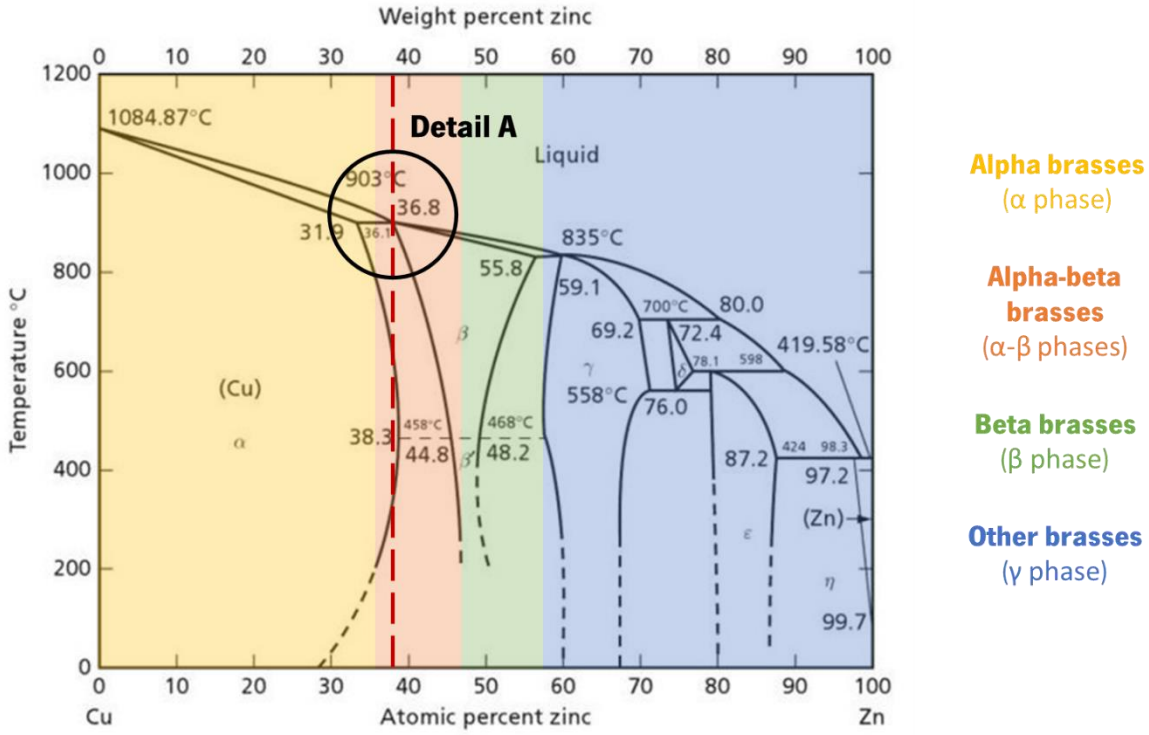

Figure 17: Cu-Zn binary phase diagram, with the main types of brasses present, as well as a vertical line representing the zinc composition.

(a) Alpha brasses (α phase):

Figure 17 shows alpha brasses have a zinc concentration of approximately 30 wt. %, at equilibrium, and a homogeneous phase (alpha) is present on the micrographs after solidification.

As the metal cools, its temperature drops and the alpha phase precipitates first (Figure 18), changing the composition of the remaining liquid. Also, if the zinc composition is higher, other phases may form on cooling, such as the beta phase and dendritic growth, resulting in poorer properties [5–7].

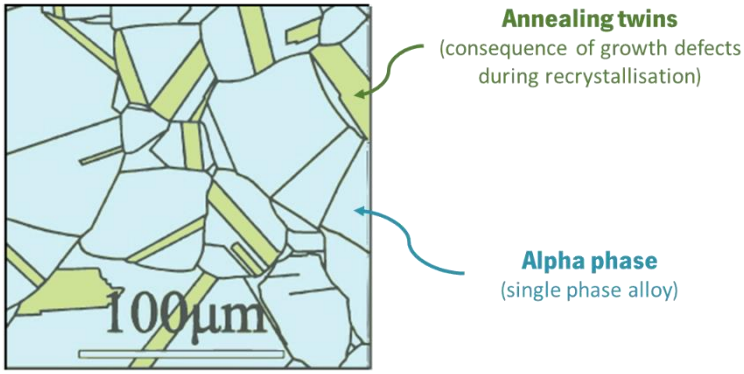

Figure 18: Schematic representation of the microstructure expected from an Alpha brass.

(b) Alpha-Beta brasses (α-β phases):

These alloys have zinc concentrations between 30 wt. % and 45 wt. % (Figure 17), at equilibrium, forming two phases (alpha and beta) after cooling.

As the metal cools, the alpha phase precipitates first (Figure 17), and according to (Cambridge) [7], it may form a Widmanstätten structure, in which the alpha phase solidifies under plates along preferential growth directions. In this case, the beta phase surrounds the alpha dendrites, as shown in Figure 19.

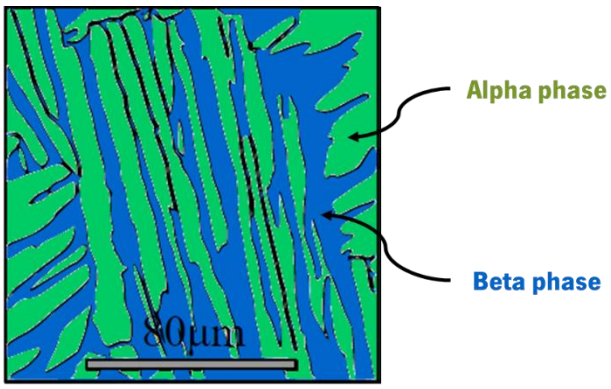

Figure 19: Schematic representation of the microstructure expected from an Alpha-Beta brass.

(c) Beta brasses (β phase):

Beta brasses are not as common as alpha and alpha-beta brasses, whose zinc composition can range from about 45 wt. % to almost 60 wt. % (Figure 17), at equilibrium. According to the Cu-Zn phase diagram (Figure 17), in this range, only a single homogenous phase (beta) is expected in the microstructure, which is harder and stronger than the previous brasses, as shown in Figure 20 [9].

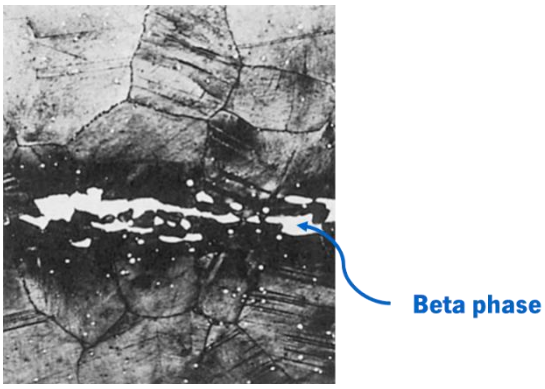

Figure 20: Micrography of Cu-Zn alloy with beta phase.

(d) Gamma brasses (γ phase):

At last, alloys with a zinc composition above about 55 wt. % (Figure 17), at equilibrium, are classified as Gamma brasses since the main phase present is, as expected, the gamma phase. As its crystal structure is particularly brittle, this type of brass is rare in general engineering applications [5].

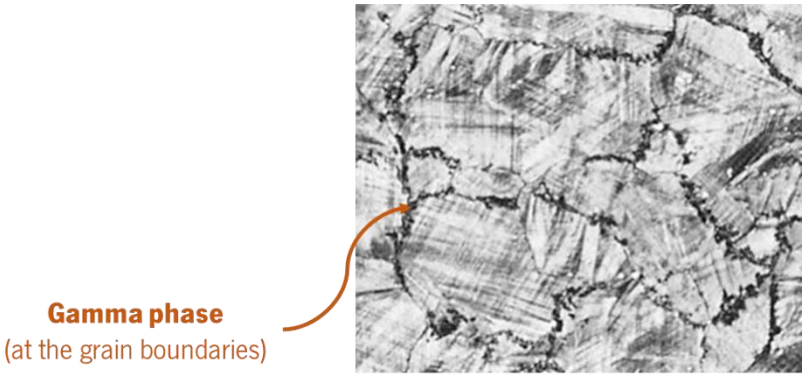

Figure 21: Micrography of Cu-Zn alloy with gamma phase.

3.1.3. THERMAL PROPERTIES

From the phase diagram in Figure 17, it is also possible to plot another chart. This cooling curve can be quite helpful in depicting the standard solidification of materials and, therefore, calculating thermal properties. Figure 22 shows a classic cooling curve for a pure or eutectic metal with some key terms, as stated by [10]:

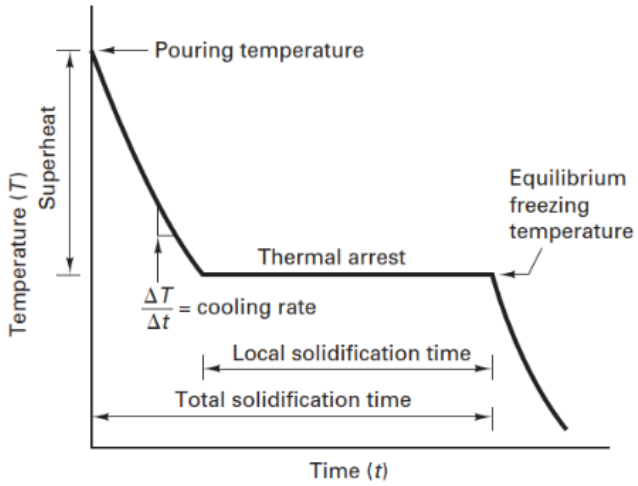

Figure 22: Cooling curve for a pure or eutectic metal.

i. **Pouring temperature**: the liquid metal's temperature when inserted into the mould.

ii. **Superheat**: temperature range between the material's pouring and freezing temperatures.

iii. **Cooling rate**: rate representing liquid or solid metal cooling. It can be considered at any point in the curve, corresponding to its slope.

iv. **Thermal arrest**: region that occurs during solidification, particularly for materials with a fixed melting point, at a precise temperature.

However, solidification will occur at a range of temperatures – solidus and liquidus. In general terms, the **liquidus temperature** is the temperature above which only the liquid phase exists in equilibrium (i.e., below this temperature, melt coexists with solidified crystals). On the other hand, the **solidus temperature** is the temperature below which one phase exists in equilibrium - quantifies the temperature at which the metal becomes completely solid according to (Madhu) [11]. Also, the area between these two temperatures (liquidus and solidus) is known as the **freezing range**.

It is important to note that the shape of the cooling curve will depend on the type of alloy used, the nature of its nucleation process and the rate and means of heat removal from the mould.

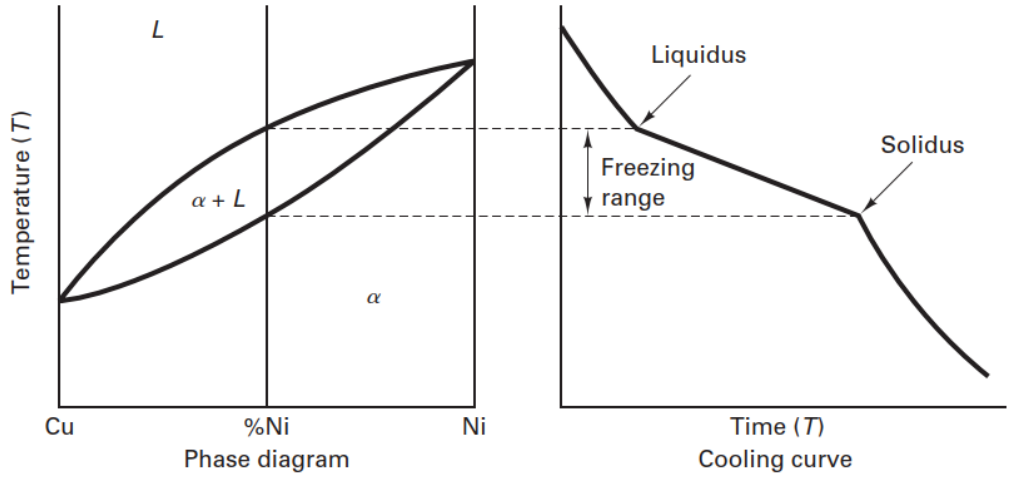

Figure 23: Phase diagram and cooling curve for hyper/hypoeutectic alloys.

Solidus and Liquidus temperatures can be determined from a phase diagram by plotting a vertical line corresponding to the zinc composition, as shown in Figure 17. Therefore, the liquidus temperature is the intersection point between the liquid transition and the vertical; the solidus temperature is the intersection between the solid transition and the vertical line, as shown in Detail A of Figure 17. This can be also seen in Figure 24 (a).

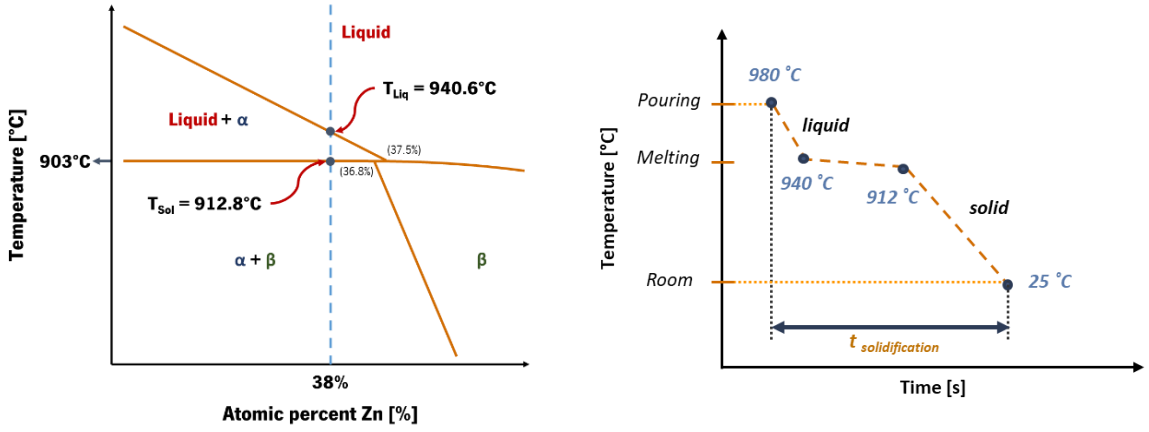

(a) (b)

Figure 24: (a) Schematic representation of the Detail A, previously mentioned; (b) Cooling curve for copper-zinc alloy ISO CB757S.

So, according to Table 3, for ISO CuZn39Pb1Al-B alloy, the zinc composition is approximately 38% and plotting this value on the phase diagram (Figure 24) gives the following thermal properties, represented in Table 4:

Table 4: Thermal properties of the alloy ISO CB757S.

Liquidus Temperature, T_{Liq} [°C]	940.6
Solidus Temperature, T_{Sol} [°C]	912.8
Thermal conductivity, k [W/m·K]	83.9

3.1.4. MELT TREATMENT

The quality of castings depends on many factors, including the design of the components; the casting process and its variables; the quality of raw materials, and the proper application of melt treatment before metal pouring into the mould [13].

Depending on the alloy in question, the melt treatment of copper ingots comprises multiple processes, as stated by (Davis) [2], such as **degassing**, **deoxidation**, **grain refining** and filtration.

The solubility of hydrogen decreases as soon as the temperature also drops. For this reason, it is necessary to remove hydrogen from the furnace or ladle before (preferably) or during the metal pouring. Otherwise, some defects, such as gas porosities, may come up.

According to Figure 6, like aluminium and magnesium, the hydrogen solubility in copper alloys is much lower at temperatures below the melting point (about 1.5 mL/100 g) and increases to almost double at temperatures above the melting point of the ingot, i.e., 1100°C. As a result, gas porosity and other related defects (excessive shrinkage, blisters, and pinholes) may occur if hydrogen remains in the metal during solidification [2].

As with aluminium and magnesium alloys, there are several possible sources of hydrogen in copper melts, including the furnace atmosphere, flux introduction, external components (ladles and other parts used in pouring and melt treatment) and reactions mould/metal interface [2].

According to (Davis) [2], among these causes, fluxes and mould-to-metal reactions are the ones that deserve more attention for being the most common ones. In the first case, most salt fluxes used in copper alloys are hygroscopic. This means that hydrogen from steam water can easily be picked up and incorporated into the melt by water decomposition, causing bubbles and gas porosities after cooling and solidification. The other characteristic (mould-to-metal reactions) is that if there is too much turbulence in the metal, air can be drawn in, causing air entrainment. For this reason, this air must be removed, especially before solidification begins; otherwise, porosity will occur for the reasons mentioned above [2].

Thus, it is crucial to understand that establishing a proper casting procedure and designing the casting system correctly will minimise the presence of hydrogen in the melt, resulting in better-quality products.

One of the most commonly used **degassing methods** is the Oxidation-reduction process, in which oxygen is introduced into the molten metal. In this case, oxygen reacts with copper to form cuprous oxide, Cu_2O, which is, therefore, inserted into the furnace, where it reacts with hydrogen, H, to produce water steam and copper, as shown in Equation (3.1):

$$2H + Cu_2O \rightarrow H_2O + 2Cu \tag{3.1}$$

When cuprous oxide is introduced into the melt, it decomposes, and hydrogen binds to oxygen because of the high affinity between these two elements. Figure 25 shows the solubility of hydrogen and oxygen in copper: for higher percentages of oxygen in the melt, the solubility of hydrogen decreases to values close to 0. Therefore, excess of oxygen can be added to ensure all hydrogen links to it. Then, a deoxidation process is applied to remove all the oxygen (in the form of water vapour).

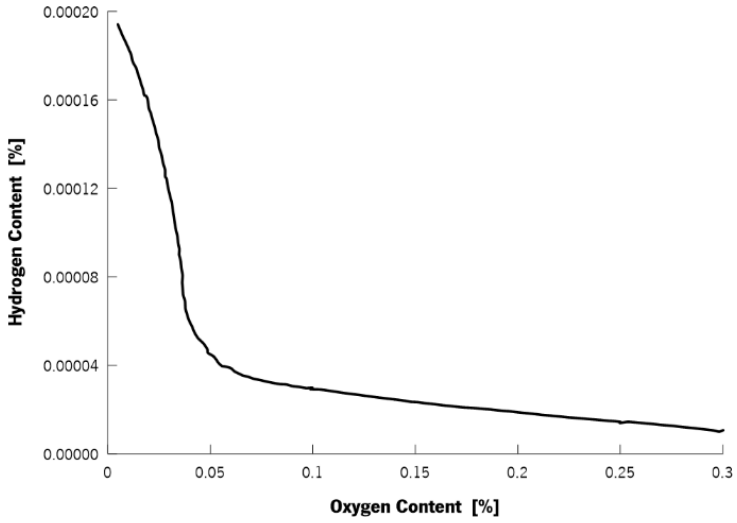

Figure 25: Graph representing the solubility of hydrogen and oxygen in copper alloys.

Alternatively, although the oxidation-deoxidation process is more frequently used for brasses, it is also feasible to use a Foundry Degassing Unit (FDU), presented in Figure 26, which is more used for aluminium alloys. The system has an impeller and motor to drive and mix inert gas (e.g., argon or nitrogen) into the molten metal. The rotation of the blades creates turbulence in the melt, allowing the inert gas bubbles to disperse, which increases the solubility of hydrogen in it. Ultimately, hydrogen is released into the atmosphere due to its lower density when compared to the alloy [14].

Although this technique is very effective in melt treatment, it is not widely applied – the oxidation-deoxidation process is preferable.

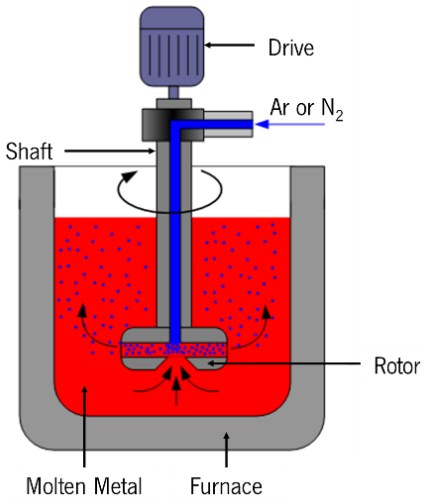

Figure 26: Schematic representation of a Foundry Degassing Unit, FDU.

Apart from hydrogen, oxygen is also a complex particle in copper alloys casting. Although it has no effect in the absence of hydrogen (because of oxygen's low solubility in copper), when hydrogen is present, it forms a fully miscible phase with the melt, leading to defects after solidification and cooling. For that reason, the deoxidation process is typically used after degassing the ingot.

Note: As mentioned before, this process is usually used together with degassing, especially when the oxidation-deoxidation process is chosen for degassing.

According to Equation (3.1), oxygen reacts with copper to form cuprous oxide, which has a high solubility in the liquid state. If this oxide is not removed, it will cause discontinuities in the casting, leading to reduced mechanical strength and porosity. In addition, **deoxidation of alloys** improves their fluidity and, therefore, their castability - components of excellent quality.

Phosphorus deoxidation is the most commonly used process because it is economical and leads to fewer problems. Phosphorous is added through master alloys - base metal material used to control or improve one or two properties – with a composition of 15%. Phosphorus reacts with copper, dissolving oxygen and forming cuprous phosphate ($Cu_2O \cdot P_2O_5$), according to the following equation:

$$2P + 4Cu + 7O \rightarrow 2Cu_2O \cdot P_2O_5 \qquad (3.2)$$

Due to its lower density, the cuprous phosphate floats then to the surface of the metal and is easily removed. This process is ubiquitous for tin bronzes, red brasses and leaded bronzes; however, it is not recommended for high-conductivity copper alloys due to the deterioration of electrical conductivity in contact with phosphorus.

Deoxidation can also be done using boron or lithium instead of phosphorus. The first case is similar to the phosphorus process. However, the reaction produces copper borate ($Cu_2O \cdot B_2O_3$) contrary to

cuprous phosphate, as mentioned in Equation (3.2). The second case simultaneously eliminates oxygen and hydrogen, which is more effective than phosphorous. However, lithium is more expensive than phosphorous, which is why deoxidation with lithium is often dismissed [2, 14, 16].

It is important to note that **yellow brasses** (ISO CB757S), silicon bronzes, manganese bronzes and aluminium bronzes do not require a deoxidation process as their alloying constituents usually absorb oxygen [2].

This step is not always mandatory for **grain refinement**, as it can be achieved by improving casting techniques. Typically, a metal with a finer grain structure is obtained by combining a low pouring temperature with a high cooling rate. This results in grains that are smaller and more ordered. However, some alloys contain aluminium or zinc which promote grain nucleation. Alternatively, other additives may also be added – lithium, iron, lead, or bismuth [14].

3.2. MOULD MATERIAL: AISI H13

In addition to analysing the copper alloy utilised in the production of the bathtub mixer, it is equally crucial to address the material composition of the dies. This information is essential for simulating the Low-Pressure Die Casting process in the QuikCAST software. The die material significantly impacts temperature distribution within the dies and will be a crucial factor in one of the simulations conducted (as detailed in Chapter 4.6.1).

Consequently, this chapter provides comprehensive insights into the key aspects concerning the tool employed.

3.2.1. CHEMICAL COMPOSITION

As illustrated by the Copper alloy ISO CuZn39Pb1Al-B, a critical aspect concerning the die tool is its chemical composition. The composition is one crucial aspect because of its application in casting simulation, including HPDC and LPDC processes. Therefore, Table 5 presents the chemical composition of the die tool used AISI H13.

Table 5: Chemical composition, in wt%, of the die tool.

Chemical element	Cr	Mo	Si	V	C	Mn	Ni	Cu
Percentage cont. [wt%]	5	1.4	1	1	0.4	0.4	0.3	0.25

As previously mentioned, the chemical composition of the H13 tool is incorporated into the software to simulate the thermal cycling of the dies. This step is crucial in assessing the tool's lifespan, especially considering that copper alloys are typically casted at elevated temperatures, often exceeding 900°C [2].

3.2.2. THERMAL PROPERTIES

In addition to the tool material's chemical composition, incorporating the thermal properties into the software is crucial. These properties are essential for constructing the thermal map of the dies in the thermal die cycling simulation. It is important to emphasize that these properties vary with temperature. Figure 27 displays, respectively, the density, thermal conductivity, and specific heat properties used to define the thermal behaviour of the AISI H13 tool material.

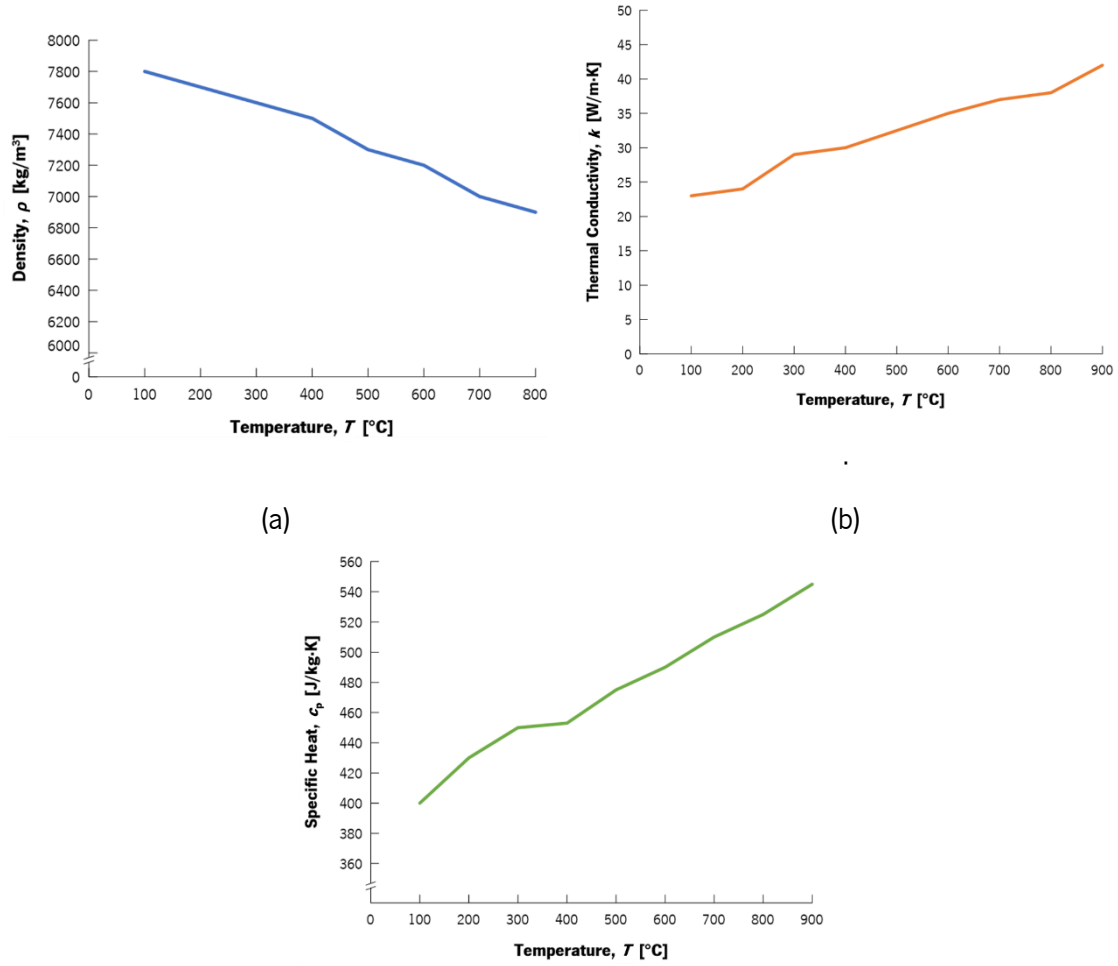

Figure 27: Thermal properties of the die's material – (a) Density, (b) Thermal Conductivity and (c) Specific Heat.

3.3. CHAPTER REFERENCES

[1] Total Materia Article, "Copper and Copper Alloys Casting Problems," *Total Materia Article*, Dec. 2002. https://www.totalmateria.com/page.aspx?ID=CheckArticle&site=ktn&LN=CZ&NM=64 (accessed Apr. 02, 2023).

[2] J. R. Davis, Davis & Associates, and W. W. Scott, *ASM Specialty Handbook - Copper and Copper Alloys*, 1st ed. 2001. [Online]. Available: www.asminternational.org

[3] Copper Development Association Inc., "C85700 Alloy ," *Copper Development Association Inc.* https://alloys.copper.org/alloy/C85700 (accessed Apr. 02, 2023).

[4] EUROPEAN STANDARD NORME EUROPÉENNE EUROPÄISCHE NORM, "Copper and copper alloys - Ingots and castings," *EUROPEAN STANDARD NORME EUROPÉENNE EUROPÄISCHE NORM*, pp. 1–76, Sep. 2017.

[5] MECHTECH GURU, "Brasses," *MECHTECH GURU*, Aug. 16, 2020. https://www.mechtechguru.com/2020/08/brasses-alpha-phase-beta-phase-gamma.html (accessed Apr. 07, 2023).

[6] Copper Development Association Inc., "Brasses." https://www.copper.org/resources/properties/microstructure/brasses.html (accessed Apr. 10, 2023).

[7] University of Cambridge, "Copper based alloys," *University of Cambridge*. https://www.doitpoms.ac.uk/tlplib/microstructural_exam/cualloys.php (accessed Apr. 07, 2023).

[8] T. Sourmail, G. H. Opdenacker, and H. K. D. H. Bhadeshia, "Annealing Twins," *University of Cambridge*. https://www.phase-trans.msm.cam.ac.uk/abstracts/annealing.twin.html (accessed Apr. 07, 2023).

[9] T. Bell, "Learn About the Different Brass Types," Sep. 10, 2019. https://www.thoughtco.com/brass-types-3959219 (accessed Apr. 10, 2023).

[10] J. T. Black and R. A. Kohser, *Materials & Processes in Manufacturing*, 10th ed., vol. 1. 2007.

[11] Madhu, "What is the Difference Between Solidus and Liquidus," Nov. 10, 2021. https://www.differencebetween.com/what-is-the-difference-between-solidus-and-liquidus/ (accessed May 05, 2023).

[12] University of Cambridge, "Interpretation of cooling curves," *University of Cambridge*. https://www.doitpoms.ac.uk/tlplib/phase-diagrams/cooling.php (accessed May 08, 2023).

[13] New-Era Technologies, "Factors Which Affect Quality of Casting Parts," *New-Era Technologies*, Jul. 24, 2018. https://www.hneco.com/Article-show-39-factors_which_affect_quality_of_casting_parts.html (accessed May 16, 2023).

[14] D. Kopeliovich, "Treatment of molten copper alloys," *SubsTech*, Apr. 06, 2013. https://www.substech.com/dokuwiki/doku.php?id=treatment_of_molten_copper_alloys (accessed May 21, 2023).

[15] D. Kopeliovich, "Degassing treatment of molten aluminum alloys," *SubsTech*, Jul. 28, 2012. https://www.substech.com/dokuwiki/doku.php?id=degassing_treatment_of_molten_aluminum_alloys (accessed May 16, 2023).

[16] KBM Affilips, "Master alloys: our spice rack for the metal industry," *KBM Affilips*. https://www.kbmaffilips.com/what-is-a-master-alloy/ (accessed May 21, 2023).

[17] Ventura Steels, "AISI H13 / DIN 2344 / H13 Steel," *Ventura Steels*. https://venturasteels.com/din-2344-aisi-h13-steel/#:~:text=AISI%20H13%20steel%20consists%20of%20chromium%2C%20molybdenum%20and,known%20for%20its%20high%20hardenability%20and%20great%20toughness. (accessed May 10, 2023).

[18] AZOM Materials, "H13 Tool Steel - Chromium Hot-Work Steels," *AZOM Materials*, Jul. 10, 2013. https://www.azom.com/article.aspx?ArticleID=9107 (accessed May 10, 2023).

[19] M. Narvan, A. Ghasemi, E. Fereiduni, S. Kendrish, and M. Elbestawi, "Part deflection and residual stresses in laser powder bed fusion of H13 tool steel," *Mater Des*, vol. 204, Jun. 2021, doi: 10.1016/j.matdes.2021.109659.

[20] D. Klobčar, J. Tušek, and B. Taljat, "Thermal fatigue of materials for die-casting tooling," *Materials Science and Engineering: A*, vol. 472, no. 1–2, pp. 198–207, Jan. 2008, doi: 10.1016/j.msea.2007.03.025.

Chapter 4 - CASTING SIMULATION

Foundries are using simulation much more these days to increase production efficiency. Simulation is an essential engineering tool as it can reduce die design time and significantly reduce costs by replacing expensive and time-consuming testing. The accuracy of the results depends on the computer's potential, but the quality depends on the tooling engineer's knowledge. If the process parameters are not similar to those used in reality (or are even wrong), the simulation results will also be inaccurate, leading to faulty conclusions.

Simulation helps to anticipate many features, such as predicting the flow pattern; the last areas to be filled; whether there is air entrapment in the mould or not; shrinkage porosity and its location; and many others. Note that simulations may be repeated several times to optimise the casting process (including the gating system and process parameters), which is the same as trial and error but less expensive and less time-consuming [1–2].

In general, a simulation flowchart could be represented as Figure 28, with the first step being the design of the cast part. This is followed by patternmaking of the part, core design and process parameter identification. This stage (process parameter identification) is where the engineer decides on the pouring and dies temperatures, the filling pressure applied (in terms of Low-Pressure Die Casting simulation), and

the most critical aspects of the casting process. The simulation is set and runs only after this, and the results are analysed. In this step, the engineer must understand whether the defects identified by the software are critical or not: if **yes**, the next step is to know their source and act accordingly; if **no** (meaning that the defects will not affect the component performance after produced), then the simulation is complete, and the die final design can be finalised and given to the tooling designer to be built [1, 3].

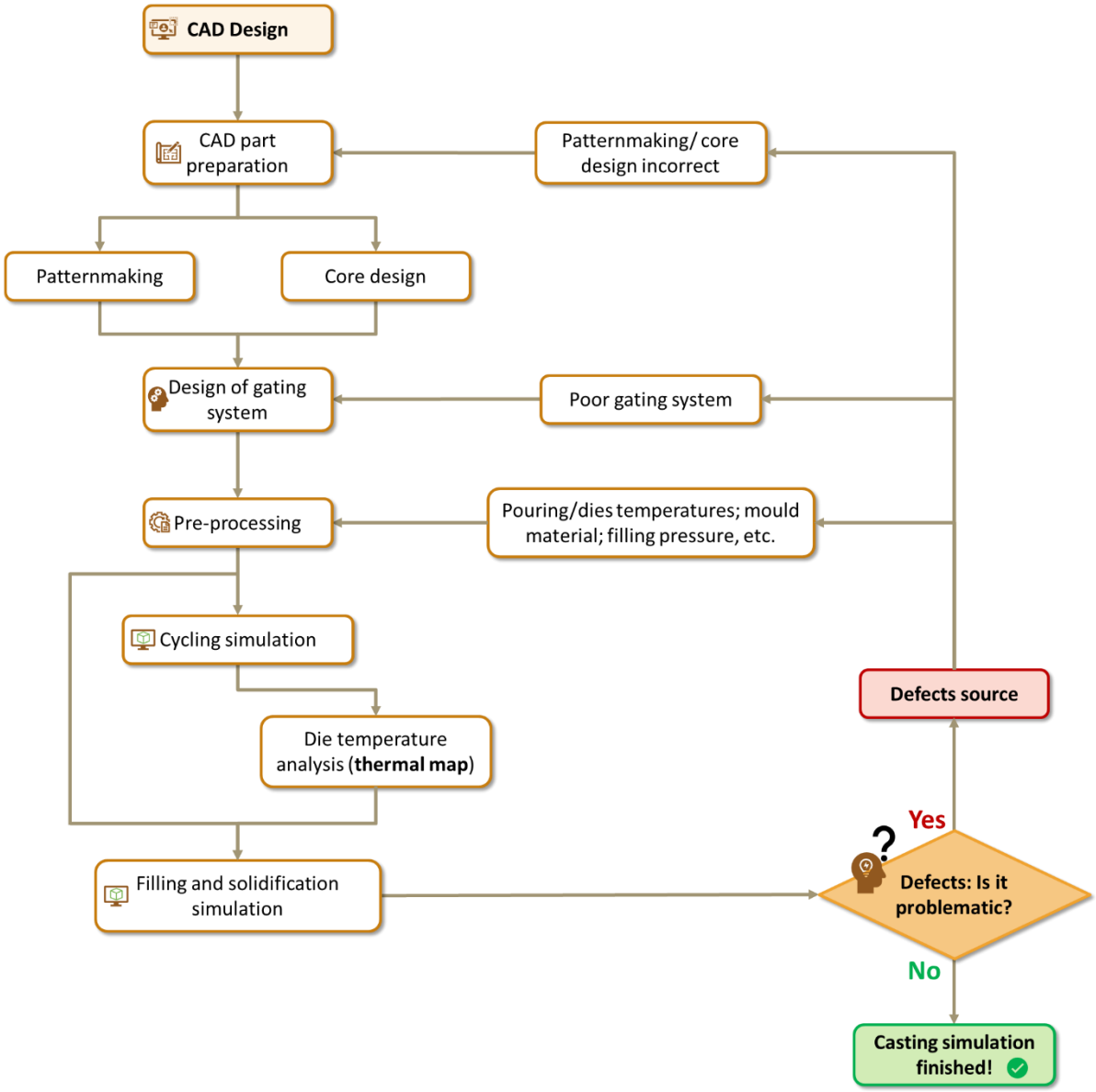

Figure 28: Typical casting part development.

4.1. NUMERICAL MODEL

ProCAST and QuikCAST are advanced casting simulation software marketed by the ESI Group. These software provide powerful tools for analysing and predicting defects in casting processes, as well as aspects related with filling and metal velocity. While both packages share standard features and functionalities, they differ in the discretization method employed, significantly influencing the simulation results' accuracy and reliability.

4.1.1. SIMULATION OF CASTING SOLIDIFICATION

The simulation of casting solidification encompasses various aspects, including **heat transfer phenomena** between the casting, dies, and the surrounding environment, which involves heat conduction between the metal and the mould, radiation exchange between the metal and the environment, and natural convection effects; release of **latent heat** during solidification of the casting; **temperature field** within the liquid-state; **formation of shrinkage porosity** resulting from the natural contraction of the casting [4].

Regarding casting solidification simulation, ProCAST uses the Finite Element Method (FEM), while QuikCAST uses the Finite Differences Method (FDM), which is simpler and requires less computing power.

The Finite Differences Method (FDM) is a simple and easily convergent technique for solving complex differential equations that are difficult to solve analytically. The domain is discretised into rectangular elements identified by discrete points and nodes. The Finite Element Method (FEM) is another technique very similar to the previous one, where the domain is also divided into elements and nodes, as shown in Figure 29 [4–5].

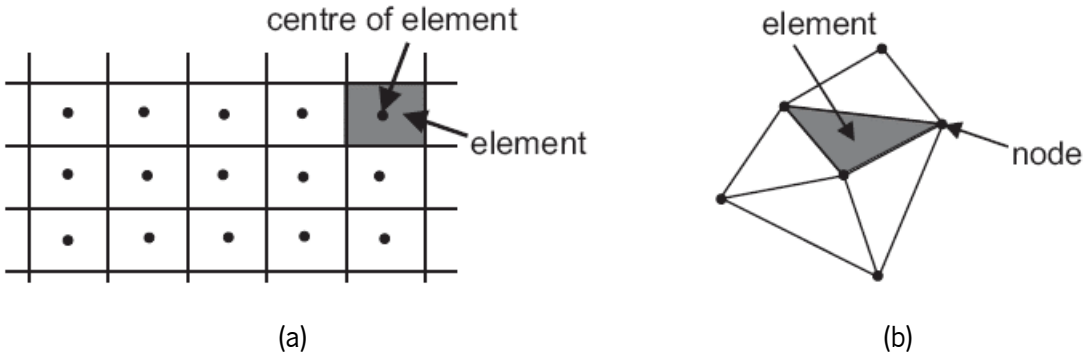

Figure 29: (a) Finite Difference Method and (b) Finite Element Method.

In FDM, an infinitesimal rectangular is placed over the boundary of the elements, and the results are obtained by averaging between each element (i.e., each element has a “weight” in the result: the

more significant the "weight", the greater its influence). This method is typically used in casting simulation to simulate temperature and flow field due to its simple mesh generation and good convergence [4–5].

On the contrary, the domain created by FEM uses an integral of the volume of each element to determine the results. The main advantage of FEM is the flexibility of its mesh method, which can quickly adapt to different boundary conditions. Therefore, this method is employed to determine the stress field of cast parts [4–5].

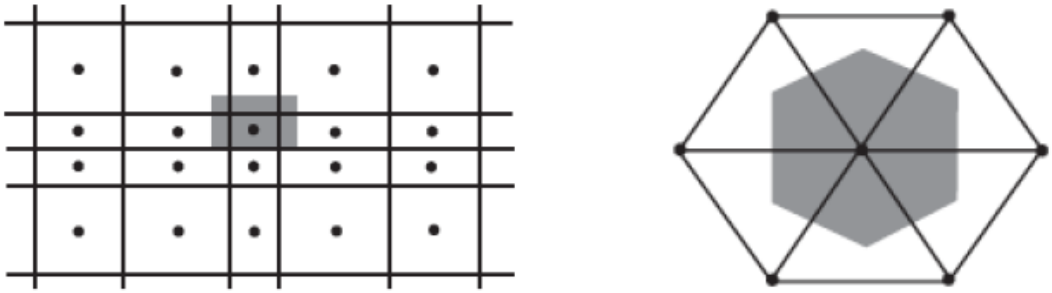

(a) (b)

Figure 30: Approximation method of (a) FDM and (b) FEM.

The workflow for casting simulation is very similar to any other simulation, starting with pre-processing, with the definition of process parameters; then running the simulation; and, finally, post-processing, with the analysis of results.

4.1.2. SIMULATION OF CASTING FILLING

During the casting filling process, the liquid metal undergoes gradual cooling, accompanied by various physical and chemical changes, such as oxidation, heat transfer and impact between the liquid metal and the mould. These factors contribute to casting defects, including air entrainment and shrinkage porosity [4].

As the liquid metal flows into the mould, it behaves as an unsteady flow of incompressible viscous liquid with a free surface. Therefore, it is crucial to accurately model and solve the flow and temperature changes during this process. This is typically achieved by solving the Navier-Stokes equations (or N-S equations): the Equation of Continuity (or Mass Conservation Equation), the Momentum Conservation Equation, and the Energy Equation. The Volume-of-Fluid equation, VOF, also describes the changing free surface [4, 6–7].

The principal challenge in the filling process lies in simultaneously solving the flow and pressure unknown values, in the N-S equations, which are inherently complex. Moreover, the temperature variation further complicates the calculations. The iterative calculation of velocity and pressure is required but can

be computationally intensive. It is important to note that sometimes the iterative results may deviate, leading to convergence issues in the simulation.

The **Equation of Continuity** can be represented as follows [6]:

$$\frac{\partial \rho}{\partial t} + \frac{\partial(\rho u)}{\partial x} + \frac{\partial(\rho v)}{\partial y} + \frac{\partial(\rho w)}{\partial z} = 0 \tag{4.1}$$

where ρ is the density of the liquid metal, represented as $[\mathrm{kg/m^3}]$; t is time, in [s]; u is the velocity of the molten metal along X axis, in [m/s]; v is the velocity of the molten metal along Y axis, in [m/s]; w is the velocity of the molten metal along Z axis, in [m/s].

The **Navier-Stokes Equations** form a set of mathematical equations that establish the relationships between a flowing fluid's velocity, pressure, temperature, and density for an incompressible fluid. These equations are fundamental in fluid dynamics for analysing the behaviour of fluid motion and understanding various physical properties. Also, they can be described in a three-dimensional domain – Equations (4.2), (4.3), and (4.4); however, since QuikCAST uses FDM, only Equations (4.2) and (4.3) are used, according to (Hall).

$$\rho\left(\frac{\partial u}{\partial t} + u\frac{\partial u}{\partial x} + v\frac{\partial u}{\partial y} + w\frac{\partial u}{\partial z}\right) = -\frac{\partial p}{\partial x} + \rho g_x + \mu\nabla^2 u \tag{4.2}$$

$$\rho\left(\frac{\partial v}{\partial t} + u\frac{\partial v}{\partial x} + v\frac{\partial v}{\partial y} + w\frac{\partial v}{\partial z}\right) = -\frac{\partial p}{\partial y} + \rho g_y + \mu\nabla^2 v \tag{4.3}$$

$$\rho\left(\frac{\partial w}{\partial t} + u\frac{\partial w}{\partial x} + v\frac{\partial w}{\partial y} + w\frac{\partial w}{\partial z}\right) = -\frac{\partial p}{\partial z} + \rho g_z + \mu\nabla^2 w \tag{4.4}$$

in which g_x, g_y and g_z are the gravitational accelerations along x, y and z axis in $[\mathrm{m/s^2}]$; μ is the kinematic viscosity, expressed as $[\mathrm{m^2/s}]$; ∇ corresponds to the Laplace operator.

Another Navier-Stokes Equation is the **Energy Conservation Equation**, represented in Equation (4.5):

$$\frac{\partial(\rho c_P T)}{\partial t} + \frac{\partial(\rho c_P u T)}{\partial x} + \frac{\partial(\rho c_P v T)}{\partial y} + \frac{\partial(\rho c_P w T)}{\partial z} = \frac{\partial\left(k\frac{\partial T}{\partial x}\right)}{\partial x} + \frac{\partial\left(k\frac{\partial T}{\partial y}\right)}{\partial y} + \frac{\partial\left(k\frac{\partial T}{\partial z}\right)}{\partial z} + S \tag{4.5}$$

where, c_P corresponds to the specific heat capacity at constant pressure, expressed as $[\mathrm{J\ kg^{-1}\ K}]$; k is the thermal conductivity, in $[\mathrm{W/m^2 \cdot K}]$; T is the temperature along the different directions x, y and z, in [ºC]; S is the source term, in [W].

Several algorithms can be applied to solve the previous equations; however, ProCAST and QuikCAST implement the SOLA-VOF model. In this computation, the SOLA solver is employed to solve the momentum and continuity equations, while the VOF model is used to handle the free surface calculus.

Hence, the **Volume of Fluid** (VOF) involves defining a function, $F(x, y, t)$, according to the Equation (4.6):

$$\frac{\partial F}{\partial t} + u\frac{\partial F}{\partial x} + v\frac{\partial F}{\partial y} + w\frac{\partial F}{\partial z} = 0 \quad (4.6)$$

The function F is assigned to every cell within the computational grid. F is set to 1 in regions full of fluid, while in regions without fluid is set to 0. Any intermediate value between 0 and 1 indicates the presence of a free surface. By determining the normal vector and the corresponding F value of each cell, it is possible to approximate the shape of the free surface with a line.

4.2. Study Case on Bathtub Mixer

The experimental work of this thesis consisted of designing the gating system for producing a bath mixer, using casting simulation to predict and prevent defects that might occur. Hence, the QuikCAST software, developed by the ESI Group, is used to determine the numerical results, which are later compared with experimental data.

The component proposed for the study (Figure 31) belongs to the company *Metalúrgica Central da Trofa, Lda.*, and is a bath mixer body typically used in bathroom showers.

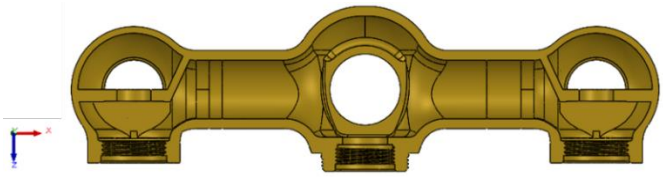

(a)

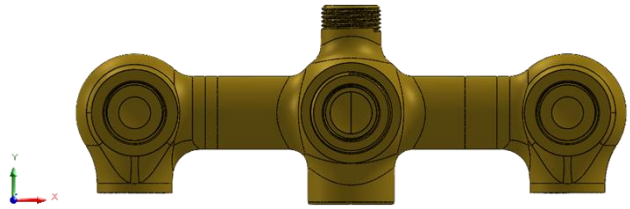

(b)

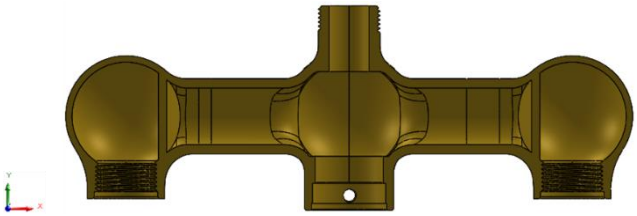

(c)

Figure 31: Bath mixer body proposed for study – (a) cut of the upper view, (b) front view and (c) cut of the front view.

The body mixer is docked to various components to assemble the shower system, such as hot and cold-water handles, taps, faucet valves, O'rings, etc. For this reason, it is necessary to ensure that the mixer meets all the tolerances specified in the drawings. Otherwise, the coupling will not be achieved. Figure 32 is a schematic diagram of the shower system assembly.

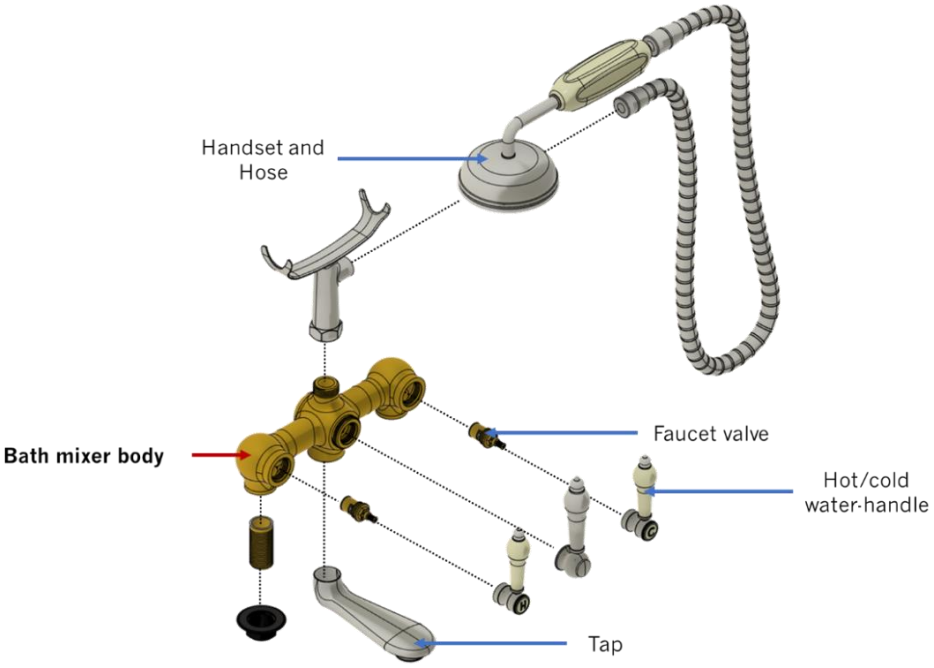

Figure 32: Schematic diagram of the bath mixer assembly.

As this is a brand-new component, the bath mixer will be produced using low-pressure die casting, and the base material will be the brass alloy ISO CuZn39Pb1Al-B, previously discussed in Chapter 3.1. After casting, it will also undergo finishing operations to separate it from the gating system and create some features, like holes and threads. Finally, the bath mixer will be subjected to chromium plating as a painting operation.

Therefore, it is necessary first to analyse the CAD drawing and identify the areas of the mixer to be machined to apply over thicknesses and compensate for shrinkage contraction during solidification. The bath mixer was split into three parts to simplify this work, as shown in Figure 33.

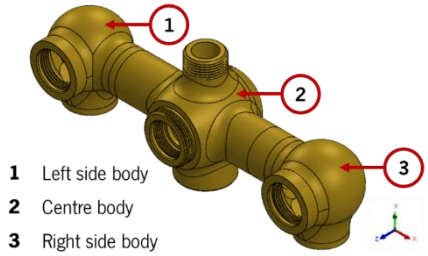

Figure 33: Division of the bath mixer into three different parts: the right/left side bodies and the central body.

4.3. CAD Casting Model

As mentioned above, this component is manufactured using casting technologies, specifically Low-Pressure Die Casting. The first analysis must, therefore, be carried out on the technical drawing for selecting the areas to be machined/cast, assigning machining thicknesses and considering a percentage to compensate for natural shrinkage.

According to the technical drawing, some features should be considered in the 3D CAD model for casting, namely:

(a) The hole in the bottom of the central body (Figure 34) must be machined as it is too small to be cast and threaded → **M6 x 1.0 mm**.

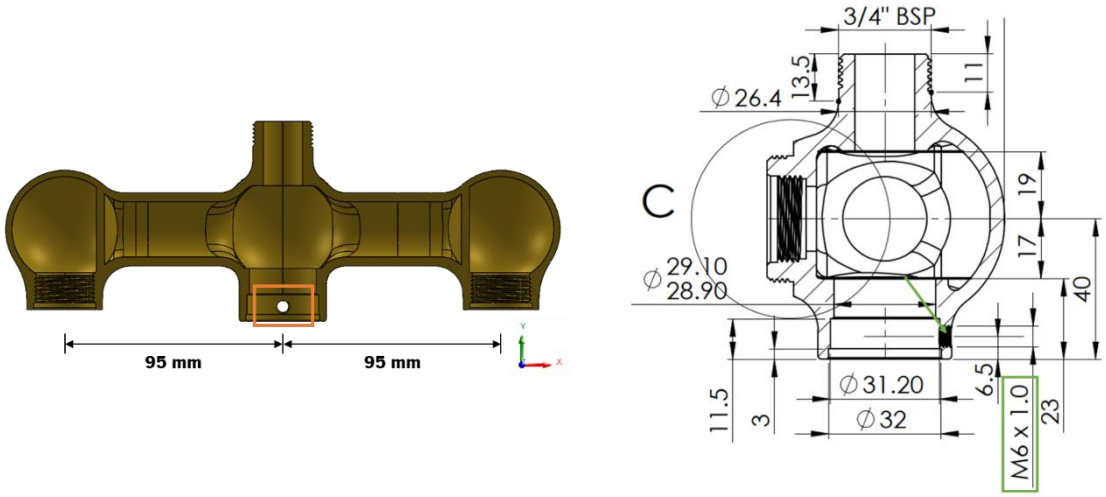

(a) (b)

Figure 34: Section view of the hole in the central body: (a) in the mixer; (b) on the drawing (detail of its position and dimensions).

(b) To ensure that there is enough material for machining, it is necessary to add "extra" material to the component (in most cases, the nominal dimensions present in the drawings are insufficient to use only). For this reason, **2 mm** was chosen as a reasonable over-thickness for the central body (Figure 35):

Note: These thicknesses are non-standard values and depend on many factors, like the alloy used for casting. For this reason, it should be chosen carefully to guarantee high-quality parts; in this case, the company MCT typically uses 2 mm as machining thickness.

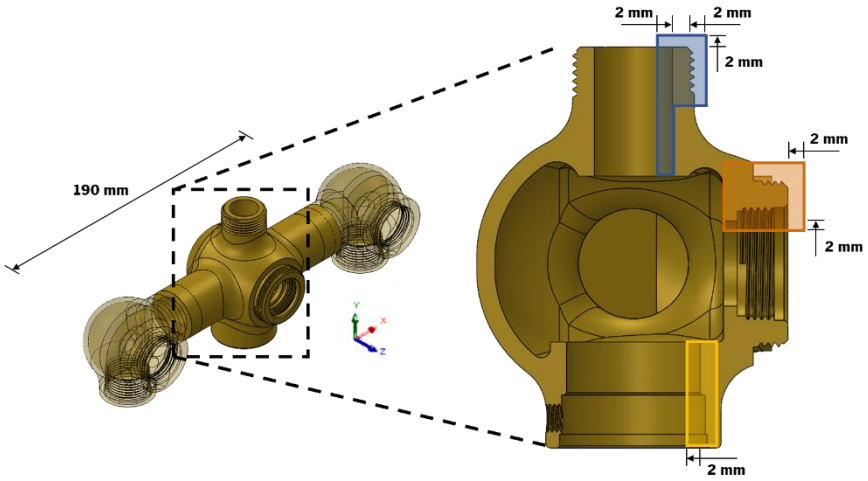

(a)

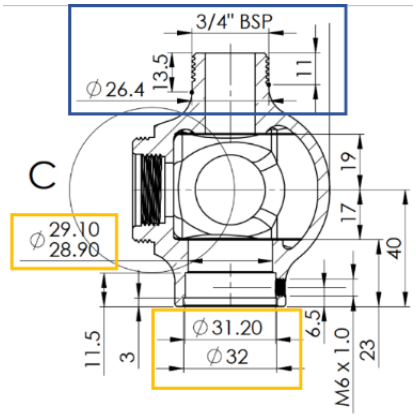

(b)

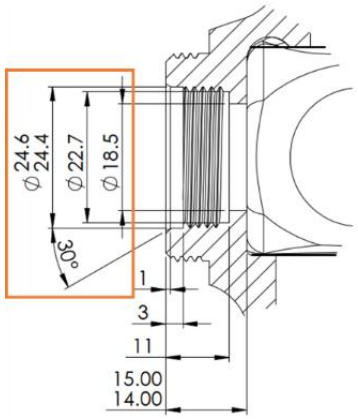

(c)

Figure 35: Areas of the central body with machining thicknesses: (a) in the mixer; (b) in the drawing and (c) in the drawing - detail C.

(c) As well as the central body, **2 mm** was chosen as the extra thickness for the tapped holes in the left and right-handed bodies, as they are symmetrical, and for the small central hole, as shown below:

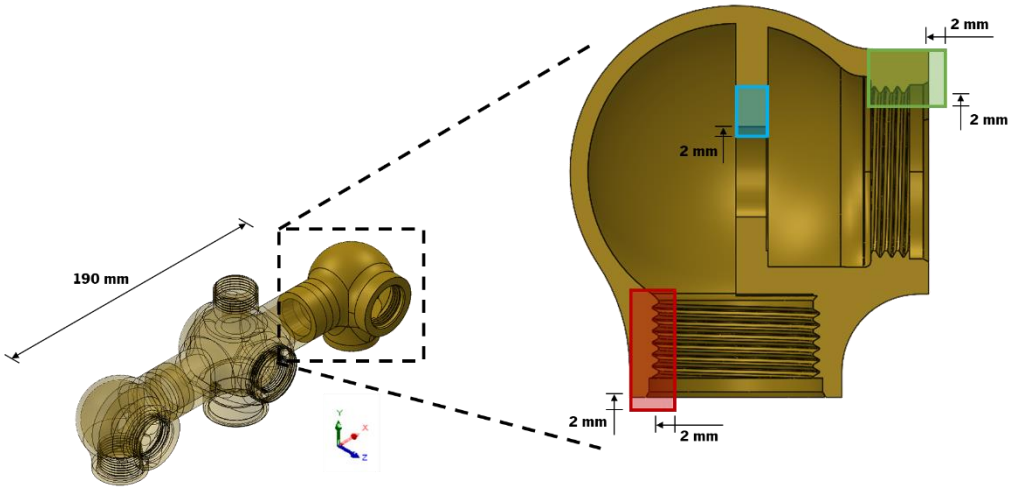

(a)

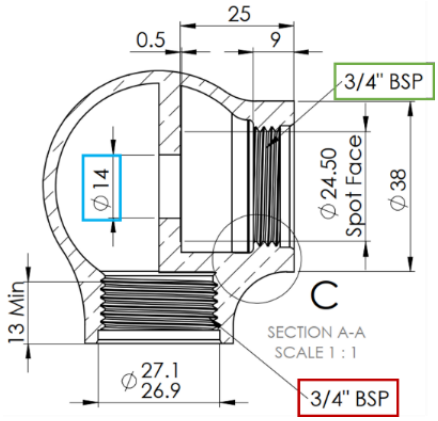

(b)

Figure 36: Areas of the left-hand body with machining thicknesses: (a) in the mixer and (b) in the drawing.

Furthermore, it is essential to add a percentage to compensate for the natural shrinkage of the component during cooling and solidification, which, for ISO CB757S, is approximately 1.5%, according to Table 1. However, this percentage should not be applied to all dimensions (e.g., using the *Scale-up* command) but only to the most critical directions, which, in this case, were along the x-axis (Figure 37).

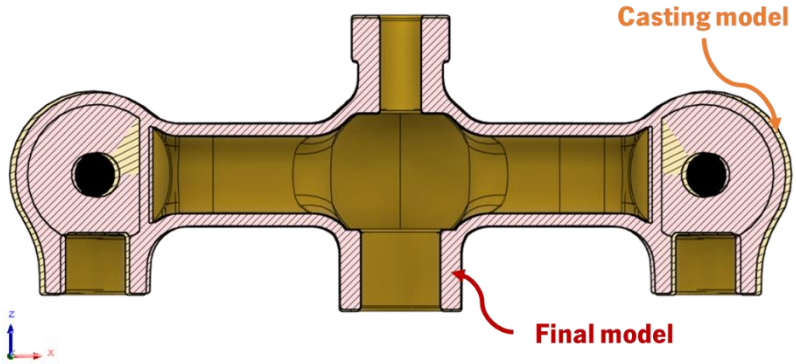

Figure 37: Casting model (in the outside) *vs* Final model after machining (in the inside).

4.4. Core Design

Once the casting model has been defined, the next step is usually the design of the cores, where several aspects need to be considered [8, 9]:

i. The cores must be strong enough to keep steady and fixed to the mould during metal pouring.

ii. The deflection of the cores must be minimal so as not to affect the final shape of the casting.

iii. The cores allow heat transfer between the metal and the mould.

iv. The permeability of the sand cores must facilitate the escape of the internal gases contained in the mould.

Regarding the body mixer, Figure 38 (a) represents the first attempt of the sand cores geometry considered. Given this configuration, using the lowest possible number of cores (ideally, three cores) would be impossible because of the central mixer body's upper and lower internal zones - Figure 38 (b); it would be necessary to use approximately five cores. Therefore, to correct this problem, since these areas are not functional, they were changed to flat surfaces, as presented in Figure 38 (a), which allows fewer core boxes to be used.

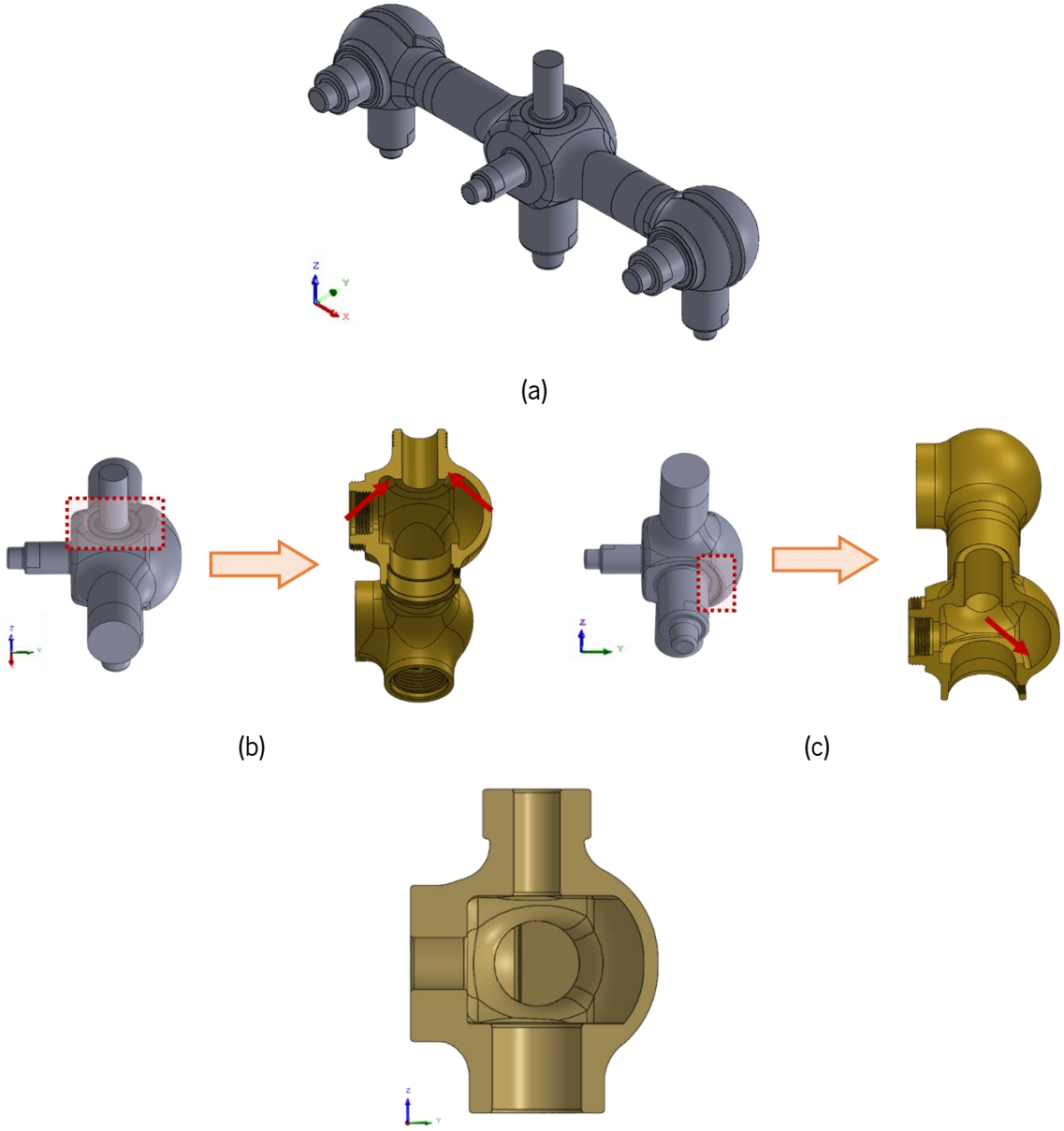

(a)

(b)

(c)

(d)

Figure 38: (a) Geometry of sand cores after the first attempt; (b) and (c) Features that obstruct using only three cores; (d) Final geometry of the bathtub mixer.

It was also necessary to divide the cores, using one of the vertical faces of the core as a reference (Figure 39), which allows the operator to easily place the cores in the mould by simply aligning one core to the other through the insert of the core.

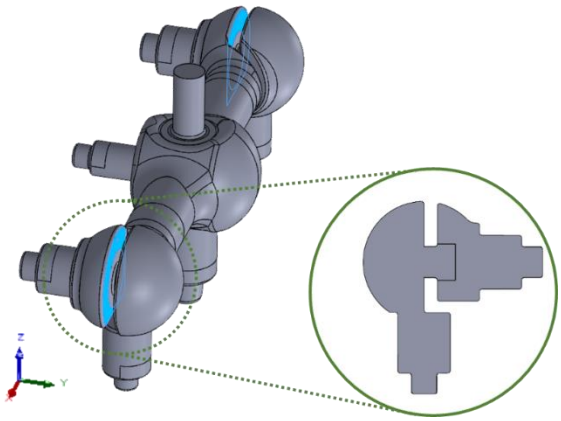

Figure 39: Division of the side cores into two, to facilitate core placing inside the cavity.

One of the most important aspects is the **draft angle of the cores**, which consists of an angle applied to all vertical faces to facilitate core extraction from the core box (Figure 40). The moulding process, casting design, and pattern greatly influence the required draft angle. If chosen incorrectly (i.e., not following ISO Standards), it can increase production costs and cause inconsistent sand cores. Therefore, foundries generally use 1° to 1.5° as the draft angle under normal conditions.

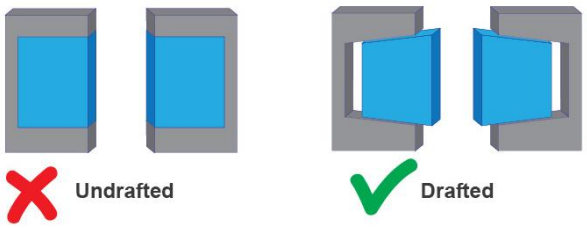

Figure 40: Diagram of undrafted parts, on the right, and drafted parts, on the left.

Before applying a draft angle to the body mixer, Solidworks allows to predict the areas where a draft angle is more likely to be required, using the Draft Analysis command. The input parameters are the direction of pull (the direction in which the two moulds will be separated), which in this case corresponds to the Y axis, and the draft angle, 1.5°, for the body mixer (Figure 41 (a)). The program then highlights the areas that entail a draft angle and those that do not, as shown in Figure 41 (b).

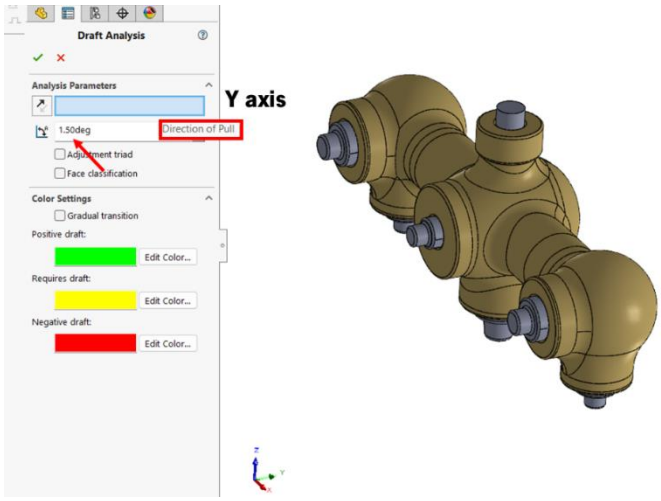

(a)

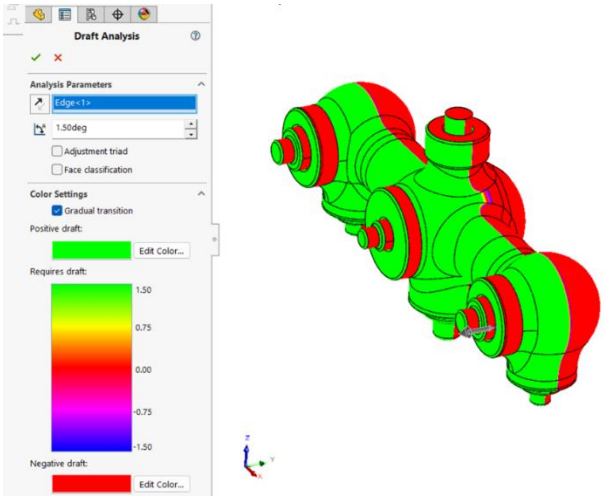

(b)

Figure 41: Draft angle: (a) input parameters; (b) areas that require draft angle in red and areas that do not require draft angle at green.

Hence, Figure 42 shows the cores after the draft angle was applied. Note that a sand trap was added to the central core's higher area to ensure it is correctly positioned in the cavity.

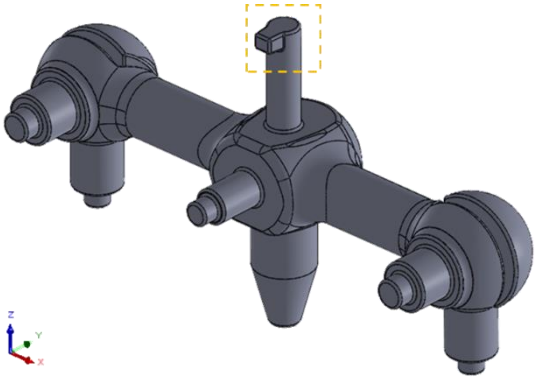

Figure 42: Final geometry of the cores with the draft angle applied and a sand trap added.

4.5. Gating Design

Once the casting model and cores are designed, the next step involves developing the gating system. According to (Nunes) [11], the gating system serves as a conduit for the molten metal to enter the dies and fill the cavity, allowing the metal to solidify and form the casting.

In Low-Pressure Die Casting (LPDC) context, the gating system must ensure complete cavity filling and compensate for casting shrinkage, effectively functioning as a riser. Therefore, a comprehensive understanding of the solidification process and casting behaviour is crucial. This chapter delves into the key considerations and principles that govern the design of the LPDC gating system [11].

4.5.1. Sprue and Runner(s) Design

The initial phase of the process entails the design of the sprue, a channel that directs the molten metal from the rising tube into one or more runners. Conversely, runners act as conduits that guide the metal towards the gate area, facilitating its entry into the cavity. In the case of LPDC systems, the sprue is positioned upward due to the furnace's placement beneath the moulds, and the metal is pressurized as it travels upwards, according to Figure 43 [11].

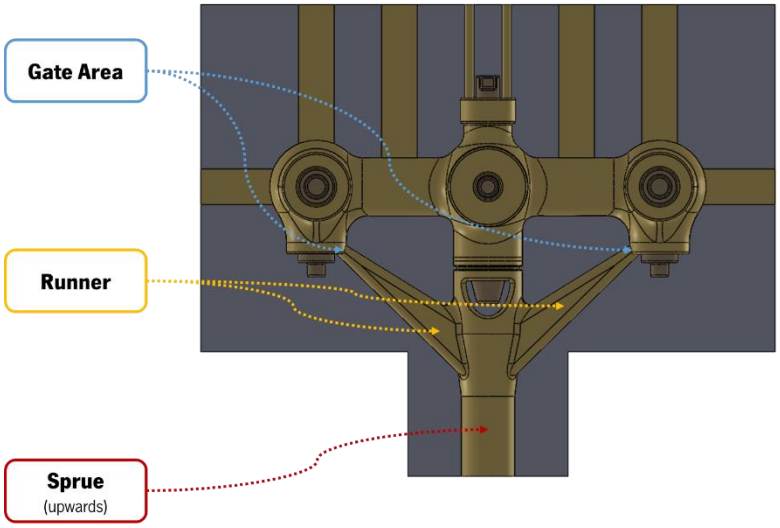

Figure 43: Example of LPDC gating system.

Concerning the runners, the arrangement for the flow of molten metal should be optimized to ensure efficient distribution. Employing multiple runners can help mitigate heat concentration on the dies. The criterion for achieving optimal runner performance involves utilizing the largest feasible cross-sectional area [12].

In Low-Pressure Casting systems, another critical consideration is the frequent implementation of runner tapering. This practice enhances the pressure of the liquid metal, reducing filling time while

upholding casting quality. Additionally, it is customary to enlarge the gate area adjacent to the casting. This adjustment slightly alleviates cavity pressure, preventing dislodging of sand from the cores and forming non-metallic inclusions. It also helps prevent metal oxidation [11].

Within the company *Metalúrgica Central da Trofa, Lda.*, a noteworthy limitation pertains to the machine in use, specifically concerning the dimensions of the sprue. With the rising tube's diameter set to 30 mm, it becomes imperative to adhere to this limit when designing the sprue. Exceeding this diameter constraint could lead to undesirable outcomes, such as reduced pressure, the formation of vortexes, and increased turbulence.

4.5.2. MOULD FILLING TIME

The gating design also requires careful consideration of the mould filling time, encompassing the duration necessary for complete cavity filling by the liquid metal. Essential to achieve high quality castings is the assurance of total cavity filling before the component solidifies or reaches a high percentage of solid fraction, which could hinder cavity filling [14].

Prolonged filling times and reduced flow rates can induce premature solidification, culminating in defects like Misruns and Cold shuts (see Chapter 2.3.2). Conversely, insufficient filling times and elevated flow rates may lead to sand core erosion and higher probability of air entrapment [15].

The optimal filling time hinges on multiple factors, including:

i. The alloy being poured.
ii. The mean thickness of the cavity.
iii. Cavity dimensions.
iv. The melt temperature of the alloy.
v. Die temperature.
vi. In LPDC systems, the maximum cavity height (including upper vents, if present).

Therefore, the mould filling time can be calculated, according to the following Equation (4.7):

$$t_{\text{filling}} = \frac{V}{A_{\text{A}} \times v_{\text{A}}} \tag{4.7}$$

in which V corresponds to the Volume of the casting, expressed in $[\text{m}^3]$; A_{A} is the gate area of the gating channel, in $[\text{m}^2]$; v_{A} is the maximum velocity of the liquid metal inside the cavity, expressed in [m/s].

4.5.3. REYNOLD'S NUMBER

In addition to the previously discussed gating considerations, another critical factor to consider during cavity filling is the Reynold's Number, which measures the fluid flow dynamics within the cavity. Equation (4.8) expresses the formula of the Reynold's Number:

$$N_{\mathrm{R}} = \frac{v \times d \times \rho}{\mu} \tag{4.8}$$

where v corresponds to the velocity of the liquid metal, in [m/s]; d is the diameter of the channel through which the metal flows, expressed in [m]; ρ corresponds to the density of the metal, in $[\mathrm{kg/m^3}]$; μ is the viscosity of the metal, expressed in $[\mathrm{N \cdot s/m^2}]$.

When the Reynold's number is below 2000, the flow is defined as **laminar**, characterized by the smooth movement of liquid molecules along straight paths without turbulence. In cases where the Reynold's number falls between 2000 and 20000, some mixing and turbulence occur, commonly encountered in various foundry gating systems, preventing air incorporation into the flowing liquid - **Transient flow**. Upon reaching a Reynold's number of approximately 20000, the flow transitions into a highly turbulent state - **Turbulent flow**. This turbulent flow disrupts the liquid stream's surface, increasing the likelihood of air being drawn into the flow and dross formation as the molten metal interacts with gases.

It is essential to highlight that this specific aspect holds particular significance in the environs of the gate area, where a substantial pressure difference exists (between the gate area constriction and the casting cavity). Hence, meticulous attention must be paid to the precise positioning and dimensions of the gating channel to prevent flow turbulence and the formation of bubbles, which can lead to gas porosity development.

4.6. LOW PRESSURE DIE CASTING: SIMULATION MODEL

The normal die-casting process fills the cavity with molten metal and solidifies it in several successive cycles. Hence, similarly, in Low-Pressure Die Casting, there are two types of casting simulation (Figure 44): first, the thermal die cycling simulation and, finally, the filling (and solidification) of the cast piece, using the thermal gradient of the die, obtained in the previous simulation.

Figure 44: Schematic representation of the simulation process of low pressure die casting.

The first simulation (**Thermal Die Cycling Simulation**) is to understand/evaluate the temperature of the mould, which gives a thermal map of it (thermal gradient). The second simulation (**Filling + Solidification Simulation**) is to understand the molten metal's filling behaviour based on the previously obtained temperature gradient.

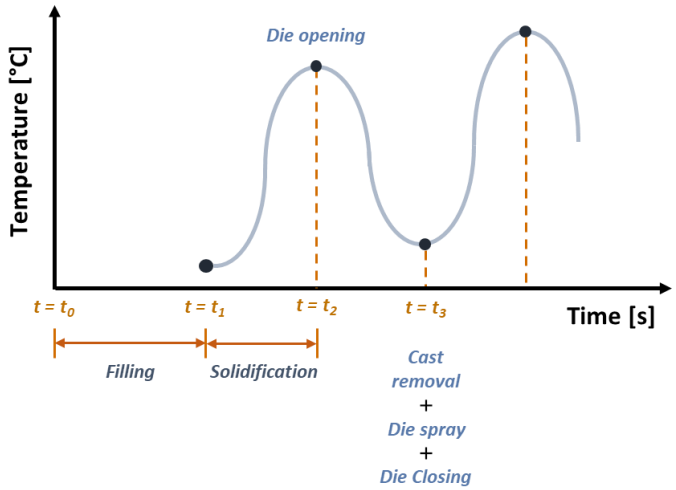

Figure 45: Typical thermal die cycling chart.

4.6.1. Thermal Die Cycling Simulation

According to (ESI Group) [16], the thermal die cycling simulation allows to:

i. Determine and optimise the number of cycles required to reach the steady state regime (in a diagram similar to Figure 45) and, therefore, simulate more accurately.

ii. Predict molten metal filling based on the temperature distribution on the dies.

iii. Determine and enhance the positions and temperatures of the heating/cooling channels.

Before defining process parameters in QuikCAST, it is necessary to primarily specify all the steps and respective times for each die cycle. As this component has no previous project and there is no record of times and steps, it used the steps of another body mixer with similar dimensions and weight, represented in Table 6.

The filling should not be included in the first simulation (Thermal Die Cycling) as it is only important for the temperatures of the dies during solidification. It is, therefore, necessary to remove this stage when applying boundary conditions.

Observing Table 6, solidification starts at 10 s, so this value must be discounted in the following steps. The filling time is added at the end, which gives a complete cycle (Table 6).

Table 6: Steps and (real and simulation) times for one die cycle.

Steps	Real times [s]	Simulation times [s]
Start of filling	0	–
End of filling/Start of solidification	10	0
End of solidification	16	6
Die opening	18	8
Cast (and cores) ejection	21	11
Start of die spraying	23	13
End of die spraying	26	16
Cores positioning	28	18
End of cores positioning	41	31
Die closing	43	33
End of cycle	45	45

Material data: *Volume manager*

Before setting the boundary conditions for the initial simulation, the material information and properties of the casting and die are listed in the Volume Manager menu (Figure 46). The volumes are then loaded into the software and characterised by pouring temperature (T_{pouring}) for cast part, core temperature (T_{cores}), and steady-state die temperature (T_{die}).

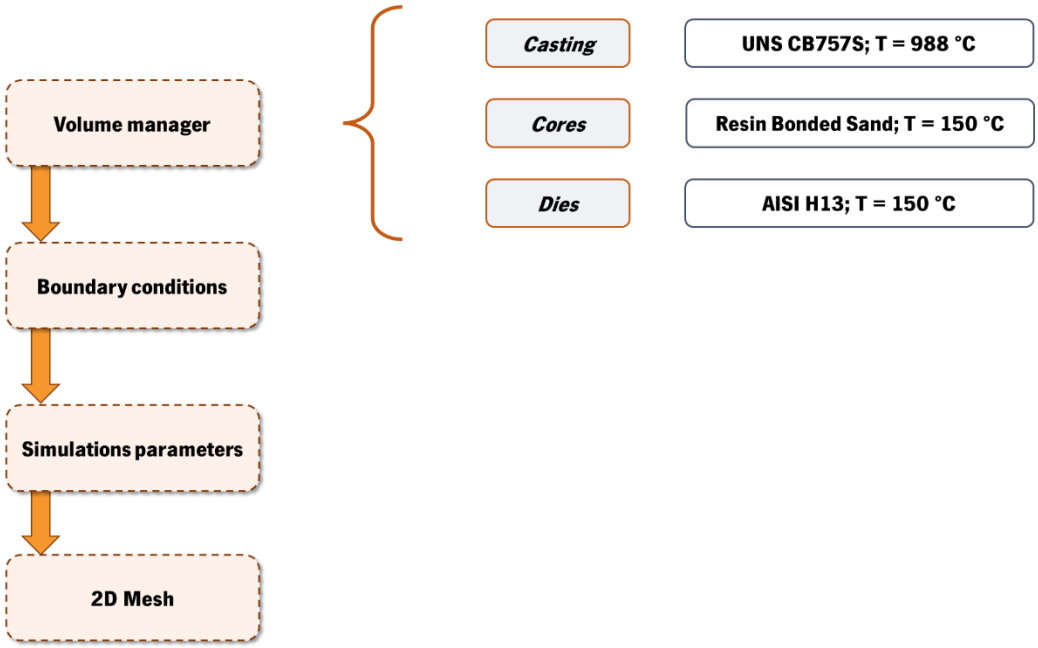

Figure 46: Characterization of the components used, for the first simulation.

The **pouring temperature**, T_{pouring}, is equal to the liquidus temperature, T_{Liq}, plus a temperature range, ΔT, according to Equation (4.9):

$$T_{\text{pouring}} = T_{\text{Liq}} + \Delta T \tag{4.9}$$

The pouring temperature must be sufficiently high to ensure smooth pouring and prevent solidification ($T_{\text{pouring}} > T_{\text{Liq}}$). The pouring temperature is influenced by alloy composition, casting dimensions (wall thickness, weight, size), mould coating, cooling system and gating system. Careful consideration of these factors ensures successful casting production [17].

A pouring temperature lower than the optimum can lead to misruns, rapid cooling of thin-wall sections, and disruption of directional solidification. This can result in defects such as misruns, cold shuts, and porosity. On the other hand, excessively high pouring temperatures can have detrimental effects, such as damaging the mould, due to extreme heat, reducing its lifespan. Additionally, it can lead to casting defects like warpage and shrinkage. Therefore, the objective is to ensure that the metal flows into all areas of the mould, especially the central cavity before solidification initiates [11, 18–19].

Hence, for brass ISO CuZn39Pb1Al-B, with a liquidus temperature, T_{Liq}, of 941°C (according to Table 4), and considering an acceptable temperature range, ΔT, of 50°C, the final pouring temperature, T_{pouring}, is determined to be **980°C**. This falls within the acceptable range specified in [20].

Resin bonded sand cores were chosen, directly selected from the material library of QuikCAST. Following the cycle outlined in Table 6, the cores are introduced into the dies after spraying. As a result, the **cores temperature** can be considered slightly higher than the room temperature (T_{Room} = 25°C), i.e., $\boldsymbol{T_{\text{Cores}} \approx 35°C}$.

As discussed in Chapter 3.2, the material chosen for the dies is AISI H13 steel, commonly employed in various applications, including moulds for brass castings, obtained from gravity and low-pressure technologies. Consequently, it is crucial to determine the **mould temperature** to ensure high-quality product production carefully. Various factors significantly influence the mould temperature, including [11]:

i. **Pouring temperature**: Higher metal temperatures during pouring result in elevated mould temperatures.

ii. **Cycle frequency**: faster cycle times increase the die's heat buildup, raising the mould temperature.

iii. **Casting shape**: Certain features, such as isolated sections, pockets, and sharp corners, increase mould temperatures.

iv. **Casting wall thickness**: Greater wall thicknesses result in higher mould temperatures.

v. **Mould wall thickness**: Thicker dies tend to have lower temperatures.

vi. **Thickness of mould coating**: Increased thickness corresponds to lower mould temperatures.

Thus, careful consideration must be given to selecting a die temperature tailored to the specific pouring alloy. Excessive temperature can subject the die to significant thermal stress, thereby decreasing its operational lifespan. Conversely, excessively low temperatures can result in premature solidification of the molten metal, giving rise to defects such as misruns and cold shuts. The optimal practice involves adopting a die temperature that ranges from 50°C to 70°C above the alloy's crystallization temperature. For the bath mixer, a **die temperature of 150°C** was chosen [18].

Boundary Conditions: *Process Condition Manager*

Following the determination of the main properties associated with the volumes employed in the simulation, the subsequent step involves establishing the appropriate boundary conditions under the previously outlined cycle (Table 6), as illustrated in Figure 47:

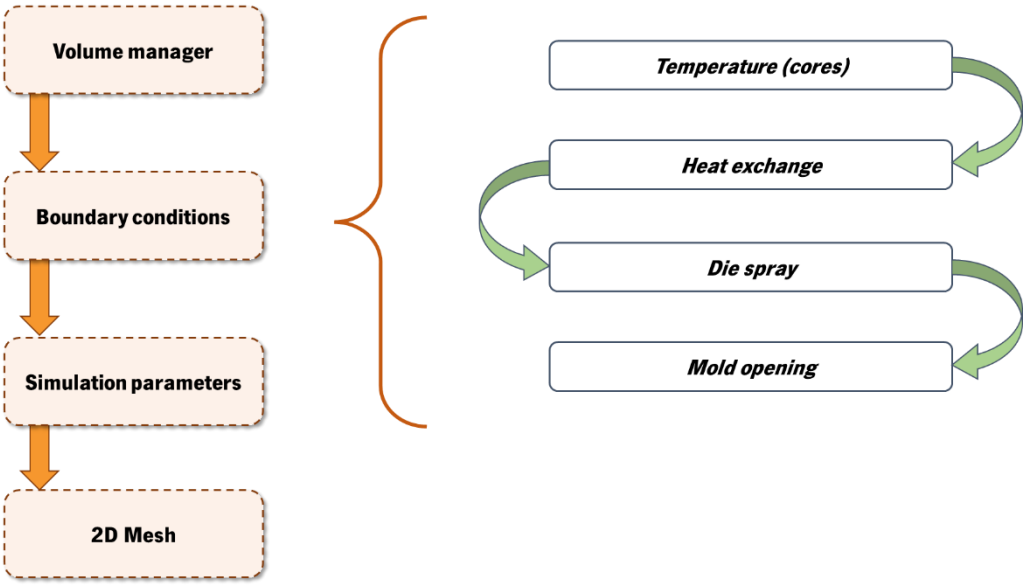

Figure 47: Boundary conditions applied to the first simulation - thermal die cycling simulation.

Analysing the cycle presented in Figure 45, it becomes imperative to determine the specific time interval corresponding to the core placement inside the mould, spanning from 18 s to 31 s. During this interval, the **core temperature** is established at 35°C. The core temperature increases in the steps preceding the core placement due to heat conduction from both the cast and the mould. As previously mentioned, the new cores have a temperature akin to room temperature, requiring a transition within 18s and 31s.

Heat transfer occurs between the die and the surrounding environment during **filling** and **spraying**, as indicated in Table 6, particularly at the external die/exterior interface. Therefore, it is necessary to define different heat transfer coefficients over time for these two situations: filling and die spraying.

Based on the information provided in Table 6, several conclusions can be drawn, as shown in Figure 48: during the first 10 s of the cycle, the heat exchange between the dies and the environment is considered an **Air exchange**; between 10 s and 13 s, the die spraying takes place with the application of a coating, which involves immersion in a water bath, in a tank - consequently, the heat exchange occurs between the dies and **water**; from 13 s until the end of the cycle, the heat exchange between the dies and the environment is once again characterized by **Air exchange**, similar to the initial phase.

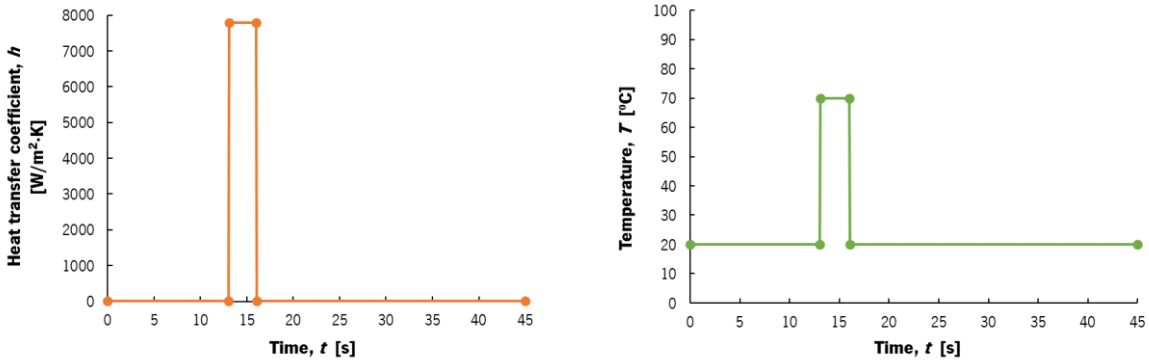

(a) (b)

Figure 48: (a) Heat transfer coefficient, *h*, and (b) Temperature, *T*, applied for the dies.

Table 7 specifies the main properties defined for water and air exchange, namely the heat transfer coefficient, *h*, and the temperature, *T*, of each one:

Table 7: Air and water adopted properties, used for defining the heat exchange condition.

Air properties	
Heat transfer coefficient, *h* $[\mathbf{W/m^2 \cdot K}]$	10
Temperature, T [°C]	20
Water properties	
Heat transfer coefficient, *h* $[\mathbf{W/m^2 \cdot K}]$	7800
Temperature, T [°C]	70

The heat transfer coefficient was determined using the HTC calculator provided by QuikCAST software. The calculation assumed an air temperature of 20ºC, while the standard value was employed for water, with an approximate temperature of 70ºC.

Die coating, a liquid coat applied to the dies plays a crucial role in enabling demoulding and extending the lifespan of the dies. This is essential due to the thermal gradient resulting from the pouring cycle of each part, which gives rise to substantial thermal stresses at the interface between the die and the cast. According to (Nunes) [11], the application of a die coat serves several purposes, including:

i. Preventing premature freezing and solidification of the cast part.
ii. Controlling the rate and direction of solidification, ensuring the soundness of the cast components.
iii. Minimizing thermal shocks.
iv. Preventing soldering of the molten metal to the dies, reducing the risk of adhesion.

By achieving these objectives, the die coat significantly contributes to the overall quality of the casted components.

When working with brass alloys, it is typical to use graphite or oil as die coatings. Applying these coatings requires pre-heating the die to a specific temperature for better mould adherence. To prevent defects in cast parts, removing the dies from the machine is recommended for maintenance purposes. During this maintenance, the dies should be cleaned and polished approximately every 8 hours to address any potential dimensional changes that may arise within the casting process and ensure the optimal performance of the dies [21].

The application of die coating on the dies is achieved by immersing the mould in vats located within the machine (Figure 88). MCT uses **GRAFICOL 85** as the coating material. Although QuikCAST does not provide a specific boundary condition to represent this immersion, the Die Spray condition can be applied. This condition allows for the definition of the surfaces of the mould that undergo immersion, as well as properties such as the heat transfer coefficient of the graphite bath, $h_{\text{Graphite bath}}$, the cooling media, and the duration of the die coating application (Table 8):

Table 8: Properties applied to the Die Spray condition.

Cooling Media	Water
Heat transfer coefficient - graphite bath, $h_{\text{Graphite bath}}$ $[\mathbf{W/m^2 \cdot K}]$	7800
Start time [s]*	13
End time [s]*	16

*These two times correspond to the mould immersion as stated in the corrected cycle - Table 6.

Specific volumes are isolated in the *Mould Opening* condition to define thermal conditions, including the heat transfer coefficient, temperature, and emissivity. As a result, three *Mold Opening* conditions (Table 9) are defined by the cycle presented in Table 6. These conditions correspond to the opening of the dies, the removal of the casting and the placement of new cores. By implementing these conditions, it becomes possible to visualize the temperature changes in the time prior to the beginning of a new cycle.

Table 9: Properties defined for the three Mould opening conditions.

Properties	Mould opening	Removal of the casting	Placement of new cores
Heat transfer coefficient – Mould/Alloy, $h_{\mathrm{Mould-Alloy}}$ $[\mathrm{W/m^2 \cdot K}]$	10	10	10
External Temperature, T_{Ext}[°C]	50	50	50
Emissivity, ε [-]	0.3	0.3	0.3
Start time [s]	8	11	11
End Time [s]	33	45	31

Simulation Parameters

After defining all the information regarding boundary conditions, it is also necessary to define the simulation parameters that rule the first simulation (Thermal Die Cycling Simulation) - Figure 49.

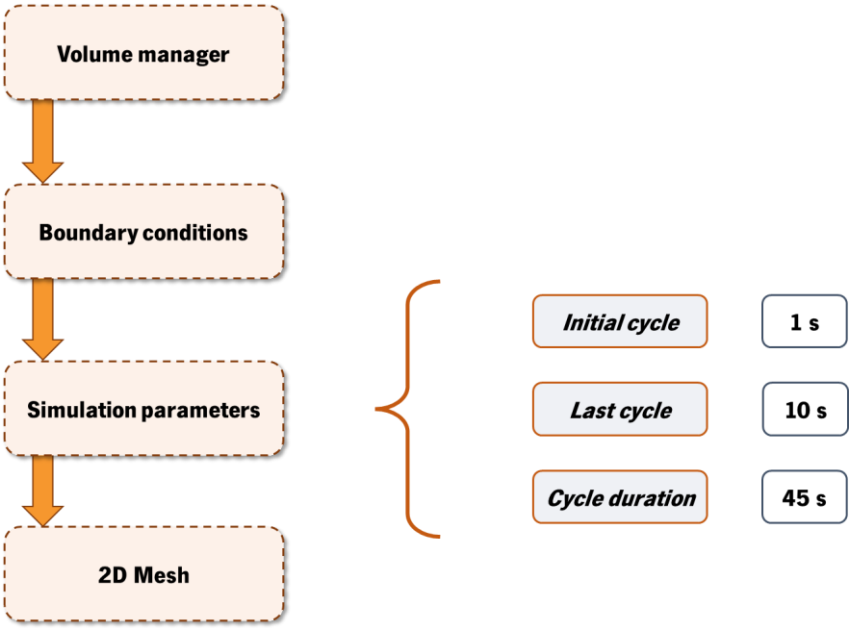

Figure 49: Simulation parameters defined for the first simulation.

In QCA General Parameters (Figure 50 (a)), the first step is to define the type of simulation as *Cycling* (the remaining parameters can be left as default, as they rule the solidification of the casting). In QCA Thermal (Figure 50 (b)), it is recommended to modify the *Frequency type* to *Time (s)* in the subsection *Advanced*. It should be noted that porosity calculations are not required for this simulation, so that the *Porosity Model* can be disabled. Finally, in QCA Cycling (Figure 50 (c)), the main cycling parameters are defined, including the initial and final cycle and the overall duration of each cycle. In this case, the overall duration of each cycle is set to 45 s, as presented in Table 6.

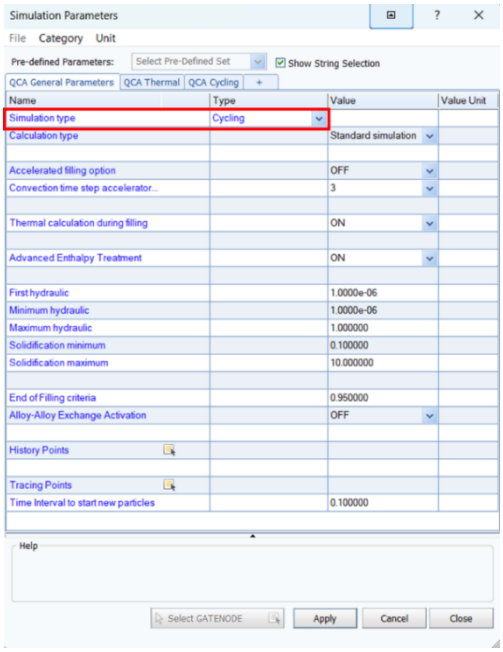

(a)

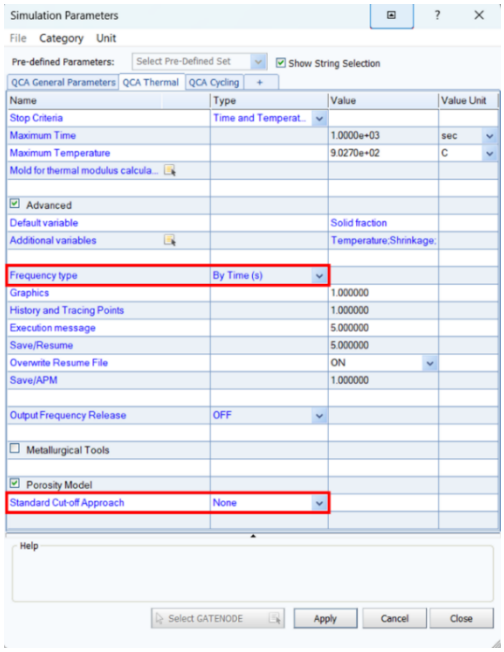

(b)

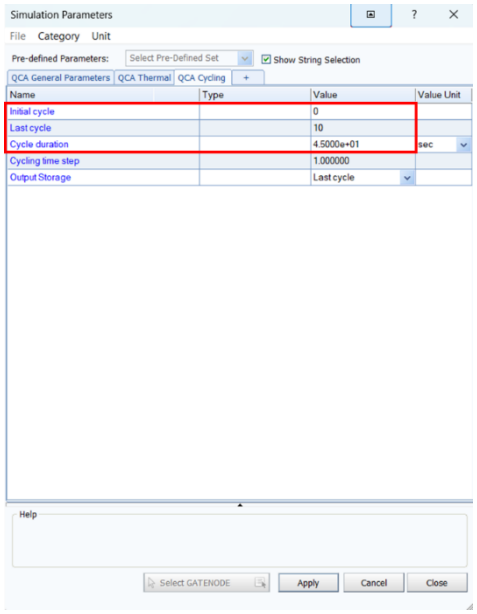

(c)

Figure 50: Parameters used for (a) QCA General Parameters, (b) QCA Thermal and (c) QCA Cycling.

2D Mesh

Finally, as mentioned earlier, QuikCAST uses the finite differences method for domain discretisation (Chapter 4.1). Consequently, it is essential to specify the dimensions of a "Grid" that is only concerned with the casting element and will be used by the Solver to apply the thermal equations.

The *Average Size* parameter (Figure 51) was set to 2 mm for each element in the areas near the previously defined Volume – *Peca*. Note that this is essential due to the calculation of thermal die temperatures is near the volume selected. Additionally, the *Maximum Growth Rate* parameter (Figure 51) determines the growth factor for elements located further away from the selected Volume. A higher value generates a coarser mesh in the surroundings, while a lower value yields a finer mesh. Therefore, a value of 1.1 mm was chosen, indicating a finer mesh configuration.

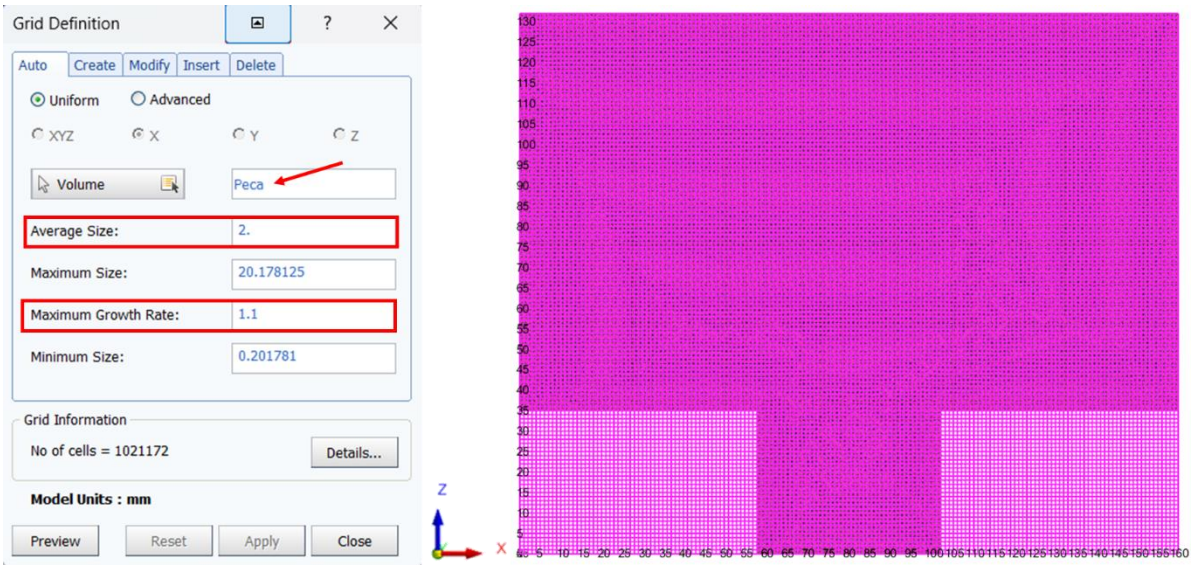

Figure 51: Parameters used for the definition of the "Grid".

4.6.2. Filling and Solidification Simulation

Based on the temperature map obtained from the thermal die cycling simulation, the next step is to proceed with the filling and solidification simulation of the cavity.

Material data: *Volume Manager*

In line with the previous simulation, it is imperative to define and modify specific properties associated with the volumes used in the model. In this particular simulation, it is crucial to ensure that the temperature of all components aligns with the temperature of the cavity immediately prior to the commencement of pouring, which is set at 150ºC. It is essential to acknowledge that this condition assumes uniform temperature distribution across all volumes, which may deviate from real-world

conditions. However, this simplification does not compromise the accuracy of the results obtained. The volume properties defined for the second simulation are shown in Figure 52:

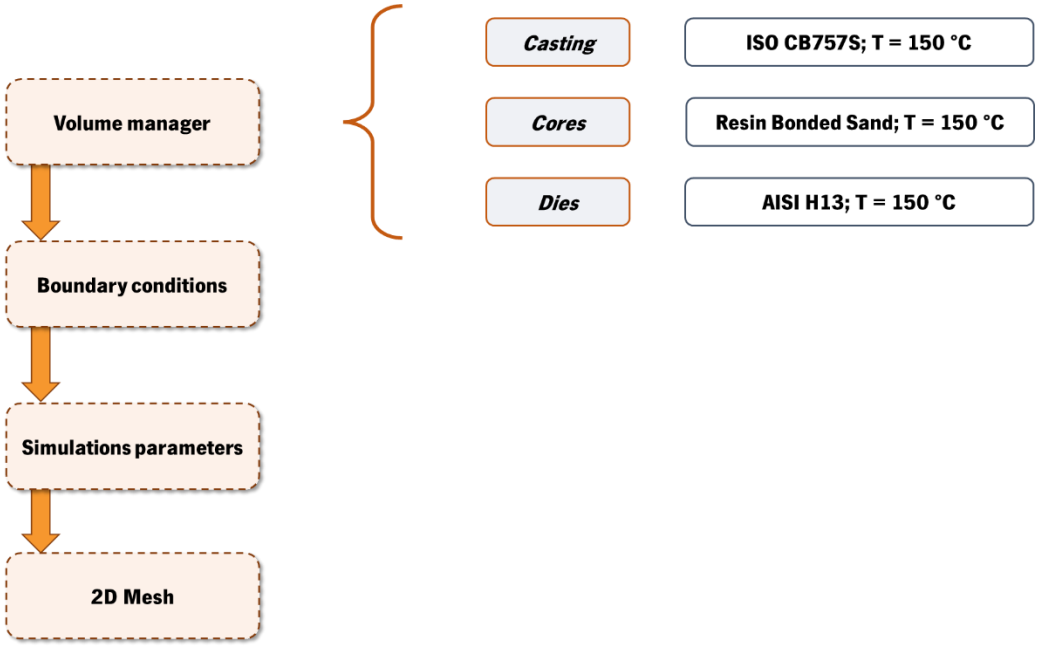

Figure 52: Characterization of the components used for the second simulation.

Boundary Conditions: *Process Condition Manager*

Following the definition of properties and materials for each volume used in the simulation, the subsequent stage involves establishing the process conditions, as depicted in Figure 53:

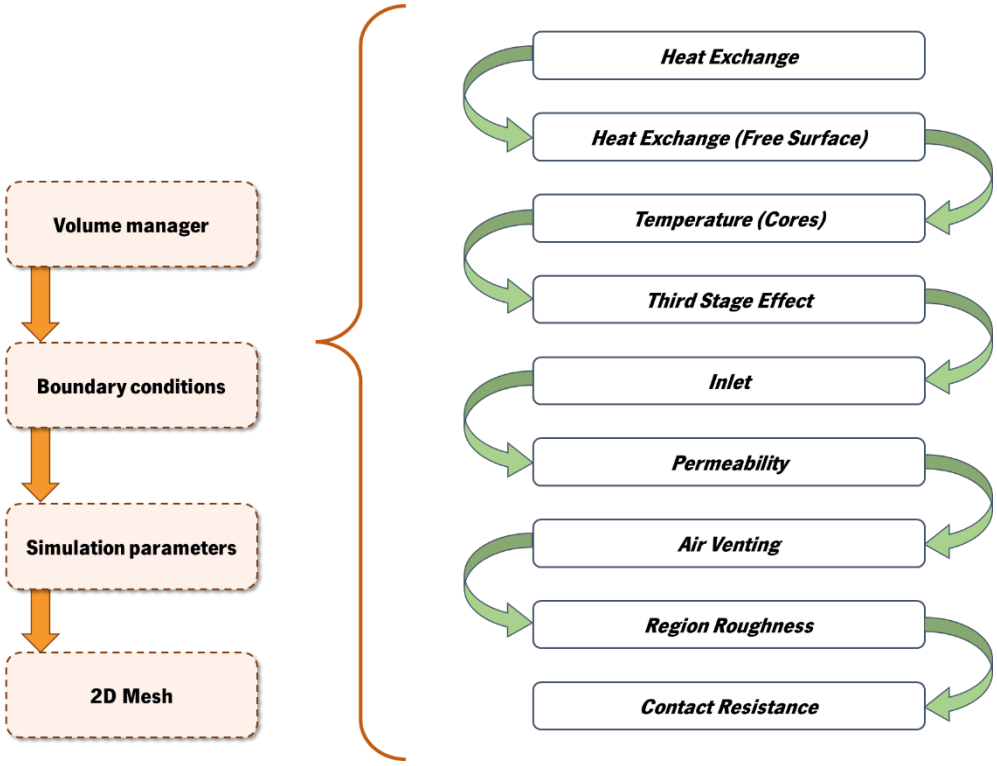

Figure 53: Boundary conditions applied to the second simulation - filling and solidification simulation.

During the filling and solidification simulation, the *Heat Exchange* condition is applied to the external surfaces of the dies, as in the first simulation. However, a natural air convection condition can be selected since the dies only meet external air during the filling process. This can be achieved by selecting the *Air Cooling* parameter from the QuikCAST library.

The second *Heat Exchange* condition pertains to the **free surface** (Figure 54) formed at the forefront of the molten metal during the filling process. This condition aims to represent the cold front of the metal, characterized by lower temperature and convection-based heat transfer with the cavity.

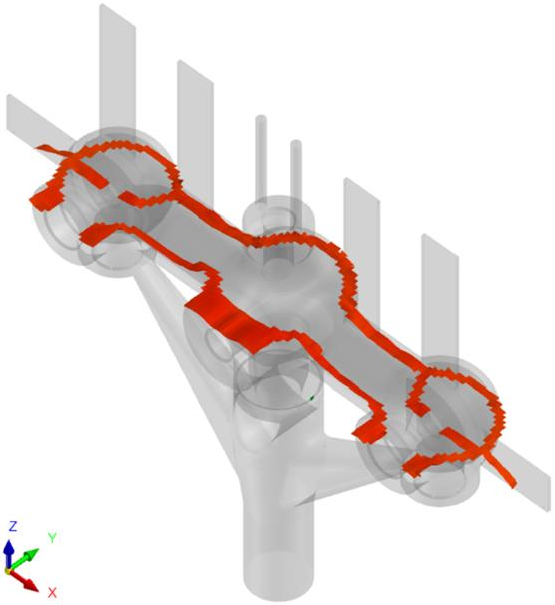

Figure 54: Free surface, during filling process.

To accurately simulate, a heat transfer coefficient, *h*, and a specific temperature, *T*, are applied. Hence, the parameters employed for this condition are outlined in Table 10.

Table 10: Parameters applied to simulate the cold front of the metal – Free surface condition.

Heat transfer coefficient, h [$\mathrm{W/m^2 \cdot K}$]	800
Temperature, T [°C]	80

In contrast to the first simulation, the **core temperature** remains constant throughout the filling process. Hence, it is necessary to assign a specific temperature for the cores. To ensure this, a uniform temperature is exclusively assigned during the filling stage, with an initial value defined (Table 11).

Table 11: *Temperature* condition parameters.

Temperature, T [°C]	35
Condition Type	Initial
Applies to	Filling

The *Third Stage Effect* condition is directly associated with defects, primarily shrinkage porosities, in components produced through LPDC, by considering the influence of pressure.

As long as the liquid metal feeding is maintained, the volumetric contraction of the alloy is compensated during solidification, resulting in a reduction in shrinkage porosity formation. However, once the feeding is halted, the volumetric contraction is calculated similarly to Gravity Die Casting, where the regions/cells that have not solidified will undergo emptying.

For the *Third Stage Effect* condition, the *Solid Fraction Cut-off* is defined as the percentage of the solid fraction of the cast part above which the feeding pressure is turned off. This parameter determines the end of solidification. In this case, a Solid Fraction Cut-off percentage of **95%** was considered, indicating that only 5% of the total cast remains in the liquid state.

In Low Pressure Die Casting, as mentioned in Chapter 2.1, the metal is introduced into the cavity by pressurizing gas or air. This can be determined either by pressure or velocity equations. Taking the second case, the **filling velocity** can be calculated using the Equation of Continuity, which relates to the mass of metal entering the cavity, which is presented in Equation (4.10) [22]:

$$Q = v_i \times A_i \Leftrightarrow \frac{V_C}{t_f} = v_i \times A_i \Leftrightarrow v_i = \frac{V_C}{t_f \times A_i} \tag{4.10}$$

where Q is the flow rate of liquid metal that enters the cavity, in $[\mathrm{m}^3/\mathrm{s}]$; v_i is the velocity at the ingate (bottom) of the gating system, in [m/s]; A_i is the gate area defined as $[\mathrm{m}^2]$; V_C is the volume of the cast part, expressed as $[\mathrm{m}^3]$; t_f corresponds to the filling time, in [s]. Note that for the velocity calculation, the liquid metal was considered incompressible. This means that the density of the metal, ρ, remains constant over time, and the filling of the cavity takes place in the laminar flow regime [22].

The application of Equation (4.10) presents a challenge as it requires prior knowledge of the filling time, t_f, which renders the calculation infeasible due to the presence of two unknown variables: the filling time, t_f, and the velocity at the ingate of the gating system, v_i. Therefore, an alternative approach must be adopted, wherein pressure input is applied instead. This involves determining a pressure-time curve that defines the filling pressure, similar to the curve shown in Figure 55 [22].

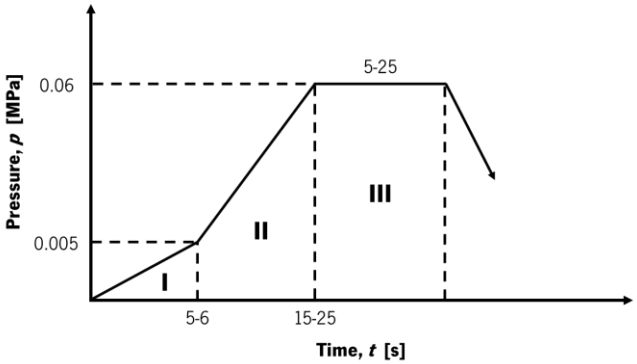

Figure 55: Pressure-time curve, typically used in LPDC.

Upon analysing Figure 55, several key observations can be made regarding the different stages of the process:

i. In the first stage (**Zone I**), pressure is applied to the molten metal to elevate it from the feed tube to the gate of the casting die, ensuring a controlled and non-turbulent flow.

ii. In the second stage (**Zone II**), the cavity of the mould is filled, and it is crucial to maintain heedful control during this stage to avoid excessive turbulence or the entrapment of air or gas, which can lead to the development of defects.

iii. In the third stage (**Zone III**), a constant feeding pressure is maintained to compensate for casting shrinkage. The duration of this stage must be carefully determined to prevent metal from falling due to gravity and to bypass excessive solidification at the gate, which could hinder the demoulding process (Figure 56).

iv. In the last stage (**Zone IV**), the pressure is entirely released, allowing the removal of the cast part.

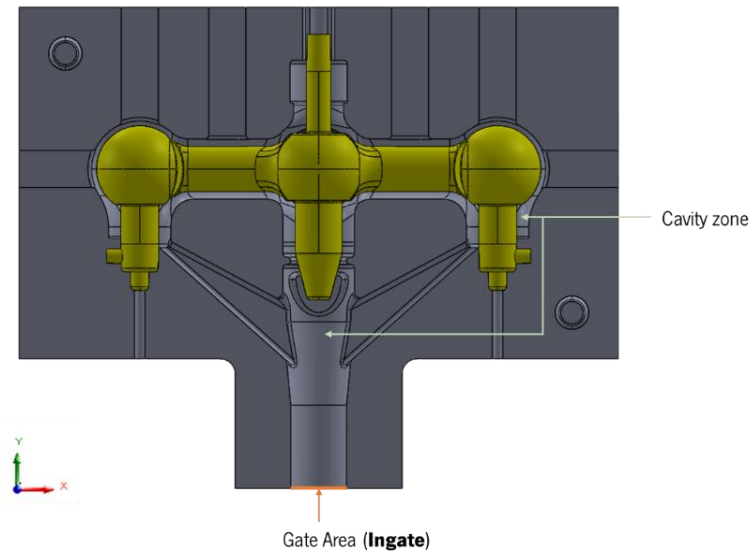

Figure 56: Identification of the Cavity and the Gate area.

For the calculation of the feeding pressure at the entrance of the dies (ingate), the Bernoulli Equation can be employed, as represented by Equation (4.11):

$$\frac{(p_{\text{ingate}} - p_{\text{rise tube}})}{\rho} + \frac{(v_{\text{ingate}}^2 - v_{\text{rise tube}}^2)}{2} + g \times Y = 0 \qquad (4.11)$$

in which p_{ingate} is the pressure at the ingate of the gating system, in [bar]; $p_{\text{rise tube}}$ is the pressure applied to the liquid metal to lift from the furnace to the entry of the gate, expressed as [bar]; ρ corresponds to the density of the liquid metal, at the pouring temperature, expressed as $[\text{kg/m}^3]$; v_{ingate} is the velocity of the metal on the gating system, in $[\text{m}^2]$; $v_{\text{rise tube}}$ is the velocity of the metal on the rise tube, also in $[\text{m}^2]$; g is the gravitational acceleration, indicated as $[\text{m}^2/\text{s}]$; Y is the height from the liquid metal at the furnace to the gating system in the dies, expressed as [m].

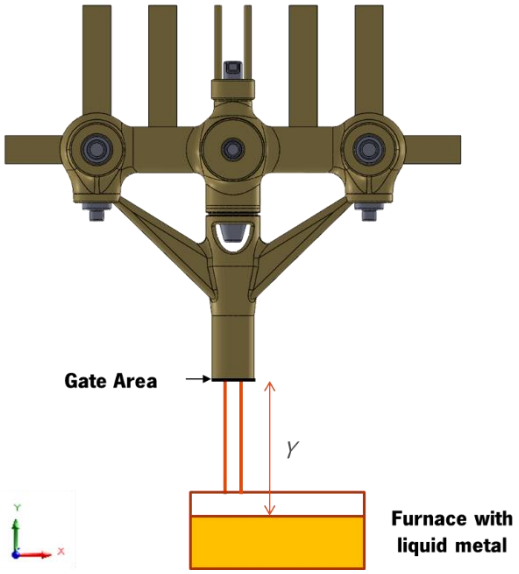

Figure 57: Height between the furnace and the gate system.

However, given the relatively low velocity of the fluid where dynamic pressure is negligible (i.e., the term $\frac{(v_{\text{ingate}}^2 - v_{\text{riser tube}}^2)}{2} = 0$), and considering a constant height, *Y*, between the fluid and the cavity with a sufficiently large volume of liquid metal in the furnace compared to the amount inside the cavity, Equation (4.11) can be simplified and reformulated as demonstrated in Equation (4.12) [24]:

$$p_{\text{ingate}} = p_{\text{rise tube}} - \rho \times g \times Y \qquad (4.12)$$

Despite the CAD models of the cores were assigned as resin-bonded sand, their interface with the liquid metal presents impermeability. This lack of permeability hinders air extraction from the cavity, obstructing the complete filling of the dies [25].

The **permeability of sand** is considered at the interface between the liquid metal and the sand cores, which is characterized by Equation (4.13) [25]:

$$P = \frac{V \times Y}{A \times p \times t} \tag{4.13}$$

in which P represents the permeability, in the SI system, which is dimensionless [-]; V is the volume of air that crosses the surface of the cores, in [m^3]; Y is the sand height, expressed as [m]; A corresponds to the section area of the cores, in [m^2]; p is the air pressure applied, expressed as [Pa]; t is the time required for the air passing through the sand, indicated as [s].

In QuikCAST, the permeability of sand is not directly represented in the SI System. Instead, a conversion factor, known as Georges Fisher value (GF value), is employed. This GF value is used to transform the permeability to an equivalent value, as described in Equation (4.14) [25]:

$$P_{\mathrm{SI}} = 1.69 \times 10^{-8} \times P_{\mathrm{GF}} \tag{4.14}$$

where P_{SI} is the permeability of sand in the SI system and P_{GF} corresponds to the permeability in the GF system, being both dimensionless [-].

Inefficient air extraction from the mould cavity is often the root cause of most visible porosities in most cast parts. When liquid metal is poured into the dies, the trapped air inside must be expelled through small holes. If these holes are not properly sized, the air remains trapped, hindering complete cavity filling and resulting in gas porosities in the casting (Chapter 2.3.1), commonly called air entrainment [26].

The size of the **vents** should be carefully designed based on the specific component to be produced. If the holes are excessively small, air may remain trapped inside the cavity. On the other hand, excessively large holes can cause a loss of pressure in the metal, negatively affecting the filling process. Ideally, the volume of air expelled from the cavity should match the volume of metal required to fill the entire mould cavity – Equation (4.15) [26]:

$$V_{\mathrm{air-cavity}} = V_{\mathrm{metal-cavity}} \tag{4.15}$$

In QuikCAST, there are two approaches for defining vents in dies [25]:

i. The first approach involves considering a **large vent**, which requires incorporating it into the die model. In this case, the die model also considers the atmospheric pressure.

ii. The second approach involves considering a **small vent**, which means it is not included in the die model. Instead, a boundary condition (*Air Venting*) is applied at the interface between the mould cavity and the vent region.

(a) (b)

Figure 58: Air Venting (a) considered in the die; (b) considered only at the interface cavity/vent.

The **surface roughness** of the metallic die has an impact on the filling process, and it is vital to account for this in the boundary conditions. The roughness value is determined based on the die material and its dimensions. In this case, the casting/cores and casting/dies interfaces have been assigned the *Average* condition, representing an acceptable value directly from the QuikCAST library.

The *Contact Resistance* condition models the resistance between molten metal and cores and dies during filling. It has a noticeable impact on the flow of metal inside the cavity. It is employed to enhance the simulation results' similarity to real-world conditions. In this case, the condition is implemented at the casting and mould, as well as casting and cores interfaces, with a thermal resistance value of $\mathbf{0.0033}\ (\mathbf{m^2 \cdot K})/\mathbf{W}$.

Simulation Parameters

After defining all the information regarding boundary conditions, it is also necessary to define the simulation parameters that rule the second simulation (filling simulation) – Figure 59.

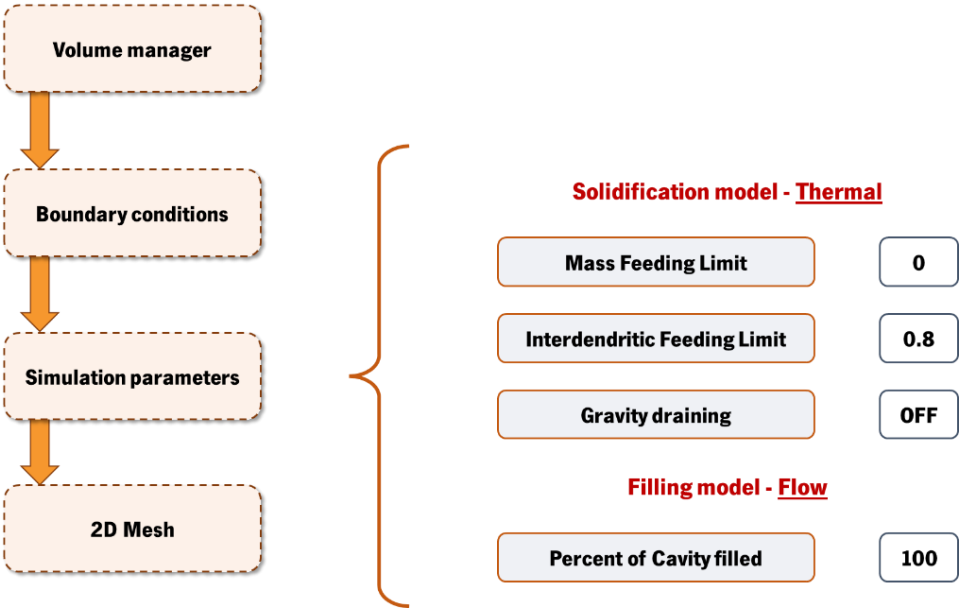

Figure 59: Simulation parameters defined for the second simulation.

In the QCA General Parameters (Figure 60 (a)), the initial step involves defining the *Simulation Type* as Flow and Thermal, with the *Calculation Type* set to Start from the mould thermal field. This choice is influenced by the filling process considering the thermal map obtained in the preliminary simulation. Additionally, it is crucial to deactivate the accelerated filling option within this window to ensure more precise outcomes. Furthermore, the parameter for *Solidification Maximum* should be configured to **0.1**, indicating that the incremental difference during solidification does not exceed this value. This refinement contributes to enhanced accuracy, although it may slightly extend computation time and stress. Finally, in the QCA General Parameters section, the *End of Filling Criteria* is established at **0.99**. This particular value is chosen as LPDC shrinkage compensation is contingent on the applied duration pressure. Opting for higher values signifies that pressure compensation is computed over an extended period.

In the QCA Thermal settings (Figure 60 (b)), a key parameter to consider is the *Porosity Model*, which governs the occurrence or absence of porosity in the outcomes. For the current scenario, it is recommended to configure the *Mass Feeding Limit* to **0**, and the *Interdendritic Feeding Limit* should be set to **0.8**. These choices are substantiated by the fact that the alloy being poured is copper zinc based, and the casting procedure employed involves the application of pressure.

At last, in the QCA Flow settings (Figure 60 (c)), except the initial simulation, the only parameter requiring adjustment is found under *Additional Variables*. Here, the parameters for Air Entrainment and Maximum Velocity are added to assess the presence of air within the cavity and determine the maximum velocity of the liquid metal inside the cavity.

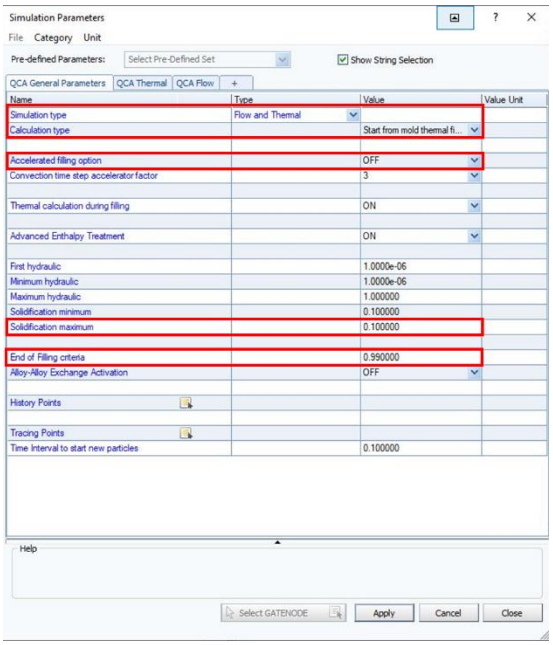

(a)

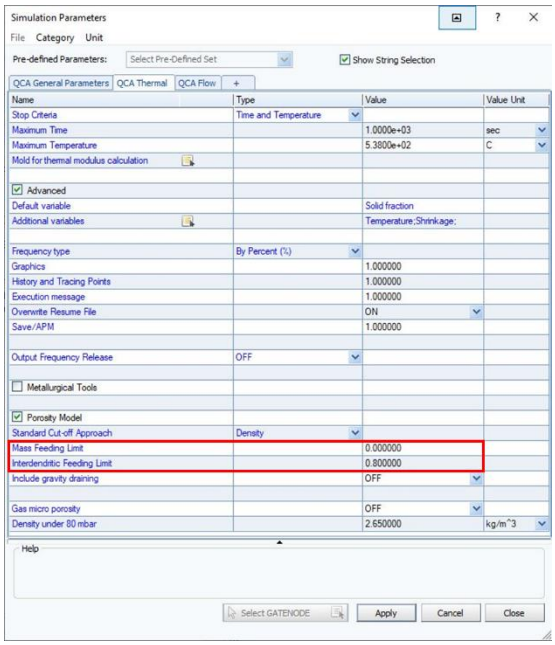

(b)

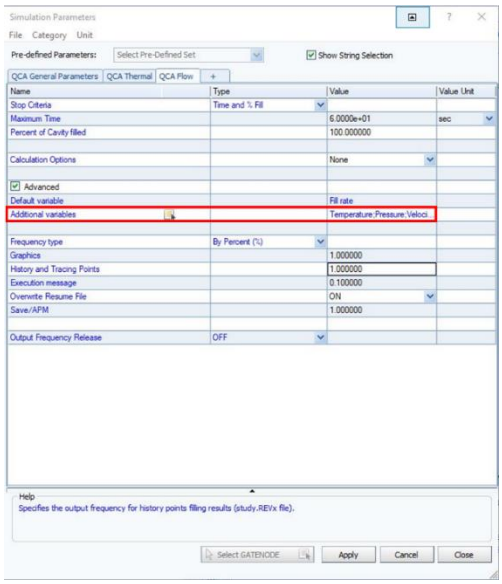

(c)

Figure 60: Parameters used for (a) QCA General Parameters, (b) QCA Thermal and (c) QCA Flow.

2D Mesh

Finally, as mentioned earlier, QuikCAST uses the finite differences method for domain discretisation (Chapter 4.1). Consequently, it is essential to specify the dimensions of a "Grid" that includes the casting and will be used by the Solver to apply the filling equations.

As defined in the first simulation, the *Average Size* parameter (Figure 61) was set to 2 mm for each element in the areas near the previously defined Volume – *Peca*. Additionally, the *Maximum Growth Rate* parameter (Figure 61) determines the growth factor for elements further away from the selected Volume. A higher value generates a coarser mesh in the surroundings, while a lower value yields a finer mesh. Therefore, a value of 1.1 mm was chosen, indicating a finer mesh configuration.

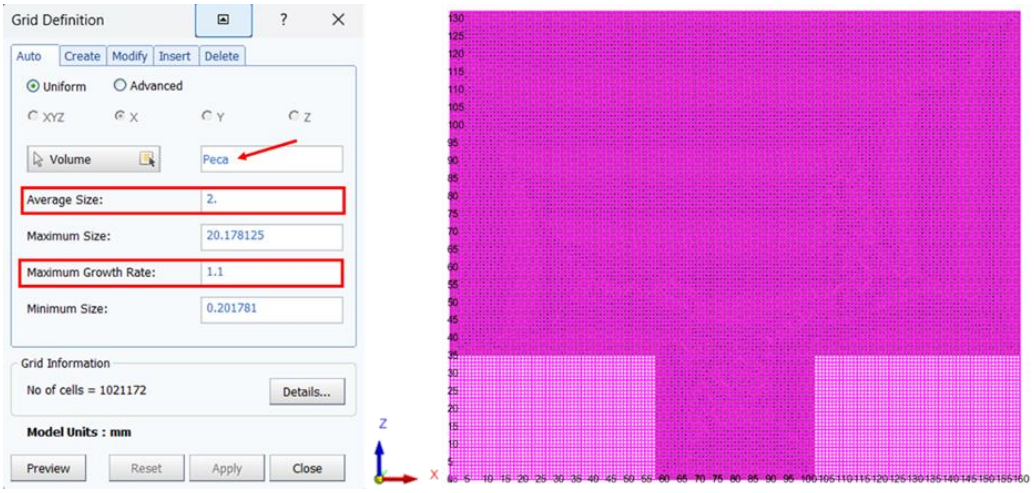

Figure 61: Parameters used for the definition of the "Grid".

4.7. CHAPTER REFERENCES

[1] NADCA, *Gating Manual*, 1st ed., vol. 1. Illinois, 2006.

[2] T. Siik, "THE VERIFICATION OF LOW-PRESSURE DIE CASTING SIMULATION RESULTS," Master of Science Thesis, Tampere University of Technology, Tampere, 2011.

[3] C. A. Monroe and C. Beckermann, "Deformation during casting of steel: model and material properties," *Proceedings of the 61st SFSA Technical and Operating Conference*, Chicago, 2007. [Online]. Available: https://www.researchgate.net/publication/268182958

[4] Z. Chen, Y. Li, F. Zhao, S. Li, and J. Zhang, "Progress in numerical simulation of casting process," *Measurement and Control (United Kingdom)*, vol. 55, no. 5–6, pp. 257–264, May 2022, doi: 10.1177/00202940221102656.

[5] H. Hendrayana, "Introduction to Groundwater Modeling," 2012, doi: 10.13140/RG.2.1.2614.4163.

[6] N. Hall, "Navier-Stokes Equations," *NASA*, May 13, 2021. https://www.grc.nasa.gov/WWW/k-12/airplane/nseqs.html (accessed Jul. 09, 2023).

[7] X. Yuwen, L. Chen, and Y. Han, "Numerical Simulation of Casting Filling Process Based on FLUENT," *Energy Procedia*, vol. 17, pp. 1864–1871, 2012, doi: 10.1016/j.egypro.2012.02.324.

[8] TheMetalCasting.com, "Casting Core Design and Analysis," *TheMetalCasting.com*. https://www.themetalcasting.com/casting-core-design-analysis.html (accessed May 29, 2023).

[9] "Key sand casting design considerations," *Engineering product design*. https://engineeringproductdesign.com/key-sand-casting-design-considerations/ (accessed May 30, 2023).

[10] "The importance of draft angle in Injection molding service," *Makenica*, Jul. 03, 2021. https://makenica.com/draft-angle-in-injection-molding-service/ (accessed May 29, 2023).

[11] R. M. Nunes, *ASM Handbook - Casting*, 4th ed., vol. 15. ASM International, 1998.

[12] Anton, "Technology and equipment for serial casting of aluminum wheels for automotive market," *SA Foundry*, May 07, 2021. https://sa-foundry.com/tehnologiya-i-oborudovanie-dlya-serijnogo-litya-alyuminievyh-diskov/?lang=en (accessed Aug. 17, 2023).

[13] ESI Group, "LPDC," 2016. [Online]. Available: www.esi-group.comwww.esi-group.com

[14] Giesserei Lexikon, "Mold filling time." https://www.giessereilexikon.com/en/foundry-lexicon/Encyclopedia/show/mold-filling-time-4680/?cHash=f23bad90680ebeb815631ca00f02db27#:~:text=Mold%20filling%20time%20Time%20needed%20by%20a%20melt,downsprue%2C%20runner%2C%20ducts%20and%20gates%20%28see%20Gating%20system%29. (accessed Aug. 18, 2023).

[15] Giesserei Lexikon, "Mold filling time in pressure die casting." https://www.giessereilexikon.com/en/foundry-lexicon/Encyclopedia/show/mold-filling-time-in-pressure-die-casting-4681/?chash=bc0ea50304f0ac5b26882d05ff58a249&cHash=8f4e0bc1dc7e5f3177906b1319199a2f (accessed Aug. 18, 2023).

[16] ESI Group, "ProCAST LPDC cycling."

[17] R. M. Nunes, *ASM Handbook - Casting*, 4th ed., vol. 15. ASM International, 1998.

[18] A&B Die Casting Projects, "How Important is Temperature when you are Die Casting?," *A&B Die Casting Projects*. https://www.abdiecasting.com/how-important-is-temperature-when-you-are-die-casting/ (accessed Jun. 17, 2023).

[19] The Library of Manufacturing, "The Metal Casting Operation," *The Library of Manufacturing*. https://thelibraryofmanufacturing.com/metalcasting_operation.html (accessed Jun. 17, 2023).

[20] J. R. Davis, Davis & Associates, and W. W. Scott, *ASM Specialty Handbook - Copper and Copper Alloys*, 1st ed. 2001. [Online]. Available: www.asminternational.org

[21] Pacific Die Casting, "Brass Die Casting," *Pacific Die Casting*. https://pacdiecast.com/brass-die-casting/ (accessed Jun. 22, 2023).

[22] H. Puga, J. Barbosa, T. Azevedo, S. Ribeiro, and J. L. Alves, "Low Pressure Sand Casting of Ultrasonically Degassed Al7SiMg Alloy: Modeling and Experimental Validation of Mould Filling".

[23] P. Fu *et al.*, "Low-pressure die casting of magnesium alloy AM50: Response to process parameters," *J Mater Process Technol*, vol. 205, no. 1–3, pp. 224–234, Aug. 2008, doi: 10.1016/j.jmatprotec.2007.11.111.

[24] M. Guofa, L. Xiangyu, W. Kuangfei, and F. Hengzhi, "Numerical simulation of low pressure die-casting aluminum wheel."

[25] ESI Group, *QuikCAST: Reference Manual*. 2014.

[26] Inc. Midland Technologies, "Reducing Porosity: High Pressure Die Casting," *Midland Technologies, Inc.*, Mar. 22, 2021. https://midlandtechnologies.com/reducing-porosity-high-pressure-die-casting/ (accessed Jul. 03, 2023).

Chapter 5 - RESULTS AND VALIDATION

The results chapter aims to present and analyse the study's outcomes on developing a gating system for the bathtub mixer using the Low-Pressure Die Casting technique. This chapter provides a comprehensive overview of the findings obtained through the application of theoretical concepts of Die gating. The primary objectives of this analysis are to assess the performance of the optimized gating system in reducing rejection rates, identify and predict potential defects in the designed model, and validate the numerical results through comparison with experimental data.

The experimental work of this thesis consisted of designing the gating system for producing a bath mixer, using casting simulation to predict and prevent defects that might occur. Hence, the QuikCAST software, developed by the ESI Group, is used to determine the numerical results, which are later assessed with experimental data.

Firstly, this chapter presents the numerical results obtained from QuikCAST. These results are based on the simulation of the thermal die cycling and then, filling processes, considering each boundary conditions used, which were outlined in Chapter 4.6.1. The numerical simulations provide insights into various aspects of the casting process, including die temperature distribution, solidification behaviour, and the occurrence of defects.

Subsequently, the focus will shift to the experimental findings, involving a meticulous visual inspection of casting samples from areas exhibiting defects. Beyond visual examination, a detailed observation under a microscope was also conducted to delve deeper into the microstructural aspects of the defects. These results will shed light on the precise origins of these defects, contributing to a more accurate understanding of the underlying factors that lead to flaws.

5.1. Numerical Results

The numerical simulation aims to predict defects in the modelled gating system for the bathtub mixer and understand the filling behaviour of the molten metal. It is important to note that the results are sensitive to the initial conditions set for the simulation. This study conducted simulations with different gating system geometries to determine the optimal design.

5.1.1. Thermal Die Cycling Simulation

In line with the discussions in Chapter 4.6.1, the initial step entails conducting the thermal die cycling simulation, which yields a comprehensive thermal mal of the die's behaviour throughout the casting process. This map eases a detailed analysis of the effects of each filling cycle on the die's properties and behaviour. Furthermore, it aids in assessing the necessity of integrating cooling systems (with water or oil) to extend the dies' lifespan and maintain their desired properties. Figure 62 illustrates the 3D model used for this simulation.

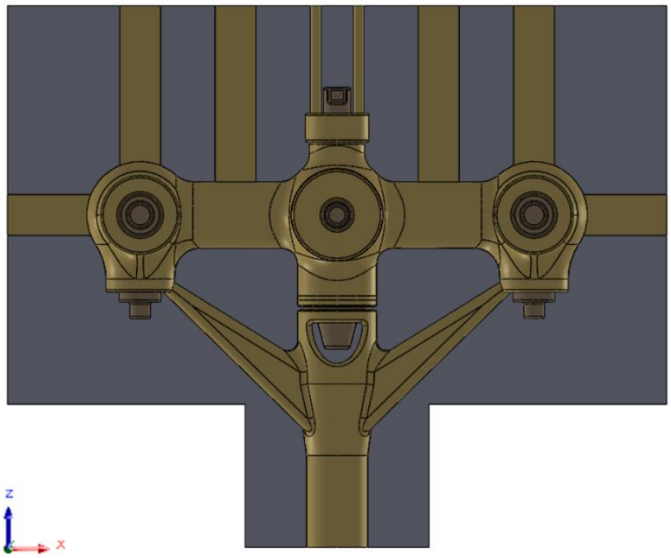

Figure 62: 3D model used for the first simulation.

Note: throughout this work, only the parameters related to the component filling were modified, while the results obtained in the thermal die cycling simulation remained constant. Therefore, the analysis of this simulation will focus solely on this configuration, considering that the subsequent geometries are identical.

The thermal map identifies critical die zones by analysing the temperature gradient during the solidification cycling process:

(a) Start of solidification (0 s → 6 s):

The thermal die cycling simulation starts with the solidification of the casting, between 0 s and 6 s, since the filling process is removed, as stated before in Chapter 4.6.1. At this stage, the entire cavity is filled, and all parts are at a high temperature, above 300°C, as the casting is poured at 988°C and initiates its solidification process, as shown in Figure 63.

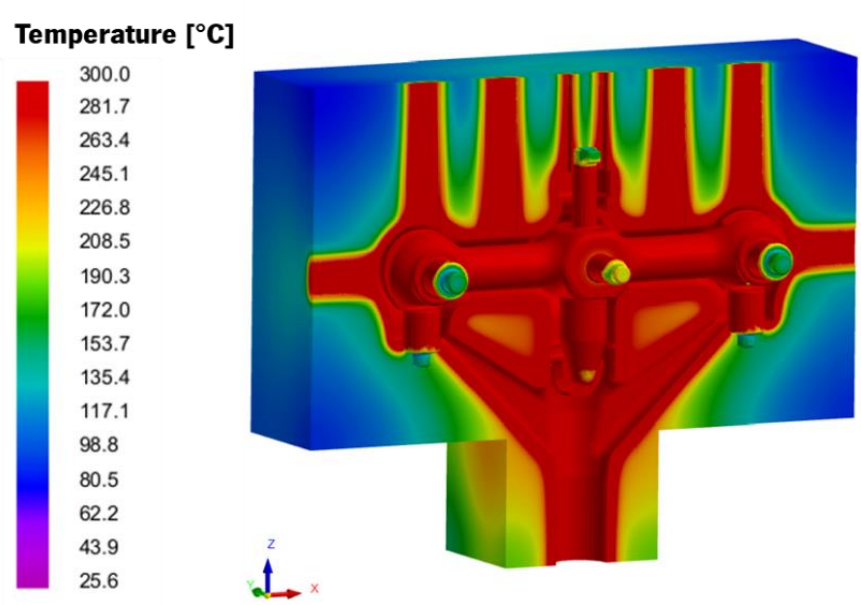

Figure 63: Temperature gradient at the beginning of the solidification.

(b) Die opening and casting ejection (8 s → 12 s):

After the complete solidification of the casting, the dies are opened, and the casting is removed from the inside. As a result, the temperature of the die drops slightly (Figure 64), decreasing from 300°C to approximately half, around 150°C, due to its contact with the external environment.

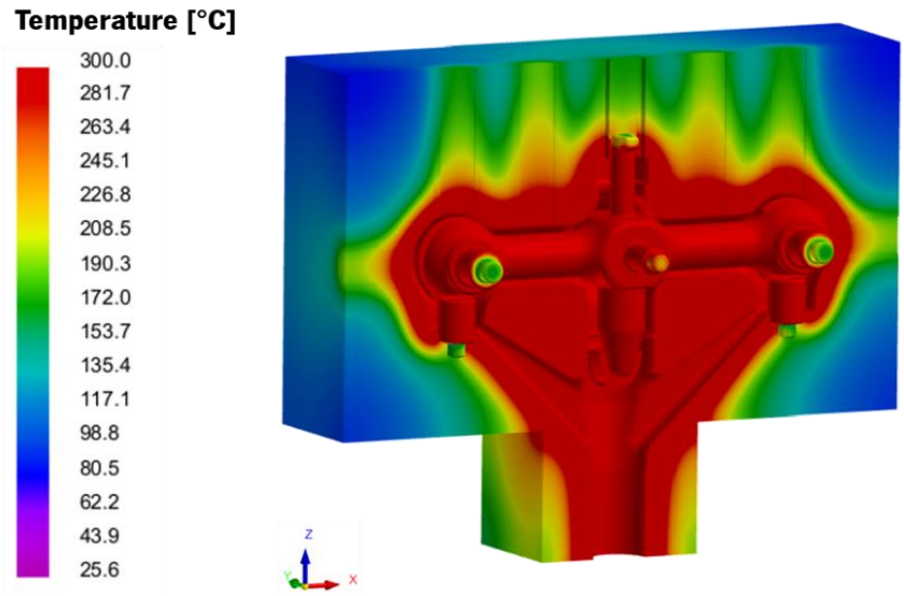

Figure 64: Temperature gradient during die opening and casting removal.

(c) Die spraying (13 s → 16 s):

After that, the dies are immersed in a water and graphite bath, inducing a rapid cooling process. The temperature of the dies further decreases from around 150°C to about 80°C, as presented in Figure 65.

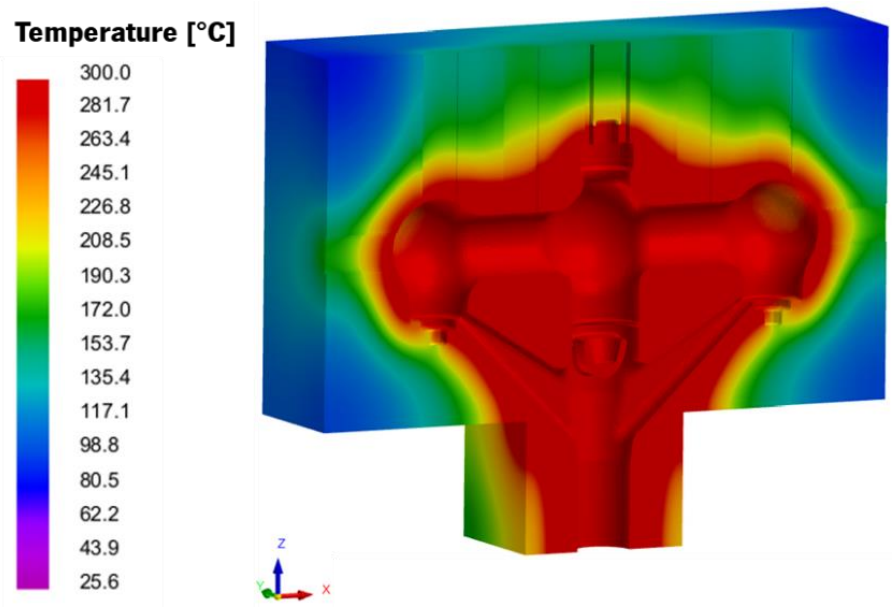

(a)

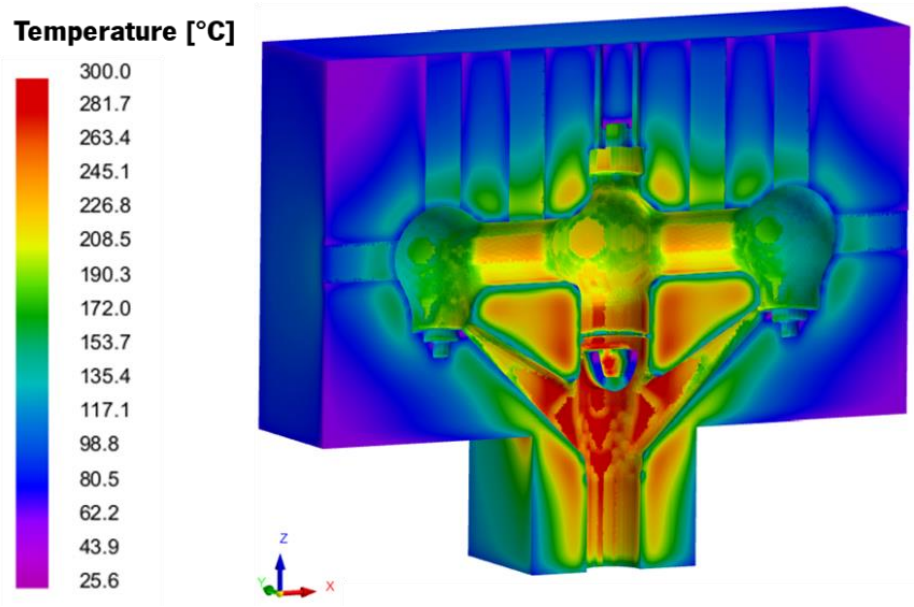

(b)

Figure 65: (a) Dies before die spraying; (b) Sudden cooling of the dies, due to die spraying on water and graphite.

(d) Die cooling in contact with the external environment (17 s → 18 s):

After plunging and cooling the dies, their temperature gradually reaches an equilibrium value as they continue cooling, as shown in Figure 66 (a). This phenomenon occurs because the interior of the moulds is not entirely cooled during die spraying, leading to the interior heating the exterior through thermal conduction. As a result, the temperature rises from 150°C to almost 300°C.

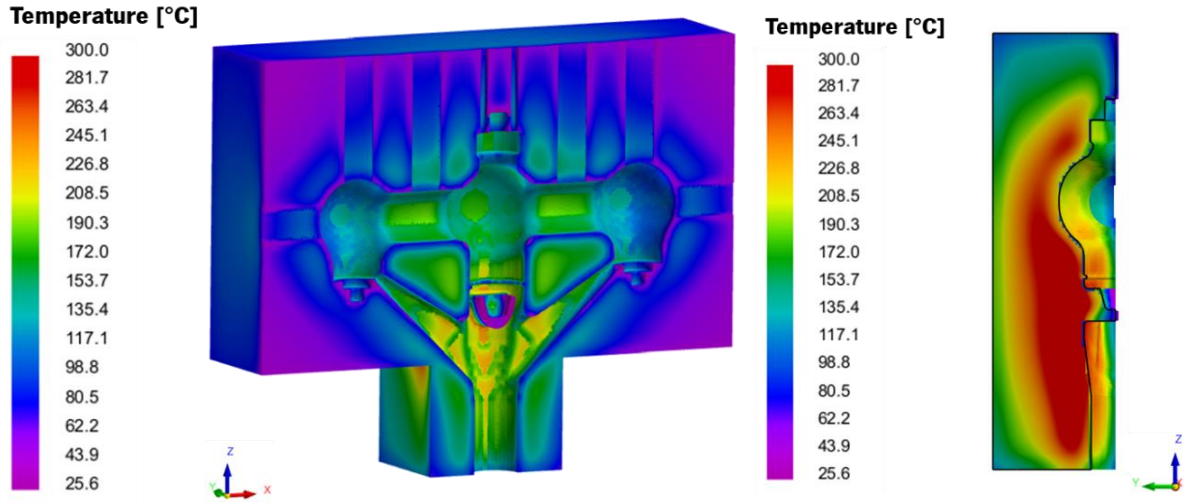

(a) (b)

Figure 66: (a) Increase of the external temperature of the die, compared to the previous stage; (b) Detail of the interior mould temperature after die spraying.

(e) Cores positioning (18 s → 31 s):

Upon analysing Figure 67 (a), it is evident that at 18 s, the cores remain at a high temperature, indicated in red, as they are still in contact with the casting. However, at 19 s (Figure 67 (b)), the new cores placed inside the mould are represented in purple and display a lower temperature (approximately 35°C), which corresponds to their initial temperature, as defined in Chapter 4.6.1.

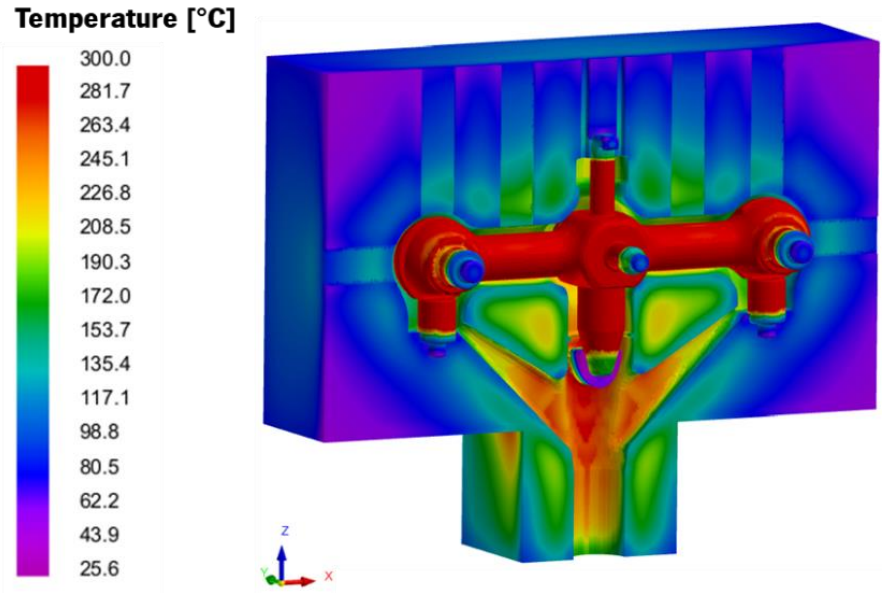

(a)

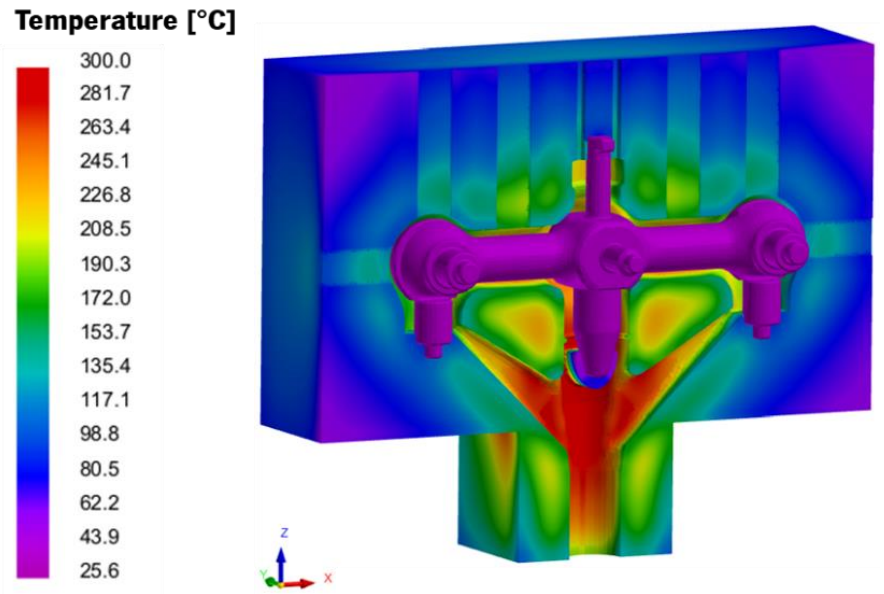

(b)

Figure 67: Cores temperature (a) at 18 s, still in contact with the casting; (b) at 19 s, after new cores are placed inside the moulding.

(f) Die closing and end of cycle (33 s → 45 s):

Finally, after the cores are placed, the dies are closed (bringing the two dies in contact with each other). The temperature of the cores increases slightly, especially in the regions in contact with each die, as shown in Figure 68. Subsequently, the moulds are closed, and the cavity is refilled until 45 s, completing a full filling and solidification cycle.

It is important to note that in this simulation, the temperatures of the dies during the filling process are not presented, as the parameters inserted are solely related to thermal cycling.

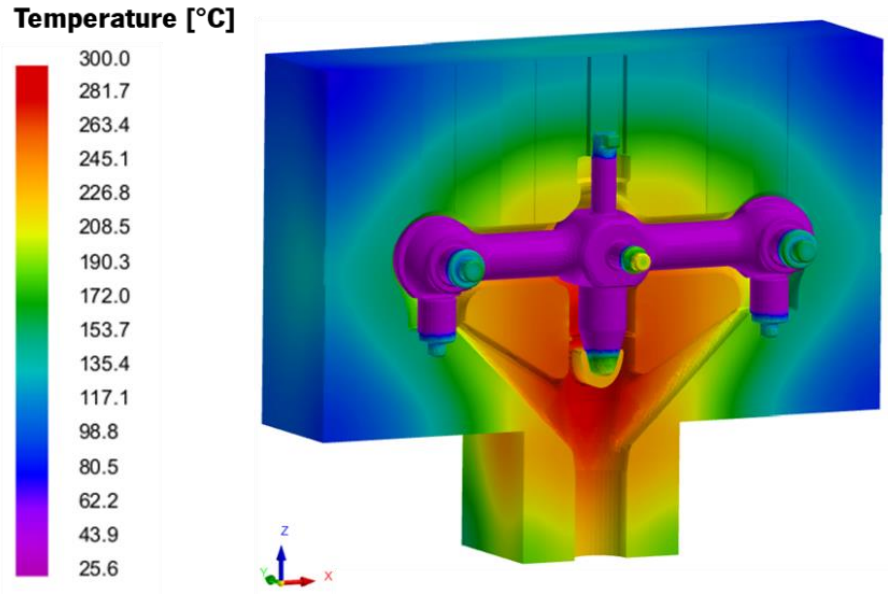

Figure 68: Die closing and increase of the cores' temperature in the areas in contact with the two moulds.

Based on the conclusions presented earlier, it is equally significant to illustrate the variation of die temperature over time. This analysis identifies the cycle at which the system converges to a steady-state regime. Figure 69 displays the locations of the points used for this analysis.

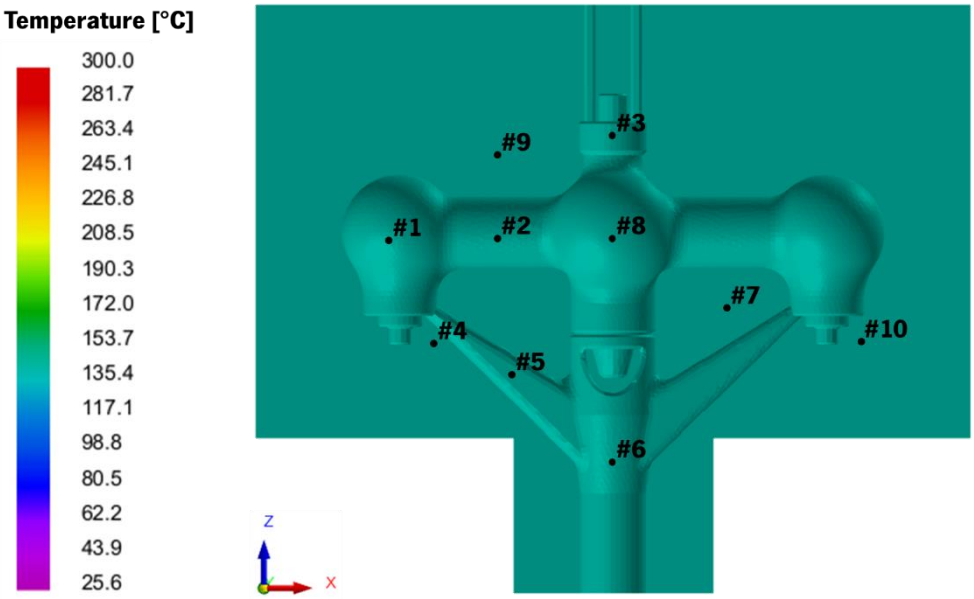

Figure 69: Location of the monitoring points used in the analysis.

Using the points in Figure 69, a temperature graph as a function of time was obtained for each point (Figure 70).

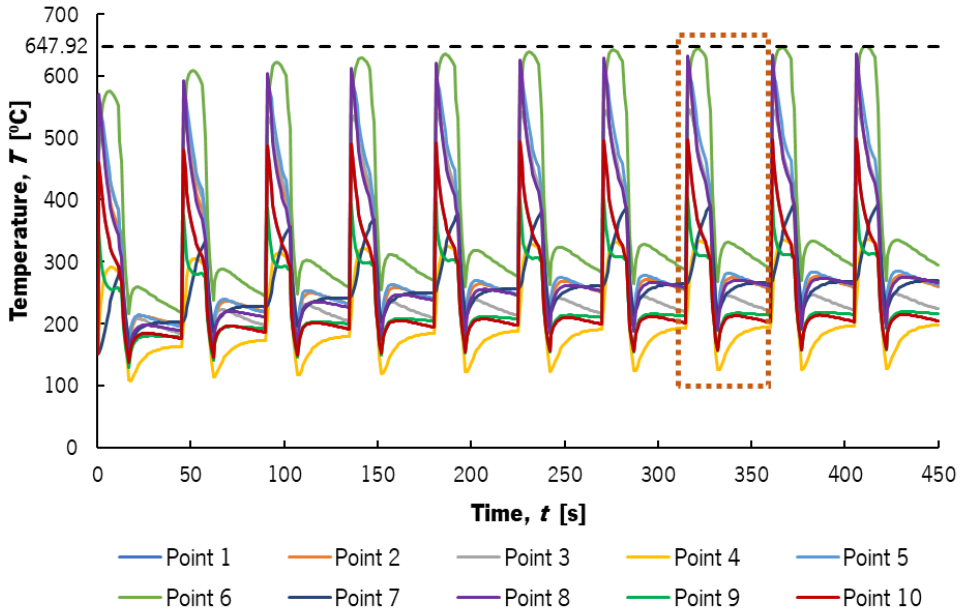

Figure 70: Graph representing the variation of temperature with time on each monitoring point.

By analysing Figure 70, it is evident that the steady-state regime is achieved after approximately **eight cycles**, indicating that the temperature behaviour remains consistent for subsequent cycles. Therefore, the thermal die cycling simulation can be simplified to only eight cycles. Additionally, it is observed that the initial die temperature (during the first cycle) is 150°C, corresponding to the initial temperature defined for each component in Chapter 4.6.1. As expected, with each cycle, the die

temperature gradually increases since it is impossible to cool down the temperature of the moulds at the end of each cycle.

Considering the sequence of cycles, it is also possible to analyse the temperature variation over time for a single cycle, as shown in Figure 71.

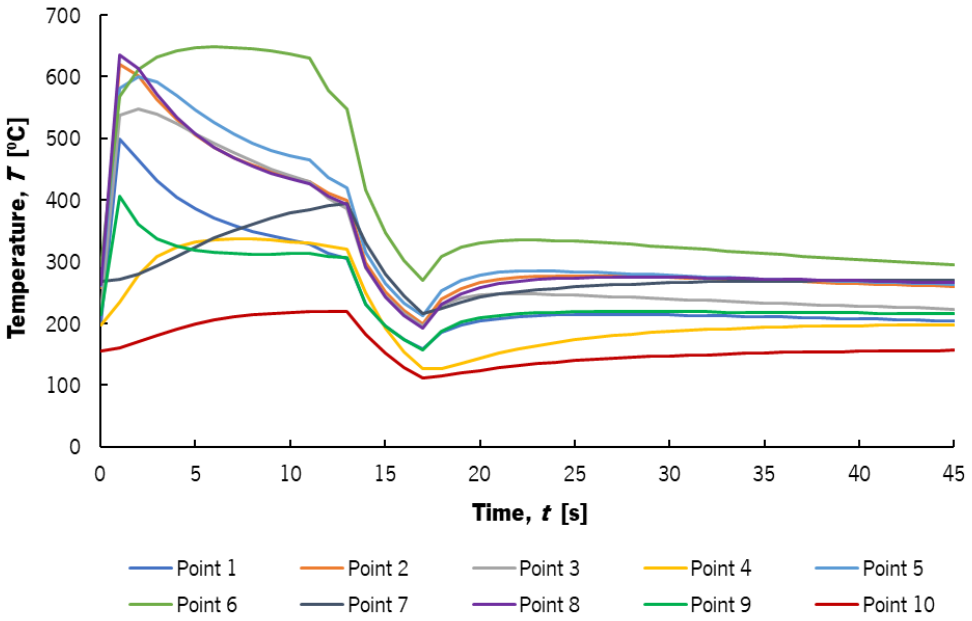

Figure 71: Variation of temperature over time, for one cycle.

Figure 71 shows that the die temperature at the start fluctuate between 150ºC and 200ºC, which corresponds to the initial cavity temperature. Following the filling process, the casting starts to solidify, resulting in an increase in temperature in all points, with Point 6 (Figure 71) registering the highest temperature. Point 6 is in the gating system, where the temperature is kept higher (988ºC) to compensate for the solidification of the entire casting. Therefore, it tends to be the last area to solidify.

Between 13 s and 16 s, there is a decline in temperature at all locations due to the immersion of the dies in the graphite bath, which is at a lower temperature (approximately 80ºC). After the bath ends at about 16 s, the temperature rises slightly.

From 16 s until 45 s, the temperature remains constant (approximately 150ºC to 300ºC), corresponding to the placement of the cores, die closing, and the end of the die cycling process.

5.1.2. Filling and Solidification Simulation

After the thermal die cycling simulation, the cavity-filling process is performed using the thermal map of the die obtained in the previous step. Hence, this chapter will focus entirely on analysing three gating system geometries used, emphasising the results of solidification.

Note: twelve different attempts were made, but to simplify this project, only the most important are discussed.

A. GATING SYSTEM V1

The 3D model used for the first iteration is illustrated in Figure 62, which is the same as for Thermal Die Cycling. Additionally, Table 12 summarizes the parameters applied to the model, which were previously discussed in Chapter 4.6.2.

Table 12: General process conditions used for the *Gating System V1*.

Pouring Temperature, T_{pouring} [°C]	988
Core Temperature, T_{cores} [°C]	35
Die Coating	Graphite

Apart from the applied conditions, it is also essential to determine the pressure curve required for the casting machine. As discussed earlier, the pressure curve employed in the simulation differs slightly from the one utilized in the machine, as the simulation does not account for the pressure required to pull the metal from the furnace to the rise tube.

Chapter 4.6.2 provides detailed documentation of the equations used to calculate the pressure curve, including the Equation of Continuity and the Bernoulli Equation. The simulation employed Equation (4.12) to determine the pressure curve. Additionally, Table 13 presents the metal's properties and the gating system's height used in the calculations.

Table 13: Metal and Gating system's properties used to determine the pressure.

Metal density, ρ [$\mathbf{kg/m^3}$]	6660.88*
Gravitational acceleration, g [$\mathbf{m^2/s}$]	9.81
Gating system height, $\mathbf{h_{gating}}$ [mm]	212.4
Rise tube height, $\mathbf{h_{rise\ tube}}$ [mm]	250

*At $T = 983.75°C$

Therefore, by replacing the values of Table 13 in Equation (4.12), the maximum pressure of 0.165 bar is obtained. Figure 72 illustrates the simulation and machine curves used for this gating system. Note that in the 3D model (Figure 62), the rise tube is not considered, which means the pressure required to lift the metal from the furnace to the rise tube is excluded from the simulation curve. Only the pressure related to the cavity-filling process is calculated and considered in the results.

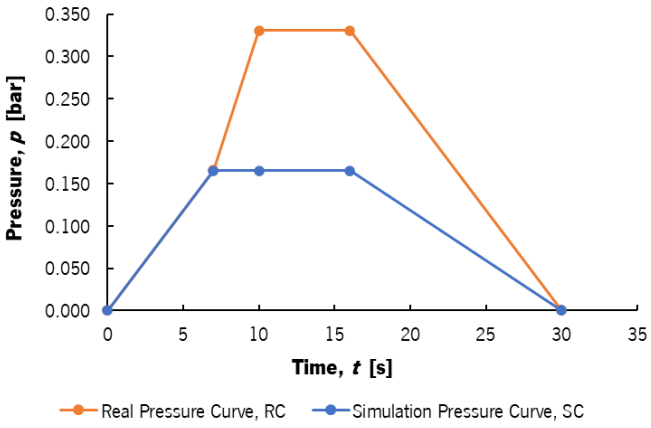

Figure 72: Simulation and real pressure curves used in *Gating System V1*.

The critical parameters used to assess the performance of the *Gating System V1* are discussed.

(a) Shrinkage porosity and Misrun:

As discussed in Chapter 2.3, shrinkage porosities are solidification defects that result from the volumetric contraction of the casting, during solidification. The component's geometry and the pouring metal influence their location and size, making it crucial to comprehend their impact on the final shape of the component. In contrast, misruns occur immediately after the filling process when the cavity is not filled, primarily due to the inefficient working of the gating system.

The results of shrinkage porosity and misruns for *Gating System V1* are shown in Figure 73. Shrinkage porosities are represented in purple, indicating empty spaces that correspond to 0% of the material. On the contrary, misruns are depicted in red or blue, appearing as empty spaces, but generally containing 100% air inside the cavity. The colour scale used helps differentiate these defects in the simulation comparison.

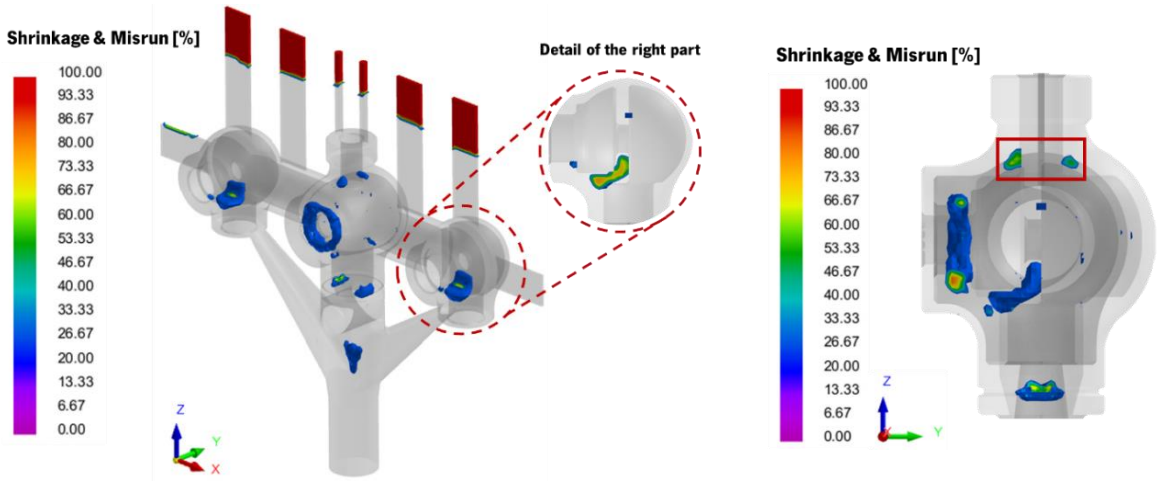

(a) (b)

Figure 73: (a) Shrinkage Porosities and Misruns; (b) Detail of Porosities and Misruns on YZ plane.

After analysing Figure 73, several observations can be made:

i. The upper body of the vents exhibits misruns, resulting from the metal not reaching the top of the mould. However, since these areas are not part of the casting, they do not affect its final shape.

ii. All three bodies of the bathtub mixer display shrinkage porosities. The side parts are prone to this defect due to varying thickness in that region (see detail in Figure 73 (a)), and therefore it is not possible to eliminate it. In the central part is a "ring" of shrinkage porosities since this area is situated inside the mould without compensation from the gating system.

iii. Figure 73 (b) reveals porosities at the upper body, which may also occur in the actual casting.

The occurrence of shrinkage porosities in the central and side bodies is primarily attributed to the solidification of the gating system (Figure 74 (a)) before the entire casting reaches a temperature below the solidus temperature. This premature solidification leads to the formation of shrinkage porosities in those regions (Figure 74 (b)).

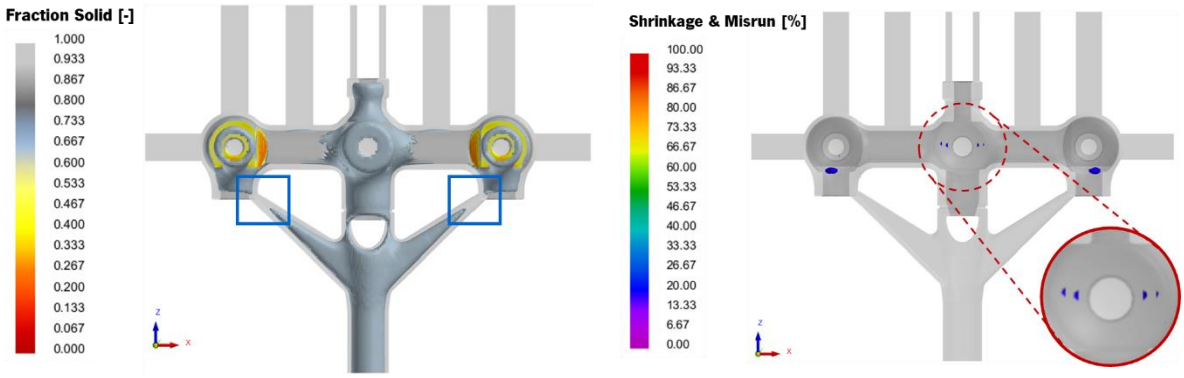

(a) (b)

Figure 74: (a) Solid fraction, after the solidification of the gate; (b) Formation of shrinkage porosity, due to the solidification of gate.

(b) Maximum velocity:

To prevent metal oxidation and the formation of porosities, the maximum admissible filling velocity (Figure 75) for the brass casting is 0.5 m/s. This value is also adopted for aluminium, as no record of an admissible maximum velocity is available for brass alloys. This conservative approach ensures a cautious and reliable casting process.

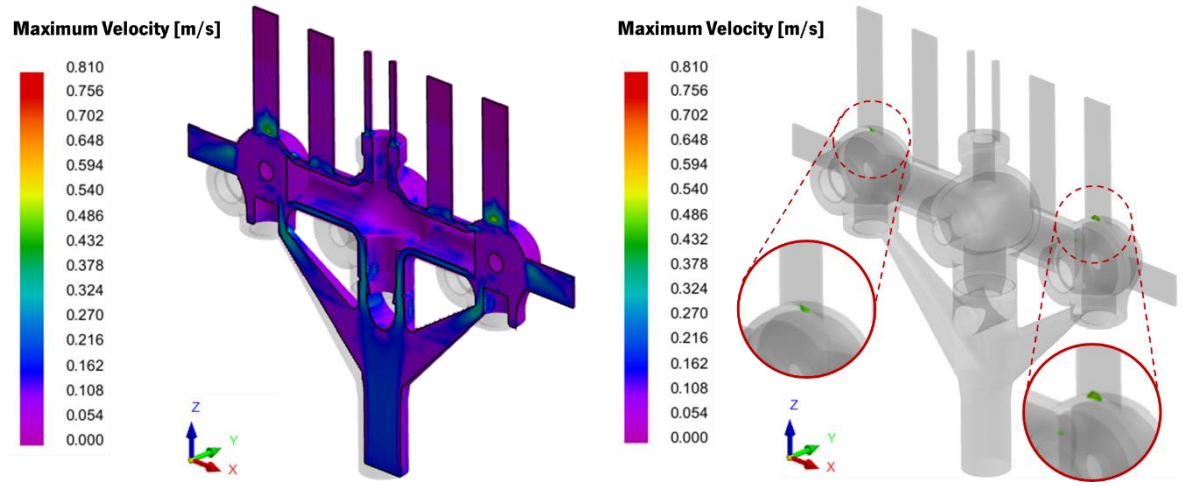

(a) (b)

Figure 75: (a) Velocity gradient of the cavity; (b) Identification of the locations where the velocity is above 0.5 m/s.

After analysing Figure 75 (a), it is evident that most of the cast part exhibits a maximum velocity significantly lower than the admissible value of 0.5 m/s. In most regions, the velocity achieved ranges from 0.2 m/s to 0.4 m/s. Only in the transition regions between the cast part and the vents is a higher velocity, as shown in Figure 75 (b). This increase in velocity is likely due to the smaller section area of the vents.

Another important parameter related to the velocity is the filling time of the system, which is the time needed to fill the entire cavity. There are no established values for this criterion; nonetheless, a range of 2 s to 3 s is acceptable. Concerning the Gating System studied, the obtained filling time of 6.11 s is slightly higher than the theoretical value.

Note: it is crucial to consider the time required for the metal to rise from the riser tube, which is also approximately 3 s. Therefore, the total filling time, including the metal rising time, falls within 5 s to 6 s.

(c) Air entrainment:

Air entrainment occurs when air becomes trapped inside the cavity during the filling process, leading to casting defects after solidification. This issue can be mitigated through a well-designed air ventilation system.

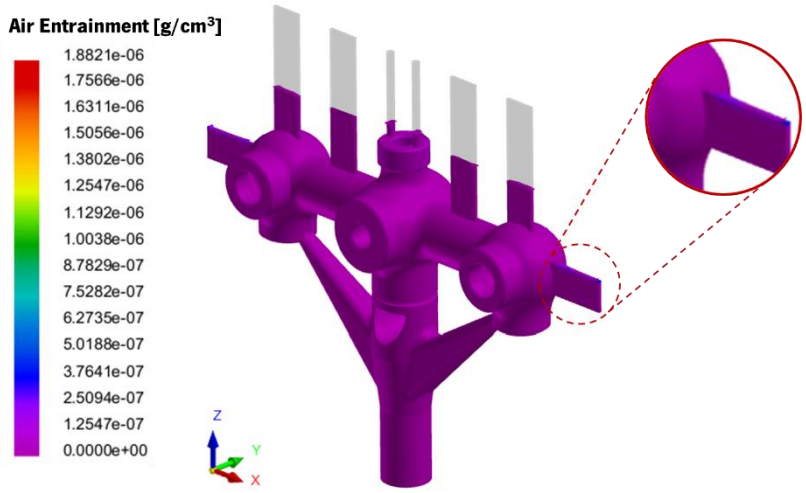

Figure 76: Air entrainment for the System V1.

Figure 76 indicates no air trapped inside the cavity, as the entire cavity is shown in purple, indicating the absence of air, as referred by the scale. This conclusion confirms that the venting system is well-designed and appropriately sized for the entire system.

Conclusions about *Gating System V1*

Based on the overhead statements, the following conclusions can be drawn:

i. Shrinkage porosities are present in all three bodies of the bathtub mixer, and they result from inadequate compensation, due to premature solidification of the gating channel (which also works as a feeder).

ii. The misruns observed at the top of the vents do not affect the final shape, as these regions will be removed after pouring.

iii. The maximum velocity of the system ranges between 0.2 m/s and 0.4 m/s, which is significantly lower than the admissible value of 0.5 m/s.

iv. The gating channel shows no air entrainment, indicating that the air ventilation project extracts all air inside the cavity.

In conclusion, increasing the gate area could minimize the formation of shrinkage defects. The location and dimensions of the vents are reasonable, and the pressure curve is also adequate. Although the filling time is slightly longer than the theoretical value previously calculated, most of the results are favourable.

B. Gating System V2

Considering the earlier conclusions, the second simulation (*Gating System V2*) employed the 3D model shown in Figure 77 (a). In this case, the gate area was increased to provide more material to

compensate for the natural contraction. The specific dimensions of the area considered are also indicated in Figure 77 (a).

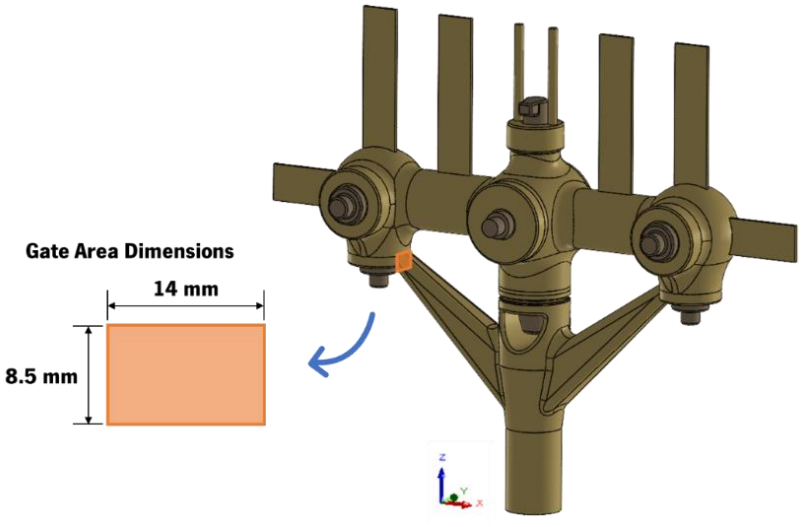

(a)

(b) (c)

Figure 77: 3D model used for the second simulation - *Gating System V2* (a) with the dimensions; Gate area in (b) V1 and (c) V2.

Since the purpose of this simulation is to evaluate the impact of the gate area on the results, the simulation parameters and pressure curve are equal to the previous simulation.

(a) Shrinkage porosity and Misrun:

Figure 78 presents the results obtained for shrinkage porosity and misruns, in the second simulation:

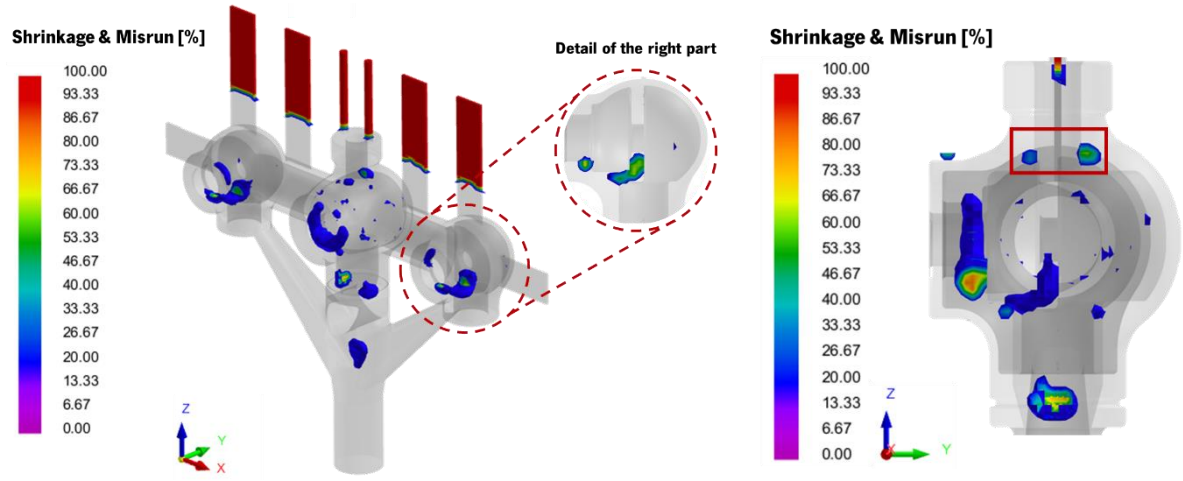

(a) (b)

Figure 78: (a) Shrinkage Porosities and Misruns, for the *Gating System V2*; (b) Detail of Shrinkage Porosities and Misruns on YZ plane.

Figure 78 displays the porosities and misruns expected to happen in the bathtub mixer, and several considerations can be made:

i. Shrinkage porosity may form in all three bodies of the casting. On the central body, there is no "ring" of porosity (Figure 78 (b)), contrary to V1. This might be a result of the higher dimensions of the gate area. The porosity on the two side bodies appears smaller but extends to the outside are where the thread is located - Figure 78 (a).

ii. In terms of misruns, similar to the previous simulation, most vents are red, indicating that these areas will not be filled with metal. Although they do not affect the final component, it is necessary to be cautious with the central body to prevent the red volume from being near the casting surface.

As expected, the formation of shrinkage porosity is directly associated with the premature solidification of the gating channel, as can be seen in Figure 79. The moment when the casting is separated from the gating channel (Figure 79 (a)) is when shrinkage appears in all three divisions of the mixer, as appears in Figure 79 (b). The separation of the casting and gating channel is the cause of shrinkage occurring in all bodies since they are not instantly above the gate area and cannot be adequately compensated.

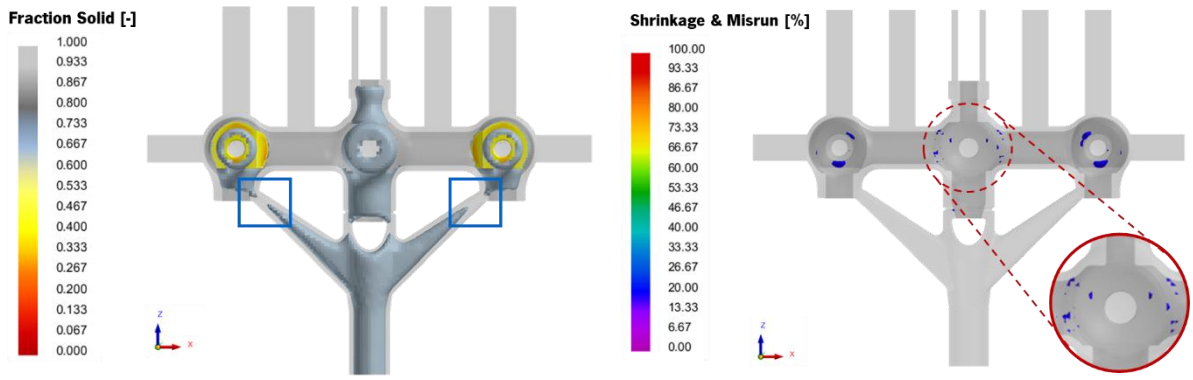

(a) (b)

Figure 79: (a) Solid fraction; (b) Formation of shrinkage porosity, due to the solidification of gate.

Regarding the filling time, this system obtained 6.8 s, which is also slightly higher compared to the theoretical value. This result was expected to be similar to the V1 model, as the pressure curve is the same.

(b) Maximum velocity:

In Figure 80, the overall graph displays the maximum velocity achieved in the bathtub mixer, during the filling process.

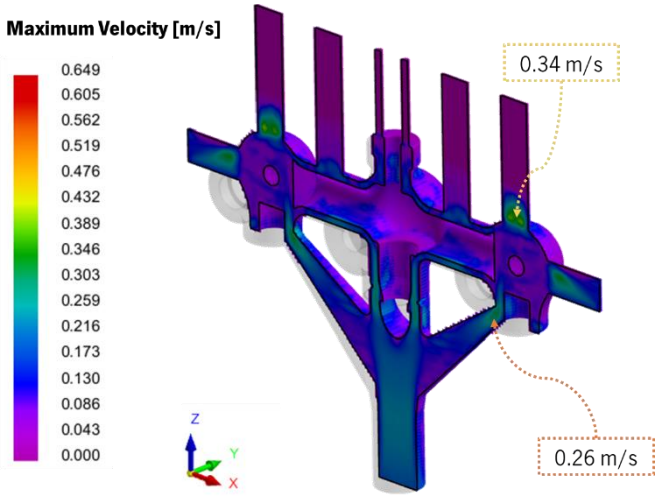

Figure 80: Maximum velocity recorded for the *Gating System V2*.

By analysing Figure 80, the maximum velocity recorded is lower than the admissible value of 0.5 m/s: the maximum values vary from 0.26 m/s and 0.34 m/s. The areas more susceptible are the gate area and near the vents because, in these regions, there is a striction in terms of areas. As mentioned earlier, according to the Equation of Continuity, this phenomenon can be linked that decreases the velocity when area increases.

(c) Air entrainment:

Lastly, it is crucial to consider that increasing the gate area also enlarges the gating system, potentially leading to more air being trapped inside the cavity. Therefore, examining the Air Entrainment parameter is important to ensure that all air is removed (Figure 81).

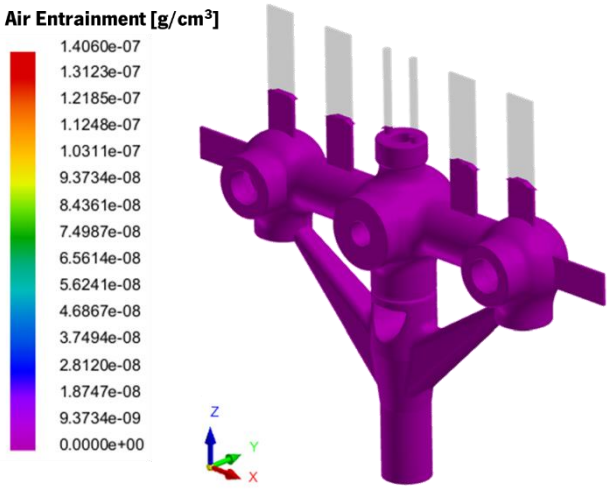

Figure 81: Air entrainment for the System V2.

Figure 81 demonstrates the successful air extraction from the cavity, as indicated by the purple colour in the model. The purple cavity confirms that the alteration to the gating channel did not impact the venting system, denoting that the current system is suitable and effective in removing air from the cavity.

Conclusions about *Gating System V2*

i. Shrinkage porosities are present in all three parts of the component, with a smaller "ring" in the central body and more extensive porosities in the side bodies.

ii. Misruns are found in the vents near the casting surface, which could be problematic in practical applications.

iii. The maximum velocity of the system remains stable and below the admissible value of 0.5 m/s.

iv. The air venting system works effectively, even though the gating channel is larger, making it adequate at any dimensions.

Considering these conclusions, modifying the pressure curve to ensure proper cavity filling is recommended, specifically regarding the venting. Additionally, the gating channel design used in V1 is more straightforward for simplicity and efficiency, as it requires less material.

C. Gating System V3

As highlighted in the conclusions of the previous system, the objective of *Gating System V3* is to consider the shortcomings of the previous attempts. Therefore, the gating channel dimensions are the same as V1 system, aiming to use less material and improve efficiency, as Figure 82 depicts.

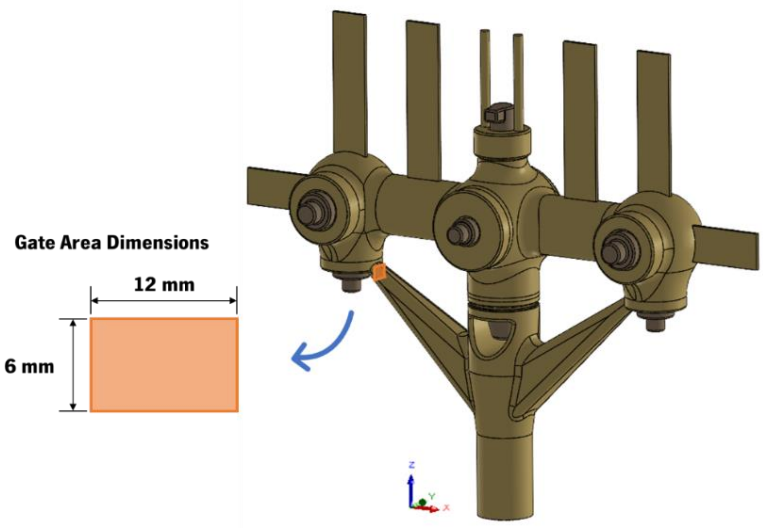

Figure 82: Dimensions of the gate area of the System V3.

Based on the previous simulation finding's, the metal's maximum height was dangerously close to the casting surface, which could compromise the final casting configuration under actual conditions. To address this concern and ensure proper filling, the parameter for gating system height, $\mathbf{h_{gating}}$, was modified to cover the entire cavity, providing an additional safety margin. Table 14 outlines the properties of the metal and gating system used to calculate the pressure.

Table 14: Metal and Gating system's properties used to determine the pressure.

Metal density, ρ [$\mathbf{kg/m^3}$]	6660.88*
Gravitational acceleration, g [$\mathbf{m^2/s}$]	9.81
Gating system height, $\mathbf{h_{gating}}$ [mm]	265
Rise tube height, $\mathbf{h_{rise\ tube}}$ [mm]	250

*At $T = 983.75$°C

Placing the values of Table 14 in Equation (4.12), a maximum pressure value of 0.180 bar was obtained. Figure 83 shows the pressure graph with the simulation and the actual curve used in the LPDC machine.

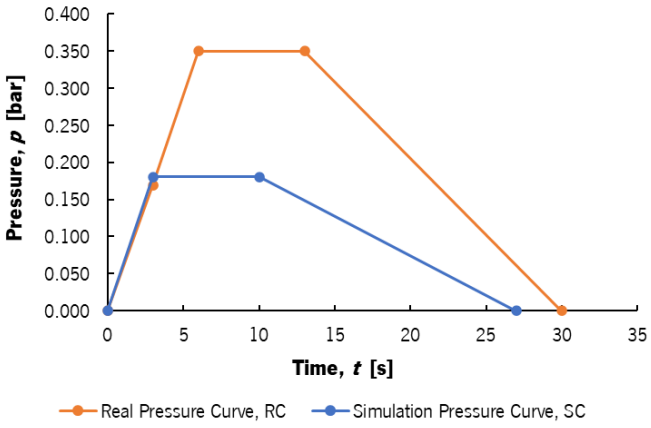

Figure 83: Simulation and real pressure curves used in the last simulation attempt.

(a) Shrinkage and Misruns:

Figure 84 shows the shrinkage porosities and misruns defects encountered for the last simulation.

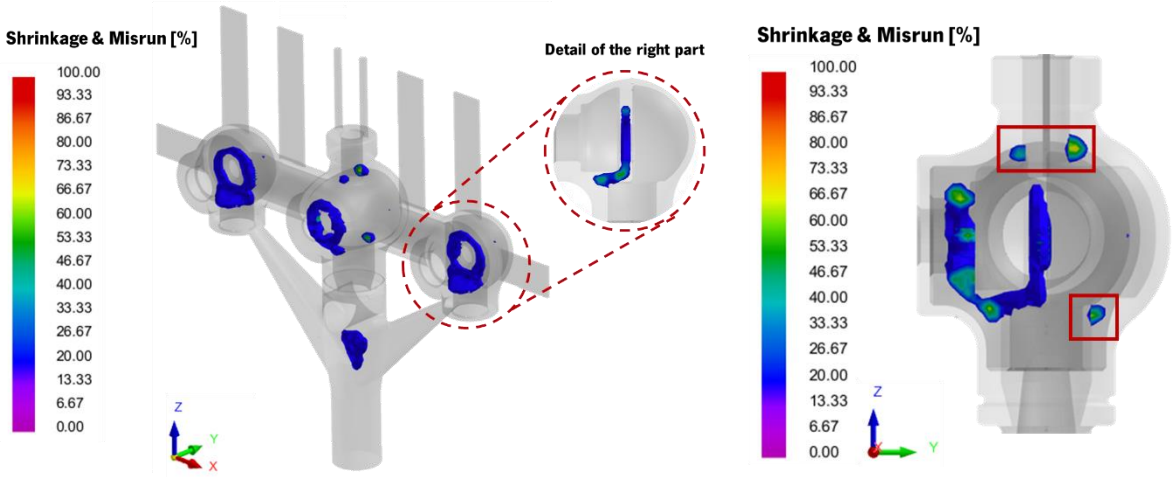

(a) (b)

Figure 84: (a) Shrinkage Porosities and Misruns, for the *Gating System V3*; (b) Detail of Shrinkage Porosities on YZ plane.

Analysing Figure 84, it is evident that:

i. Similar to the previous simulations, shrinkage porosities are prominent in all three bodies. The side bodies show more pronounced shrinkage, especially in the central thicker wall (see detail in Figure 84 (a)). The central body still exhibits a prominent "ring" and some minor porosities Figure 84 (b).

ii. As expected, there is no evidence of misruns. The pressure applied considered the entire height of the casting cavity, ensuring that even the vents were filled with metal.

Furthermore, these porosities are attributed to the premature solidification of the gating channel – as shown in Figure 85 (a). It is evident that as soon as the casting is completely separated from the gating channel, shrinkage porosities appear, as illustrated in Figure 85 (b).

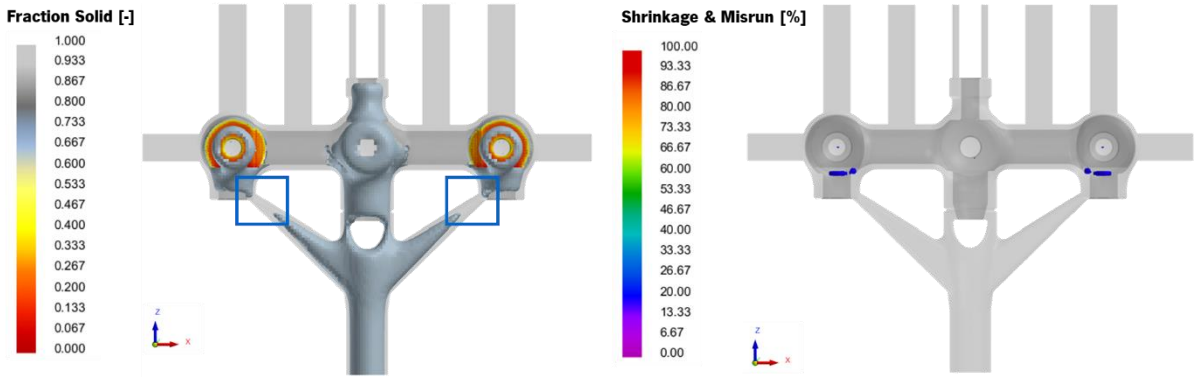

(a) (b)

Figure 85: (a) Solid fraction; (b) Formation of shrinkage porosity simmultaneously to the gate closing.

Regarding filling time, the *Gating System V3* obtained a time of 2.88 s, which is considerably lower than the theoretical value. This decrease in filling time can be associated to the slightly higher pressure used in this simulation compared to the other options.

(b) Maximum velocity:

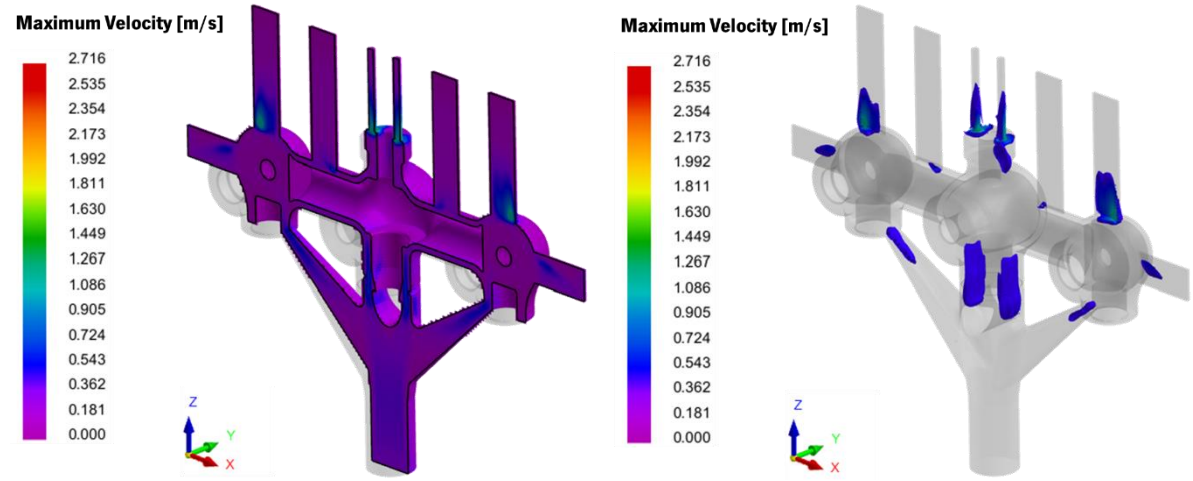

(a) (b)

Figure 86: (a) Maximum velocity for the V3 version and (b) regions of the mixer where the velocity exceeds 0.5 m/s.

In Figure 86 (a), it can be observed that the velocity gradient is significantly higher compared to the previous versions, with the regions of highest velocity corresponding to the entrance of the vents and gate areas. The increase in speed is directly related to the higher pressure applied. Analysing Figure 86 (b), it becomes evident that the velocity in the gate areas and the entrance of the vents exceeds 0.5 m/s,

with the maximum velocity recorded being approximately 0.8 m/s (primarily located in vents). These areas, vents, are not part of the final bathtub mixer, so any potential oxidation due to the high speed does not compromise the entire system, as they are removed after metal pouring and solidification.

(c) Air entrainment:

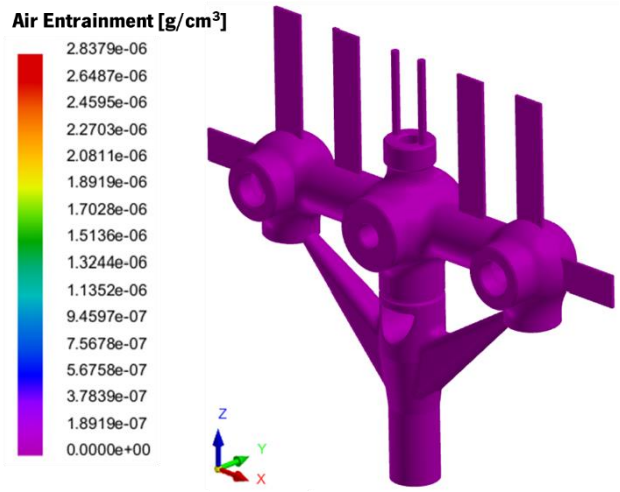

Figure 87: Air entrainment for the last simulation.

As expected, Figure 87 confirms no indication of air entrainment inside the cavity, thanks to the efficient venting system demonstrated in the previous simulations.

Conclusions about *Gating System V3*

Based on the results shown, the following conclusions can be inferred:

i. Similar to the previous versions, shrinkage porosities are present in all three bodies of the mixer. The side bodies exhibit more pronounced porosities due to the thicker wall; there is a possibility of these not occurring.

ii. No misruns are expected, as the pressure applied considers the total height of the cavity and moulds.

iii. The velocities recorded are higher than the other versions, mainly due to the increase in the maximum pressure value.

iv. There is no evidence of air being trapped inside the cavity, which confirms the effectiveness of the venting system.

D. COMPARISON OF RESULTS

Considering the results obtained from the three simulations, it is essential to compare them to choose the configuration that best suits the production of the bathtub mixer. For this purpose, Table 15 presents a comparative analysis of the results.

Table 15: Comparison between all the systems tested.

Parameters	***Gating System V1***	***Gating System V2***	***Gating System V3***
Mass of casting, m_{casting} [kg]		1.765*	
Mass of filling system, m_{filling} [kg]	3.013*	3.045*	3.013*
Yield of casting, η_{casting} [%]	60	60	60
Shrinkage porosity	Yes, in all three bodies	Yes, in all three bodies	Yes, in all three bodies
Misrun	Yes, in all vents	Yes, in all vents (near the casting surface)	No
Feeding pressure, p_{feeding} [bar]	0.165	0.165	0.180
Filling time, t_{filling} [s]	6.9	6.8	2.9
Maximum velocity, $v_{\text{máx}}$ [m/s]	0.11 to 0.5	0.13 to 0.4	0.4 to 0.8
Air entrainment	No	No	No

*At $T = 20°\text{C}$

Analysing Table 15, it can be observed that:

i. All three configurations show **similar casting yields**. However, Gating System V2 has a higher mass for the filling system.

ii. Shrinkage porosities are present in all systems, with smaller porosities in the side bodies for the first two systems.

iii. Misruns occur in the vents for the first two systems but not in the last one due to the higher pressure (0.165 bar *vs* 0.180 bar).

iv. The filling time is the **same** for Gating Systems V1 and V2, and it is almost twice as long as V3 (also related to a higher value of pressure).

v. Gating System V3 has a **high metal speed**, with regions exceeding 0.5 m/s, while the rest systems have similar velocity gradients.

vi. All systems effectively prevent air entrapment inside the cavity.

Considering all conclusions, it is evident that *Gating System V1* stands out as the **most optimal configuration**, and its parameters will be used and tailored to the real-world scenario.

5.2. Model Preparation for Production

To produce the bathtub mixer, *Metalúrgica Central da Trofa, Lda.* employs the LPDC machine of the IMR BPC 155H model, as depicted in Figure 88 (a). This compact and highly flexible model makes it suitable for achieving high production rates. The operating procedure mirrors the one described in Chapter 2.1. In this context, the molten metal is introduced into the cavity using air pressure.

(a)

(b)

(c)

Figure 88: (a) LPDC Machine of the IMR BPC 155H model, (b) Actuator with the dies and (c) Rising tube with the heating nozzle, to avoid premature solidification of the metal.

The LPDC machine can seamlessly transition between different stages of the production process, including die immersion for heating and preparation and the actual filling process. The machine's design is modular, as illustrated in Figure 88 (b). An important feature to highlight is the presence of a heating nozzle located on the rising tube. This nozzle extends from the furnace to the mould entrance, as shown in Figure 88 (c). Including this heating mechanism is vital to prevent premature solidification of the metal as it ascends the rising tube.

Table 16 presents key characteristics of the IMR BPC 155 H machine [1]:

Table 16: Characteristics of the IMR BPC 155 H machine.

Maximum die dimensions [mm]	500
Maximum die thickness [mm]	200
Maximum die weight [kg]	150
Maximum (die) close force [N]	8000
Working pressure [bar]	60
Electric power installed [kW]	132
Dipping tank capacity (for immersion of the dies) [L]	500 (2 Tanks, in total)
Gross weight [kg]	9000

The preceding chapter covered the iterative process to determine the optimal filling system (*Gating System V1*) for the study case. While this configuration exhibited excellent performance with fewer shrinkage porosities, appropriate filling time, and velocity, it is essential to modify and adapt the model for casting in the Low-Pressure Die Casting.

Additionally, the preparation of the model included designing the two moulds and the core boxes (for the two types of cores), considering the specifications of the machines used for casting and cores. Therefore, a series of steps were implemented in the bathtub mixer model, as follows:

(a) As described in Chapter 4.4, the cores were divided into three parts to ease their production and placement into the moulds. Although their coupling geometry was not mentioned in the simulation, it is essential to the production process. The central core has two protrusions on each connection to the other cores (Figure 89), and these features also have drafts to facilitate assembly. Likewise, the side cores have corresponding drafted holes at the same positions to ensure a proper fit:

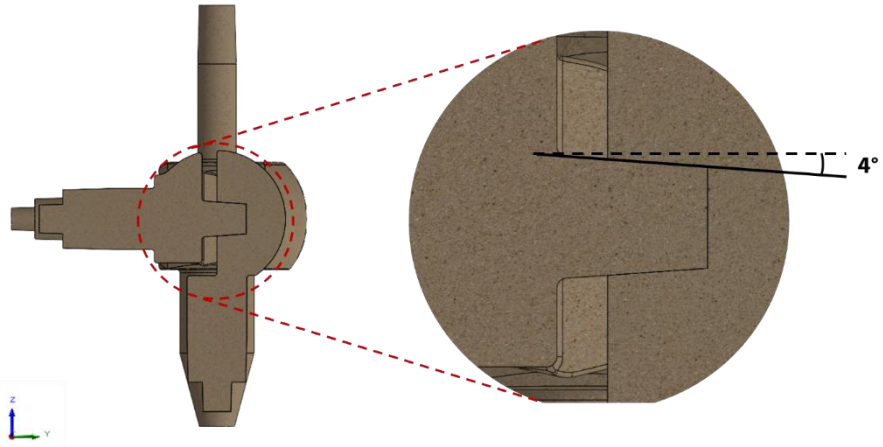

Figure 89: Central and side cores connection with a draft angle of 4°.

(b) The two small vents (with a diameter of 5 mm) positioned at the top of the cavity, as represented in all 3D simulation models, were replaced by a larger vent (Figure 90). This modification allows for better extraction of gasses from the central core.

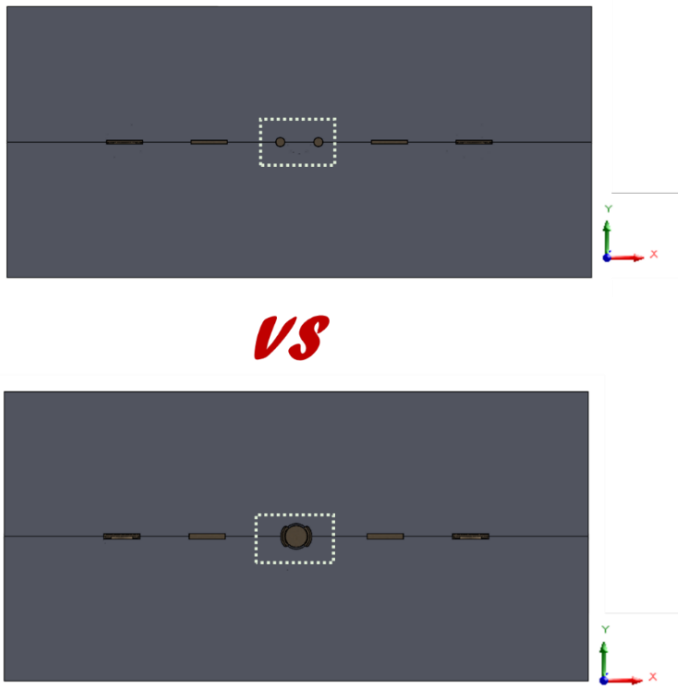

Figure 90: Replacement of the two small vents by a larger vent at the top of the cavity (Top view).

(c) To position and orientate the two side cores into the cavity, a small hole was created to guide the core and prevent dislocation when the die closes, as shown in Figure 91. Additionally, two small vents were added at the bottom to facilitate the extraction of gases from the cores – as seen in Figure 91.

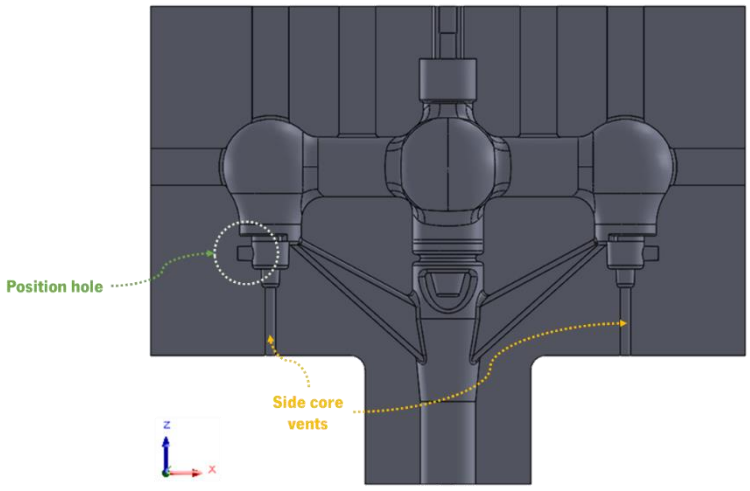

Figure 91: Position holes and side core vents locations.

(d) Subsequently, two 14 mm holes were created at specific positions, as depicted in Figure 92. These holes guide the two moulds when closing, ensuring that the casting remains appropriately aligned during the process, thus avoiding defects such as Mismatch or Shifts - Chapter 2.3.3.

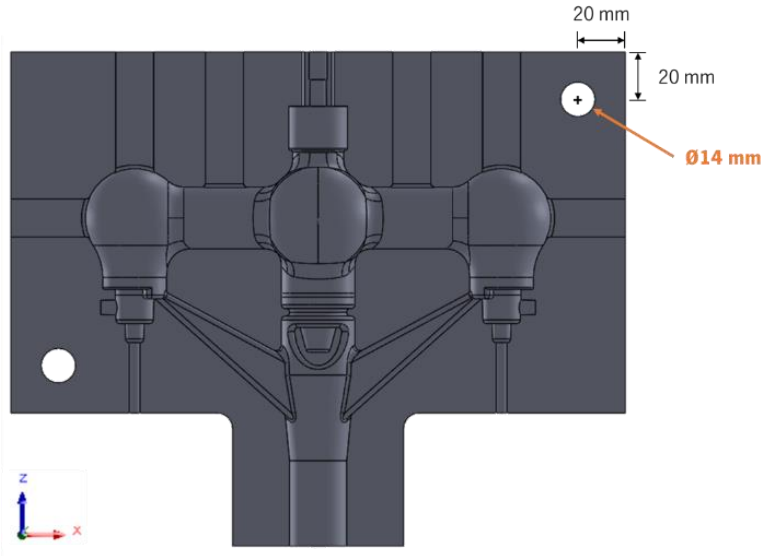

Figure 92: Position and dimensions of Guide holes.

(e) Next, three small holes were put into the mould to provide an escape path for gases generated from the contact of high-temperature metal with the sand cores. These holes are strategically positioned at the centre of each central core fitting, as illustrated in Figure 93.

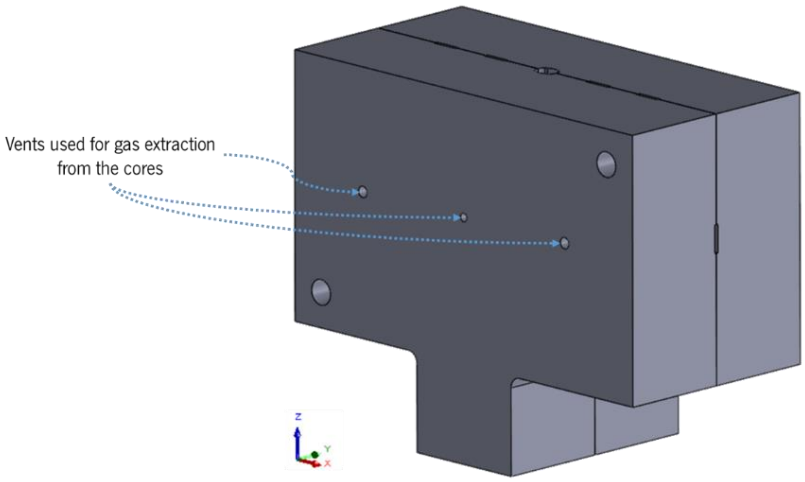

Figure 93: Vents positioned at the centre of each central core fitting in the mould.

(f) Lastly, eight holes, in total, were included in the two moulds to facilitate fitting the dies into the Low-Pressure Die Casting machine. The dimensions of these holes are indicated below:

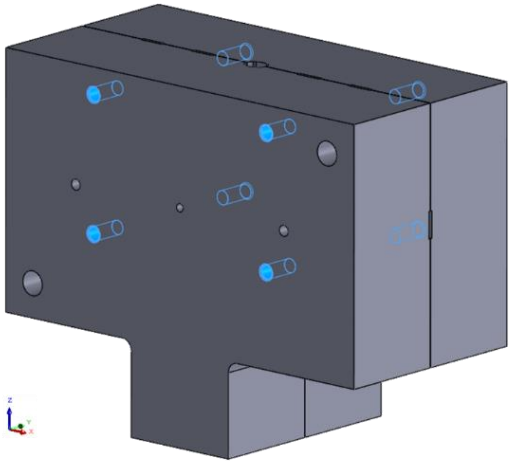

Hole Type	 Countersink
Type	Bottoming Tapped
Size	M12
End Condition	Blind: 12 mm

Figure 94: Fitting Holes and their specific dimensions.

The final 3D model of the dies and core boxes were sent for tool production, as represented in Figure 95 and Figure 96.

(a)

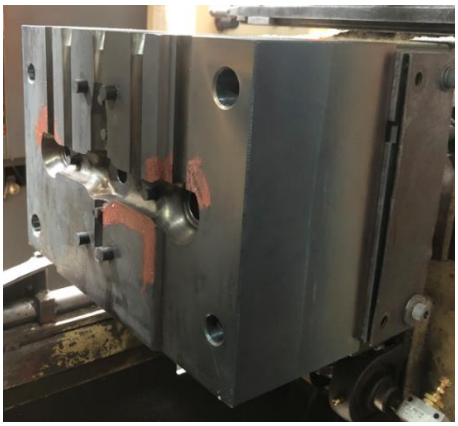

(b)

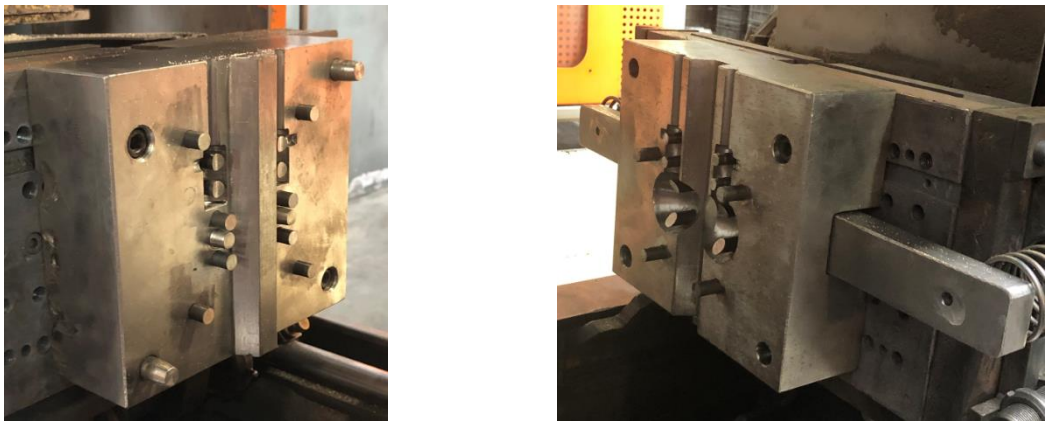

(c) (d)

Figure 95: Core boxes for the (a), (b) central core and the (c), (d) side cores.

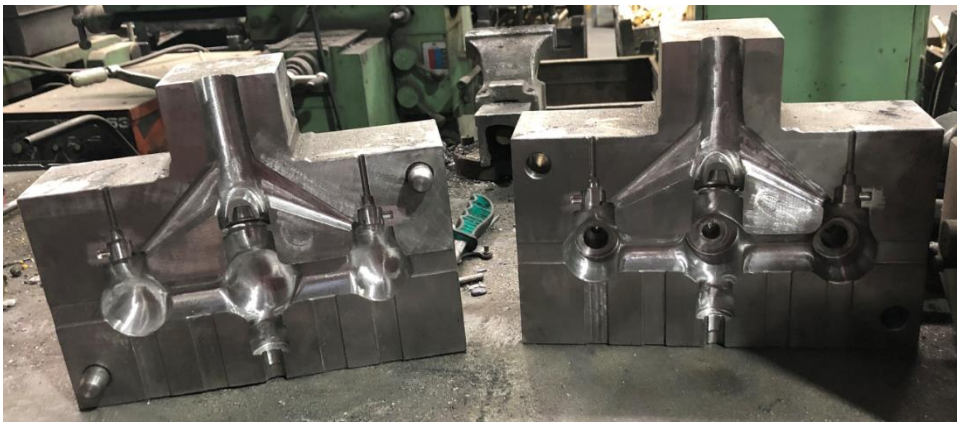

Figure 96: Final dies used for the production of the bathtub mixer.

5.3. Comparison of Numerical and Experimental Results

The experimental results aimed to compare and validate the QuikCAST software's numerical simulations. The objective was to assess the accuracy and reliability of the numerical model as a predictive tool. This validation process allows for a critical evaluation of the numerical model's performance and predictive capabilities, ensuring its robustness and accuracy in simulating the casting process.

After pouring and solidification, the probes were visually inspected to identify any defects. A microscopic examination was conducted for regions with detected defects to determine if they originated from shrinkage, due to lack of shrinkage compensation, or from trapped gas from the cores inside the cavity. Therefore, the forthcoming chapters will provide a detailed description of all the results and conclusions from the bathtub mixer study.

5.3.1. VISUAL ANALYSIS OF CASTING SAMPLES

As previously mentioned, the primary objective of these experimental data is to validate and assess the accuracy of the numerical predictions. Thus, the initial focus was on examining the presence of misruns, as they are associated with the filling process and can be detected immediately after pouring and removal from the dies. Figure 97 depicts the mixer after it was taken out of the machine and the correspondent numerical results obtained.

(a) (b)

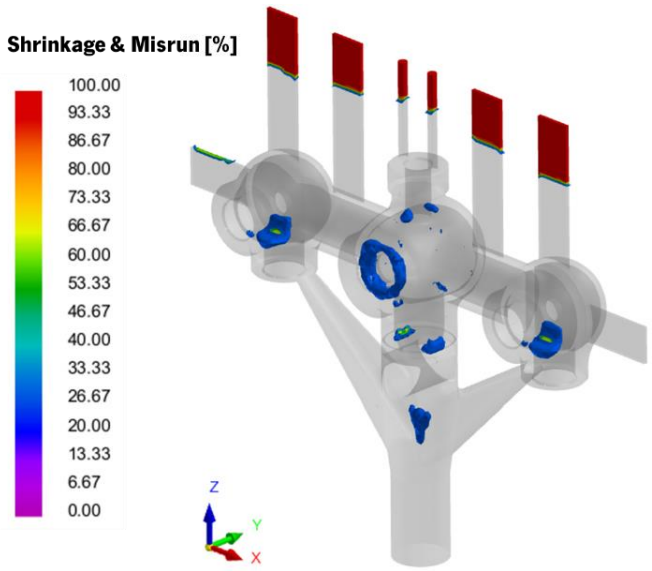

(c)

Figure 97: Bathtub mixer after being removed from the LPDC machine, with the gating system in (a) front view and (b) rear view; (c) Numerical results obtained for this configuration.

Figure 97 (a) and (b) shows that the mixer exhibits no misruns, which aligns with the numerical results - Figure 97 (c). The absence of these defects confirms that the filling system effectively ensured the cavity's complete filling, as predicted by the simulation.

Note: In Chapter 5.1.2, the maximum velocity and air entrainment parameters did not show any problematic values, regarding the numerical results. The maximum velocity recorded was below 0.5 m/s, and no air was observed inside the cavity. As a result, these aspects will be omitted in the subsequent sections.

Regarding the central issue with the study case (Shrinkage porosity), the numerical results (Chapter 5.1.2) indicated that the bathtub mixer was expected to show defects in all three bodies, with the central body exhibiting a "ring" of this defect. Additionally, the two side bodies might display smaller porosities at their bottom.

To further examine these predicted flaws, after removing the casting from the machine, it was cut and separated from the gating system, and the vents were also removed. As the expected defects were located inside the mixer, it was cut in different planes, as shown in Figure 98.

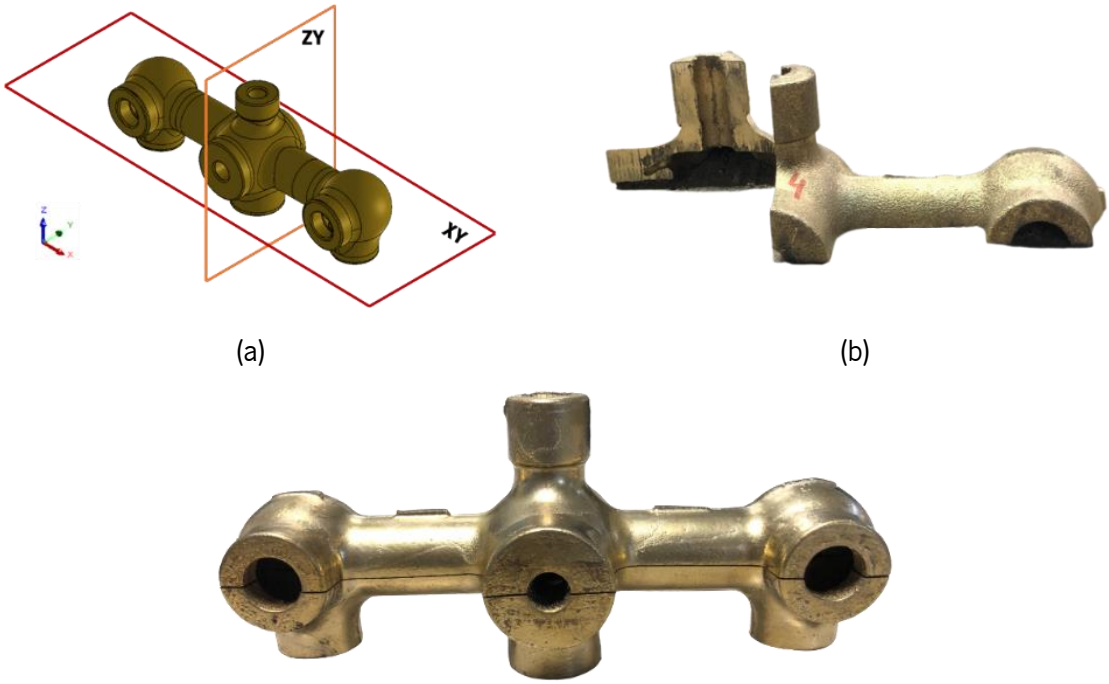

(a) (b)

(c)

Figure 98: Planes used to cut the mixer – (b) ZY plane and (c) XY Plane.

In the XY plane, the encountered defects were primarily located at the top of the casting, specifically at the central body, consistent with the numerical results shown in Figure 99 (a).

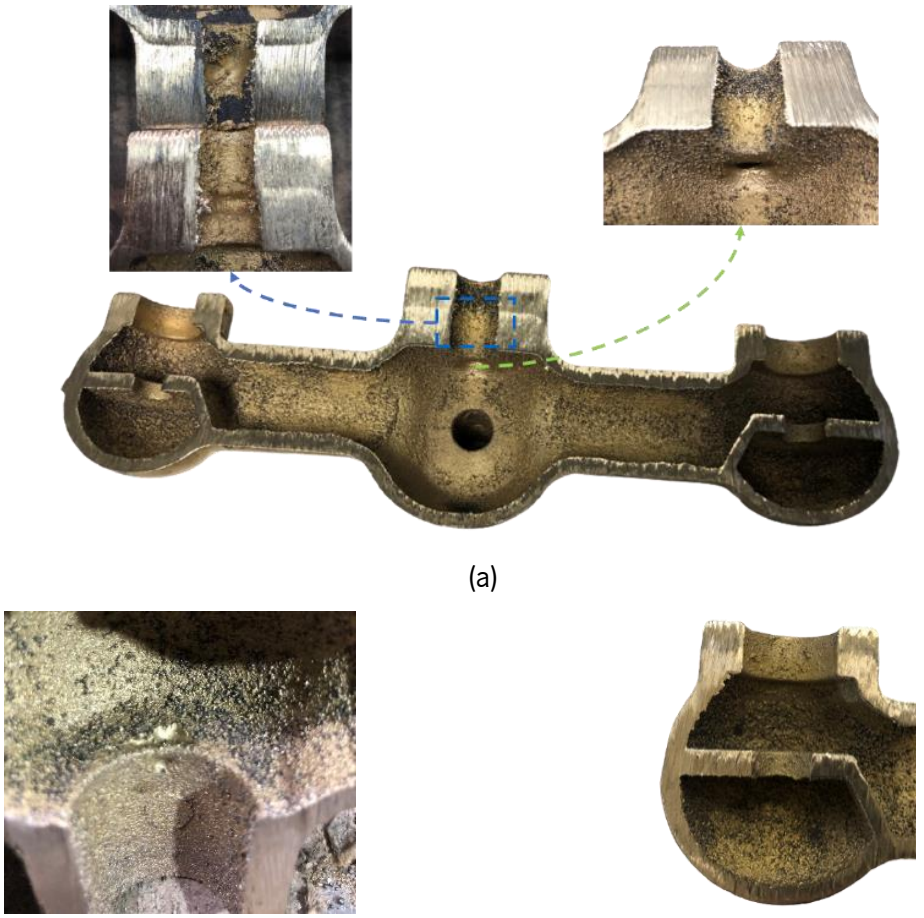

(a)

(b)

(c)

Figure 99: (a) Bathtub mixer cut in XY plane, in which blue and green represent the defects found; (b) Minor defects encountered at the bottom of the central body and (c) Detail of the left-side body.

Upon analysing Figure 99 and comparing it with the numerical results, it is evident that the "ring" of porosity mentioned earlier resulted in a more profound defect. Besides, some shrinkage porosity is present in the bathtub, indicated in blue in Figure 99 (a), at a location where the gating system cannot compensate. In contrast to expectations, no flaws were found on the side bodies - Figure 99 (c).

Therefore, for better understanding, Figure 100 presents a comparison between the numerical results and the actual results obtained in the casting process:

(a)

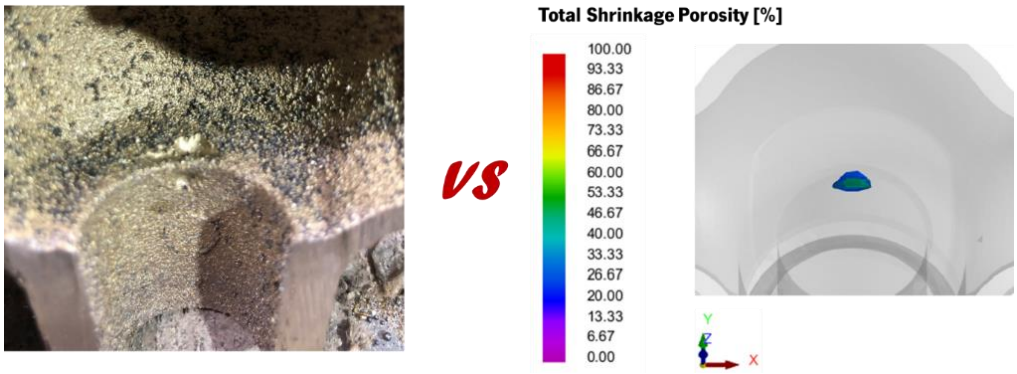

(b)

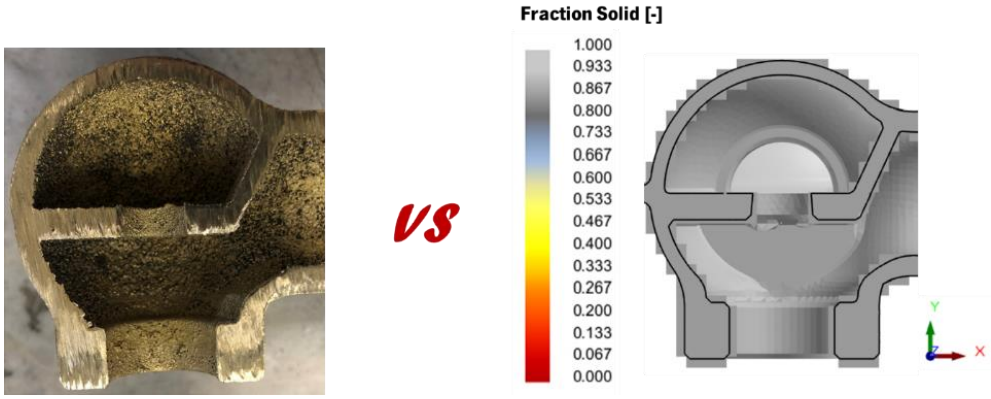

(c)

Figure 100: Comparison of real and numerical results (a) on the XY plane; (b) of the minor porosities and (c) of the side bodies.

Upon comparing the experimental and numerical results mentioned above, it becomes evident that the predicted shrinkage porosity closely resembles the actual defects observed (Figure 100 (a) showcases a deep depression in the flaw), highlighting the challenge in compensating for the gating system.

Similarly, the minor flaws present on the central body – as depicted in Figure 100 (b) – align precisely with the predicted locations, indicating high accuracy in the solver's predictions. However, it's important to note that no apparent defects are observed in the side bodies (Figure 100 (c)). The absence

of flaws in this region may be attributed to a potential misapplication of one of the boundary conditions, especially considering that the painted core must be accurately represented in the simulation.

Considering the comparison between the discussed experimental and numerical results, two potential causes of the defect observed in Figure 100 (a) can be identified:

i. **Natural contraction of the mixer**: The presence of the defect may be attributed to the natural contraction of the bathtub mixer during solidification. The gating channel is designed to compensate for this contraction by supplying additional molten metal. However, due to the gating channel's location within the mould, it may not effectively reach certain areas of the casting, such as the one depicted in Figure 100 (a). As a result, the natural contraction in this region could lead to the formation of the defect.

ii. **Gas Entrapment from Cores**: Another potential cause is the entrapment of gases from the sand cores inside the cavity. During the casting process, the high-temperature molten metal contacts with the sand cores, which can release gases. Since no vents are inside the mould (as shown in Figure 101), these gases may become trapped in the casting after pouring. The entrapment of gases can create voids or defects, making it challenging to achieve a sound component.

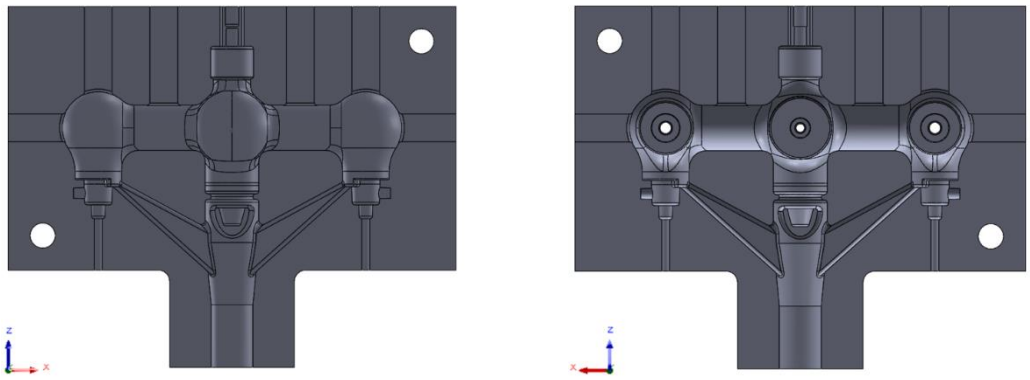

(a) (b)

Figure 101: Dies' interior without vents for extract gases - (a) left and (b) right moulds.

To gain a deeper understanding and determine the primary cause of the defect, a more thorough analysis of the specific region is essential. One approach is examining the region's metallurgy, providing insights into the defect's shape and dimensions.

5.3.2. MICROSCOPIC ANALYSIS OF THE MICROSTRUCTURE OF THE DEFECT

As previously mentioned, one approach to identifying the origin of the defect shown in Figure 100 (a) involves analysing its microstructure to understand its formation.

Gas porosities are flaws that arise when air or other gases become trapped within the cavity during solidification. Air becomes confined in the metal's interstices and cannot escape until the initial stages of

solidification, coinciding with the decrease in hydrogen solubility (as illustrated in Figure 6). Consequently, gas porosities exhibit rounded, smooth, and polished surfaces.

In contrast, shrinkage porosities develop due to the casting's contraction during solidification, stemming from liquid metals having a lower density than solid counterparts. This characteristic contributes to its irregularity, sharp edges, and distorted appearance observed in shrinkage porosities, setting them apart from gas porosities.

For this reason, two distinct sample types were selected to conduct a microscopic examination: one taken from the exact location as the defect and the other from an unaffected region (serving as a "standard group"). Figure 102 provides visual clarity regarding their respective positions.

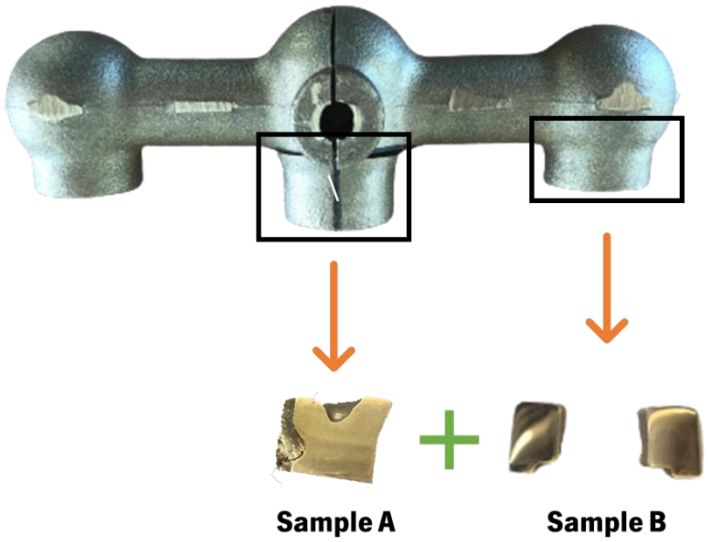

Figure 102: Location of the casting samples used - Sample A corresponds to the defect zone and Sample B corresponds to the "Standard Group".

Figure 102 illustrates that both samples underwent through polishing, cleaning, and chemical etching procedures. These steps were taken to facilitate the observation of microstructures under an optical microscope. The images captured are showcased in Figure 103 below:

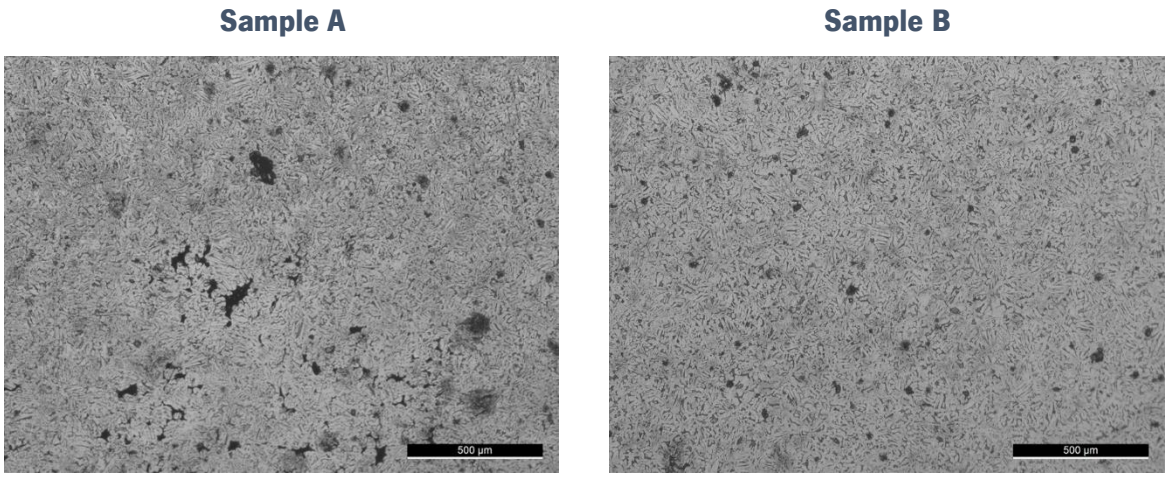

(a)

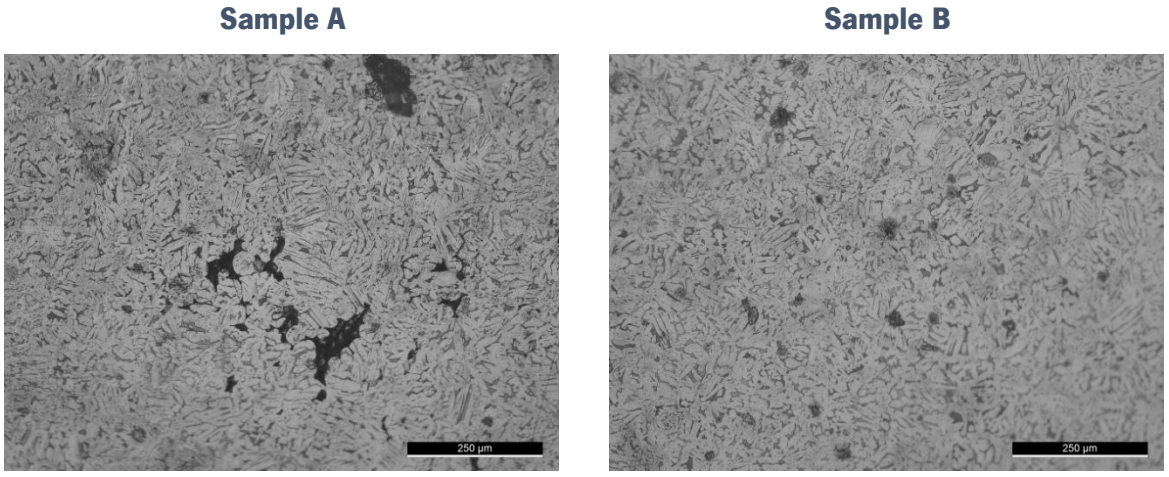

(b)

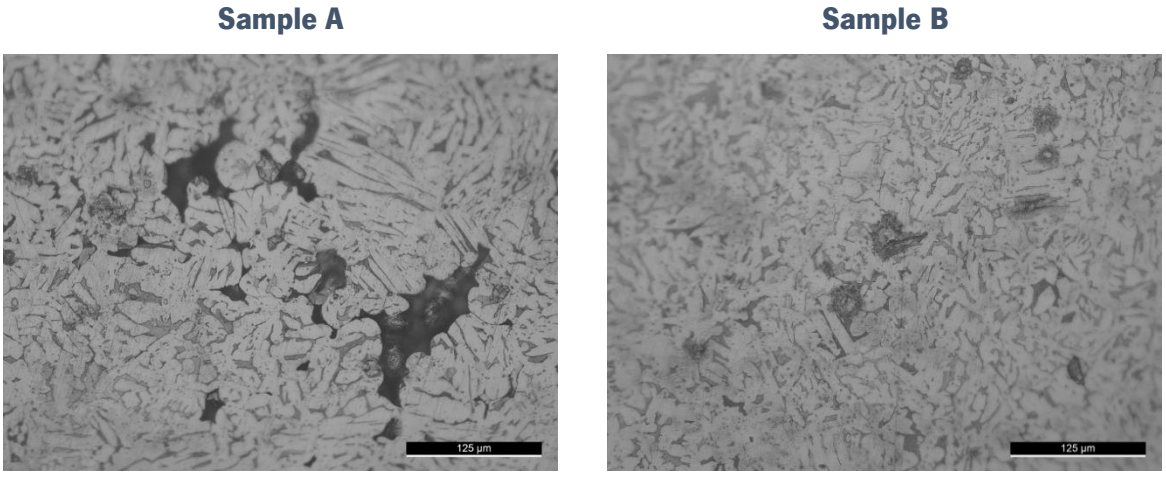

(c)

Figure 103: Microstructures obtained for the Samples A and B at different magnifications (a) 500 µm, (b) 250 µm and (c) 125 µm.

Analysing Figure 103, the following observations can be made:

i. The microstructure of Samples A and B corresponds to the expected phase diagram (Figure 17), with the alpha phase, α, appearing white and the beta phase, β, appearing dark. For this reason, the α-phase is present in the interstices of the β-phase and is more predominant due to its later formation.

ii. Sample A, from the defect zone (Figure 102), exhibits clear evidence of shrinkage porosities characterized by sharp and jagged edges. These flaws are evident in the 125 μm images - Figure 103 (c).

In summary, it becomes evident that the most prominent defect observed in the bathtub mixer (Figure 102) is a shrinkage porosity, often referred to as a Pipe defect, as seen from the conclusions previously outlined. This type of defect can be classified as an Open Shrinkage Porosity, as depicted in the schematic representation shown in Figure 104 (a). Prominently, this type of defect is characterized by its jagged edges and irregular shape, as observed in the microscopic analysis.

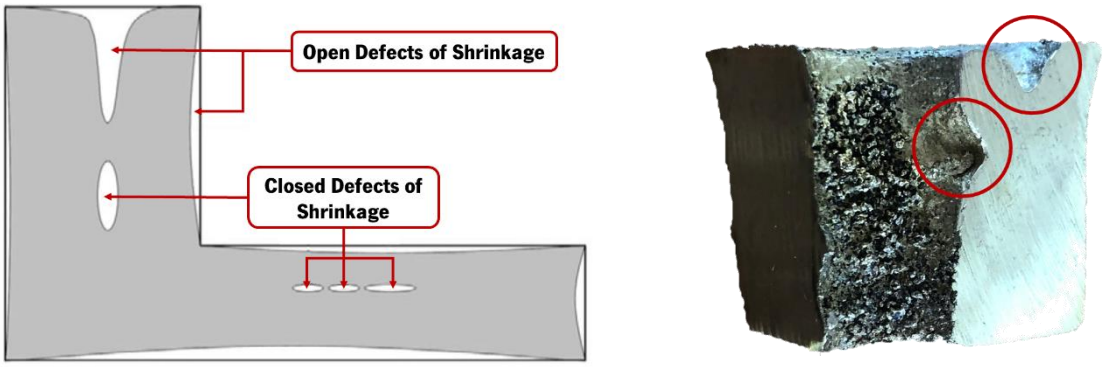

(a) (b)

Figure 104: (a) Types of shrinkage porosities; (b) Open shrinkage porosities observed in the casting, also known as Pipes.

5.4. CHAPTER REFERENCES

[1] IMR, *IMR brochure*. IMR, 2017.

[2] O. Chahem, "PROCESS ANALYSIS - IMR," *Prezi*, Oct. 09, 2018. https://prezi.com/p/ytlyjmvgaryh/imr-project-process-analysis/ (accessed Aug. 10, 2023).

[3] "17 Types of Casting Defects: Understanding Their Causes and Solutions," Jul. 19, 2022. https://www.rapiddirect.com/blog/17-types-of-casting-defects/ (accessed Aug. 10, 2023).

[4] S. Wong, "22 CASTING DEFECTS AND HOW TO PREVENT THEM IN YOUR PRODUCTS," *Intouch Quality*, Jul. 12, 2023. https://www.intouch-quality.com/blog/21-casting-defects-and-how-to-prevent-them-in-your-products (accessed Aug. 10, 2023).

Chapter 6 - CONCLUSIONS

The conclusion of any work plays a vital role in providing an overview of the entire project. In this chapter, some essential aspects of the project are summarized, and three main topics are addressed:

1. **Key challenges encountered**.
2. **Project's Contribution**.
3. **Future Work**.

The project focused on Low-Pressure Die Casting, which offers many advantages such as high metallurgical quality and flexibility. However, it still faces challenges, including gas and shrinkage porosities, defects that can compromise the final quality of cast products. Understanding the properties of the alloy used, including thermal properties and microstructure, played a crucial role in compensating for these defects during the development of gating systems.

6.1. PROJECT'S SUMMARY

The study aimed to evaluate the viability of utilizing QuikCAST casting software for manufacturing a copper-based Bathtub Body using Low-Pressure Die Casting (LPDC). The primary objective involved

creating a casting system, predicting potential defects, and comparing numerical and experimental outcomes.

Significant contributions were made towards achieving an optimized gating system for LPDC technology throughout the various phases of project development. The final design considered certain limitations related to the production line and the alloy, including thermal properties and chemical composition.

This work highlights the practical applicability of casting simulation in foundries, particularly in predicting the dimensions and positions of defects in castings. Consequently, the company can reap several benefits, including cost reduction, as there is no need to produce dies for testing each new component. Additionally, production time reduces significantly as new gating systems are developed more efficiently.

The success of the optimized gating system can be attributed to the comprehensive casting simulation process. This process predicted die temperatures through Thermal Die Cycling simulation and provided insights into metal velocity, temperatures, and air entrainment through Filling Simulation.

Regarding the Thermal Die Cycling Simulation, based on 10 points taken from the moulds, it was determined that a steady-state regime was reached after 8 cycles. This indicates that the subsequent cycles behaved consistently. Therefore, the simulation can be simplified to run for only 8 cycles. Concerning the Filling simulation, the iterative method led to generating three optimized solutions, which were compared to identify a viable solution for implementation in the industry. The final solution, *Gating System V1*, exhibited favourable characteristics, including a high Casting Yield (60%), a lower defect rate (present in all three bodies), and an appropriate filling time (approximately 6.9 s).

Furthermore, microscopic analysis shed light on the defects observed in the cast parts, which were attributed to either shrinkage or gas porosities. The analysis confirmed that the defects were, in fact, shrinkage porosities, as detailed in Chapter 5.3.2.

In summary, the implemented gating system contributes significantly to reducing the company's high rejection rate of 50%, resulting in numerous advantages in terms of cost savings, time efficiency, and the quality of the final product.

Additionally, it demonstrated the feasibility of employing QuikCAST software in Low-Pressure Die Casting (LPDC) simulation. The comparison of numerical and experimental results underscored the software's efficacy in enhancing the casting process. By accurately predicting defect locations and optimizing system designs, QuikCAST holds the potential to significantly reduce manufacturing costs, minimize rejection rates, and accelerate product development timelines.

6.2. KEY CHALLENGES ENCOUNTERED

As with any academic research study, the extensive investigative aspect of the project is time-consuming yet essential for obtaining a fundamental grasp of the technology's concepts and, consequently, for devising implementable solutions in the industry.

In the case of this work, the development of a gating system for LPDC technology necessitated a comprehensive and meticulous research effort. This approach was adopted to minimize the potential introduction of errors that could compromise the final solution.

The primary challenges encountered revolved around aspects related to the design of the filling system and its core equations. These challenges stemmed from the limited research and literature in this specialized field.

Another challenge was the need for more information about casting simulation, especially concerning the specific software employed, QuikCAST, in contrast to other more widely recognized commercialized software solutions.

6.3. FUTURE WORK

While this work primarily emphasized the development of an optimized gating system for Low-Pressure Die Casting technology, several other factors could also be valuable in reducing the porosity typically observed in this industry.

Melt treatment is one of the most crucial aspects of achieving high-quality castings, and it would be essential to evaluate the influence of implementing it during production, in addition to continuously monitoring the chemical composition.

Another important aspect concerns the re-melting of castings with defects. While the company performs cleaning to remove most impurities, not all is removed, such as core sand. When castings with defects are placed back into the furnace, these impurities (that do not melt) can result in slag inclusions when dissolved with the other pure metal. Therefore, it would be advantageous to investigate whether cleaning the interior of components to remove all the particles present is required.

Finally, concerning Thermal Die Cycling simulation, there is an opportunity for further research involving the analysis and comparison of die temperatures (numerical and experimental). Since MCT employs both copper and steel dies, this research can offer insights into determining the lifespan of each material. It can also help assess the feasibility of implementing cooling systems within the dies commonly employed in producing aluminium wheels. Brass is poured at a higher temperature than aluminium, making die temperature management a crucial aspect of the process.